Pullout behaviour of hooked-end steel fibres in self-compacting concrete

Vítor M.C.F. Cunha,
Joaquim A.O. Barros, José M. Sena-Cruz

Report 07-DEC/E06

School of
Engineering

Department of
Civil Engineering

University
of Minho

Azurém, 4800-085 Guimarães, Portugal
Tel. (+351) 253 510 200 – Fax (+351) 253 510 217 – Email: secG@civil.uminho.pt

ACKNOWLEDGMENTS

Notation and symbols

Abbreviations

ACI	American concrete institute	-
FRC	Fiber cement composite	-
LVDT	Linear displacement transducer	-
ITZ	Interfacial transition zone	-
RKN	Runge-Kutta-Nyström	-
SFRSCC	Steel fibre reinforced self-compacting concrete	-
UTS	Ultimate tensile strength	-

Greek letters

ε_f	Fiber strain	-
ε_c	Concrete strain	-
η	Factor that simulates the steepness pullout curve descending branch	-
κ_{b1}	Bond modulus of the real fibre	N/mm^3
κ_{b2}	Bond modulus of the fictitious fibre	N/mm^3
κ_e	Secant spring coefficient	N/mm
μ	Friction coefficient	-
ν_m	Poisson coefficient of the matrix	-
ν_f	Poisson coefficient of the fibre	-
θ	Fibre inclination angle	$^\circ$
σ	Normal stress	N/mm^2
σ_f	Normal stress in the fiber	N/mm^2
σ_{max}	Maximum pullout stress	N/mm^2
$\sigma_{b,max}$	Maximum tensile stress due to bending	N/mm^2
σ_{fu}	Fibre rupture stress	N/mm^2
σ_n^{ext}	Normal stress due to external loading??	N/mm^2
σ_n^{shr}	Normal stress due to shrinkage	N/mm^2
σ_y	Yielding stress of the fibre	N/mm^2
τ	Bond stress	N/mm^2
$\overline{\tau}$	Average bond stress	N/mm^2
τ_{crit}	Critical shear bond resistance	N/mm^2
$\tau_f(s)$	Frictional stress for the fiber slip δ	N/mm^2
$\overline{\tau_f}$	Constant friction bond	N/mm^2
τ_0'	Frictional bond stress	N/mm^2
ω	Fibre volume deformed under shear	mm^3
ξ	Damage coefficient of the shear stress deterioration	-
Γ	Bond energy of the interface zone	N/mm

Contents

LIST OF FIGURES

LIST OF TABLES

CHAPTER 1

Literature survey

1.1 Introduction

Short and randomly distributed fibers are often used to reinforce cementitious materials, since they offer resistance to crack initiation and, mainly, to crack propagation. In fibre reinforced cementitious composites, FRC, of low fibre volume fraction the principal benefits of the fibres are effective after matrix cracking has occurred, since fibres crossing the crack guarantee a certain level of stress transfer between both faces of the crack, providing to the composite a residual strength, which magnitude depends on the fibre, matrix and fibre-matrix properties. The mechanical performance of FRC is highly influenced by the fibre dispersion, since the effectiveness of fibres depend on how the fibers are oriented, their location and arrangement within the cement matrix. Considering the above-mentioned and that fiber and matrix are bonded together through a weak interface, study of the interfacial behaviour is important for understanding the mechanical behaviour of such composites.

The effectiveness of a given fiber as a medium of stress transfer is often assessed using a single fibre pullout test, where fiber slip is monitored as a function of the applied load on the fiber (Naaman and Najm, 1991; Banthia and Trottier, 1994; Li and Chan, 1994; Groth, 2000). Several test and specimens configurations have been developed for measuring the fiber pullout load versus slip response. These kind of tests can be performed with a single or multiple fibres. The case of a multiple fiber pullout test, where a certain number of fibers are loaded simultaneously instead of a single fibre, is difficult to perform. Moreover, the correlation between the results with a random distributed fibre composite is also complicated, due to these kind of tests being commonly performed with all fibers aligned (Bartos, 1981). Ouyang *et al.* (1994) performed pullout tests on multiple fibers with different inclinations. However, the correlation with a random distributed fibre composite is difficult, since the inclination of the fibers in each

specimen was the same.

In spite of the belief sometimes held that no correlation exists between the behaviour of fiber in a single fiber pullout test and its behaviour in a real composite (Hughes and Fattuhi, 1975; Maage, 1977), the data derived from single pullout tests can give relevant contribution to optimise the properties of fibre reinforcement cement composites. The available research indicates that there is not an ideal test or model to fully predict the mechanical behaviour of steel fibre reinforced concrete, even for the basic case of uniaxial tension, since the relationships withdrawn from the uniaxial tension test can not be representative of all fibre types and cement matrices. However, from the analysis of the fiber reinforcement mechanisms in a single pullout test, the key aspects of the overall behaviour of a composite material tested under uniaxial tension can be assessed.

The post-cracking behaviour of random discontinuous fiber reinforced brittle-matrix composites can be predicted by the use of a composite bridging stress - crack opening displacement relationship, $\sigma - w$. Several authors developed micro-mechanical models for obtaining the $\sigma - w$ relationship, since for quasi-brittle materials, the stress-crack opening relationship that simulates the stress transfer between the faces of the crack has a significant impact on the behaviour of a structure after its cracking initiation. In case of FRC, the $\sigma - w$ relationship can be approximated by averaging the contributions of the individual fibers bridging the matrix crack plane, defining for this purpose probability-density functions of the centroidal distance of fibres from the matrix crack plane, and of the orientation angle (Li *et al.*, 1991). Visalvanich and Naaman (1983) derived a semi-empirical model to simulate the tension - softening behaviour of a cement based material reinforced with discontinuous randomly distributed steel fiber. In this work they assumed a purely frictional fiber/matrix interface and the possibility of fibre fracture was not contemplated. Based on the assumptions of the latter model, Li (1992) developed an analytical model which take into account an additional frictional effect called snubbing effect (factor which considers the angle effect of nonaligned fibers on the pullout load). Maalej *et al.* (1995) extended the latter fiber pullout model by explicitly accounting for potential fibre tensile rupture.

The latter models, which are based on an averaging process of all the forces that are carried out by the fibers over a crack plane, by modeling the main mechanisms on a single fibre pullout can provide the general material composite behaviour with reasonable accuracy. However, they do not account for some aspects, such as, fiber bending rupture, and matrix spalling at the exit points of inclined fibres. Moreover, the possible interaction between neighbouring fibres, as well as, the modification of the matrix modulus and packing density by the addition of fibres are neglected in the above-mentioned models.

Another difficulty on the prediction of the post-cracking behaviour of a composite in a real

structure is that the material behaviour in a test specimen may differ from the behaviour of a real structural element. It is well described in literature, that various casting procedures, as well, structural shapes may result in predominant fibre orientation into parallel planes (Stroeven, 1986; RILEM TC 162-TDF, 2002), or in the case of steel fibre reinforced self-compacting concrete along the flow itself (in the fresh state) and the flow along the walls (Grünewald and Walraven, 2003). The fiber orientation nearby the walls of a structural element will not be representative of the material, but of a structure (Stroeven, 1986). A predefined orientation of the steel fibres parallel to the tension direction in a test specimen may result in overestimating the post-cracking mechanical properties of the steel fiber reinforced concrete, when compared with specimens with equal amount of fibers, however with a random fibre orientation.

1.2 Pullout behaviour of steel fibres (micro mechanical)

In this section it will be discussed the pullout behaviour of straight steel fibres and hooked-end steel fibers from a micro mechanical point of view. The mechanical behaviour of other steel fibres types will be discussed more briefly in a posterior section, not from a physical point of view, but from the overall mechanical behaviour performance standpoint. The most relevant aspects to determine and understand the pullout load – slip relationship of a fibre will be focused. The interfacial transition zone, ITZ, is also referred here in a succinct and qualitative way, in order to help understand further micro-mechanical considerations.

1.2.1 Fibre-matrix interface

A fibre reinforced cement composite is composed by the mixture of aggregates, cement paste and fibre, bonded to each other at an interface, which is commonly called the interface transition zone, ITZ. The properties of this zone depend on many parameters, such as the nature of the binder, the presence of additions, and the water/cement ratio. The properties and bonding quality of the interface plays a primordial role on the behaviour of the composite material. In fiber reinforced cement composites, the ITZ behaviour has, even, a more relevant role on the mechanical behaviour of FRC than in plain concretes, since the fibre aspect ratio is considerably high, and, therefore, the contact surface area is larger than that of the aggregates.

The formation of ITZ can be explained by the wall effect, since there is a non-efficient packing of the cement particles in the fresh state, which leads to a high amount of empty space that only will be partially filled with hydration products. The syneresis process (Chandra, 2002) can also justify the morphology of the ITZ. During syneresis, the exudation of the cement gel produces the release of the water molecules from the gel structure. This leads that the particles

arrangement of the originally homogeneous mass, at the contact surfaces, will readjust into two separate parts, a water rich and a solid rich mass.

In spite of existing several explanations for the formation of the ITZ, the main outcome withdrawn of the ITZ formation is that all these phenomena at this zone result in a significantly higher porosity than in the bulk paste, and also in an increase amount of calcium-hydroxide (CH) crystals (Figure 1.1(a)). For this reason the ITZ has substantially lower strength and stiffness when compared to the bulk cement paste (Diamond and Huang, 2001). Test results of the microhardness of concrete around the steel fibre (Wei *et al.*, 1986) indicate that the microhardness in the ITZ is lower than in the bulk cement matrix (Figure 1.1(b)), and that the width of the interface zone is of about 75 μm. Bentur and Mindess (1990) determined with a SE Microscope that the width of the ITZ ranges from 20-50 μm, whereas Li and Stang (1997) points out values on the order of 40-70 μm thickness.
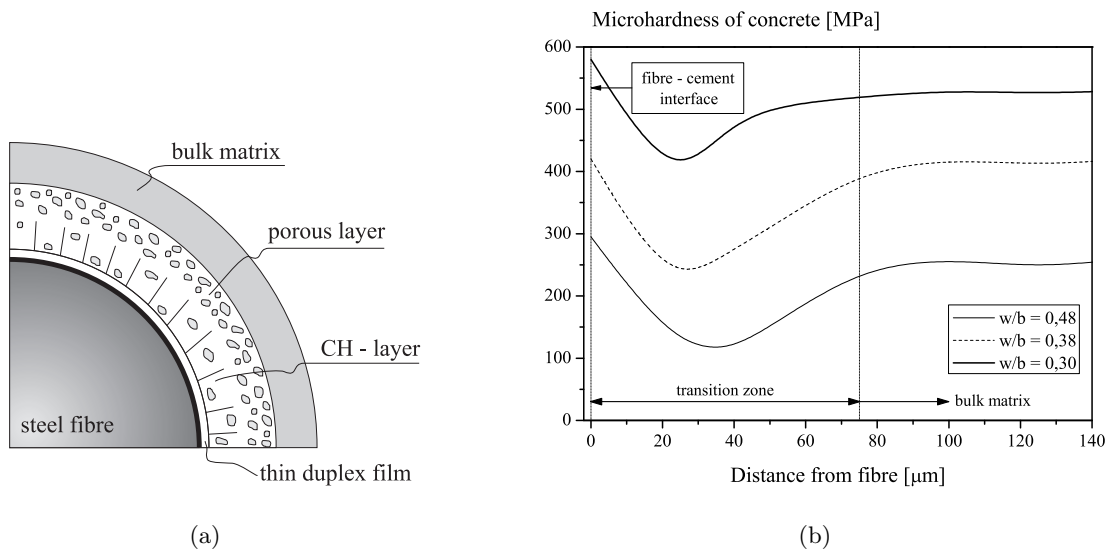
Figure 1.1: Interface transition zone: (a) Transverse cross-section through a steel fibre (adapted from Bentur and Mindess (1990)); (b) Results of microhardness tests around steel fibres (adapted from Wei *et al.* (1986)).

Densification of the ITZ strengthen the transition zone and thus, enhance the fiber/paste interfacial bond strength. This can be accomplished with the reduction of water/cement and/or the use of microfillers, e.g. microsilica. This can be observed in Figure 1.1(b), where the strength of the ITZ increases with the reduction of the water/binder ratio. However, not always densification of the transition zone results in bond strength improvement (Li and Stang, 1997). There are other parameters which influence the hardness of the ITZ. In fact with the

increase of aggregate porosity, in general, bond strength increases, since the binder impregnates more deeply the aggregate border, extending the adhesion zone more to the interior. On the other hand, the absence of porosity in steel fibres surface will extend the adhesion zone to an outer zone from the fibre. The debonding of the surround interface between the fiber and the paste occurs at a weak zone, at a certain distance from the fibre surface (Wei *et al.*, 1986; Bentur and Mindess, 1990), and not in the actual contact paste-fibre surface, being a direct consequence of the differences between the ITZ structure and the rest of the cement paste (see Figure 1.1(b)).

1.2.2 Bonding

The micromechanical behaviour of fiber reinforced cementitious composites is somehow very complex, in part due to the presence and combined action of several mechanisms of bond. According to Naaman and Najm (1991) the principal bond mechanisms during the pullout of a fibre that contribute to the ductility of the composite material are: adhesion, friction, mechanical and fibre interlock.

The adhesion or chemical bond is the bond between the fibre and concrete matrix which surrounds it, which is related to the properties of the interface transition zone. The chemical bond is the first mechanism to be activated on the pullout. During this initial phase, the fibre and matrix deformations are fully compatible, in such a way that the bond of the fibre-matrix interface does not suffer any damage. As previously said, fiber matrix interface can upon depend on several parameters and also be improved by several ways. However, due to the brittle nature of adhesion, the bond improvement observed in a single pullout test does not translate in an equal improvement at the composite level (Naaman and Shah, 1976). After full debond is attained, frictional stresses are generated when this component is mobilised, in a general manner, due to the abrasion and compaction processes on the interfacial zone throughout the slipping of the fiber along its channel.

The mechanical bond can be obtained by fiber deformation processes. This leads to local interaction between fiber and matrix on the millimetre scale, and from a macroscopic point of view can be regarded as a roughening effect (Li and Stang, 1997). All steel fibers at the present days have their bond improved through mechanical deformations (e.g. crimping, indenting, or adding at their ends hooks, paddles or buttons), since this technique has proven to be the most effective one in improving fiber - matrix bond (Banthia and Trottier, 1994; Li and Stang, 1997). While for a smooth fibre, the slip mainly depends on the break down of chemical adhesion and on friction, for deformed fibres (e.g. crimping, indenting or hooked - end) it is generally accepted that the chemical bond can be neglected in favour of the mechanical bond between

the fibre "deformations" and the surrounding concrete (Maage, 1977). Finally, fiber to fiber interlock exists only in high volume fraction of fiber reinforcement (e.g. $\simeq 10\%$ of steel fibers in SIFCON (Homrich and Naaman, 1987)) where the fibers are in contact with each other. For the current volume fraction of fiber reinforcement used in conventional fibre reinforced composites, fiber to fiber interlock should be not taken into account.

The type of bond was also categorised by Bartos (1981); Gray (1984) in accordance with the nature of stress transfer and type of interface:

- **Shear bond**: Transfer of the parallel stresses to the longitudinal axis of the fibre. When mobilised, this type of bond assures the deformation compatibility between fibre and matrix. If the shear bond stress exceeds a limit value, it will be observed a relative displacement of the fibre towards the cementitious matrix. In this case, shear bond in a length where a relative displacement between the fibre and matrix occurs, corresponds to a friction phenomena.

- **Tension bond**: This stress component enables to resist forces perpendicular to the interface. This type of bond can be mobilised by phenomena due to mechanical stresses (e.g. Poisson coefficient), or due to physical phenomena (e.g. concrete shrinkage). This radial bond is usually ignored in models for a single fibre. Remark that, however, for a random fibre distribution over a cementitious matrix, the fibre interaction with each others can produce local confinements, which could better mobilise this kind of bond (Kelly and Sweben, 1976).

On the other hand, the average fibre orientation and fibre spacing influences the efficiency of a group of fibres. The pullout resistance may decrease as the distance between fibre decreases, due to the higher probability of mutual influence of the fibres stress fields (Naaman and Shah, 1976).

1.2.3   Critical embedment length

The failure mode of the fibre reinforced concrete is highly influenced by the stress transfer between the fibre and cementitious matrix. After matrix cracking, and for a straight fibre without anchorage, it can be observed two failure modes: the fibre rupture, the fibre sliding.

The most elementary model consists on balancing the forces on a straight fibre submitted to traction load. Assuming the hypothesis of an uniform distribution of the adherence, $\bar{\tau}$, over the fibre, it is possible to define a critical embedment length:

$$L_{f,crit} = \frac{\sigma_{fu} \cdot d_f}{4\bar{\tau}} \tag{1.1}$$

where σ_{fu} and d_f are, respectively, the fibre rupture stress and diameter. If the fibre embedment length is higher than the value of $L_{f,crit}$, the fibre will fail, if not, the fibre will slide.

This simplest model is the basis of the fibre-matrix association study. The reinforcement mechanisms in this case depend on the mechanical properties of the material, the adherence phenomena between the fibre and the matrix, and the geometrical dimensions of the fibres. However, there are other parameters that influence the reinforcement mechanisms, such as: the fibre orientation respect to the load, the fibre geometry configuration (e.g. fibres with anchorages or corrugated) and the fibre-matrix interfacial bond stress that is not constant over the fibre embedded length.

1.2.4   Pullout mechanisms of aligned fibres

Straight fibres

Generally, the overall mechanical behaviour of a straight steel fibre can be described as the combination of two mechanisms: debonding of the surround interface and frictional slip of the fibre. Afterwards the embedment fibre length is fully debonded (from outer surface to the interior of specimen prism), the fiber pullout occurs under frictional resistance.

The pullout behaviour of an aligned fibre can be represented by a load-slip curve as shown in Figure 1.2. In the first phase of the pre-peak branch, the pullout load almost linearly increases with the slip. However, before the peak load (B) is attained, usually, a nonlinear phase in the pullout load-slip curve is observed. Therefore, in the pre-peak branch two distinct phases are usually observed. The first one, a linear ascending part (OA) which is associated with the elastic or adhesive bond. The second part of the pre-peak branch (AB) starts with the microcracking of the ITZ, corresponding to the initiation of the debonding process. The non-linearity observed in this part is regarded as an indication of an interfacial crack propagation (Shah *et al.*, 1995). The interfacial crack stably propagates up to the peak load, and is usually designated as the critical crack length.

After the maximum load is reached, the load decreases with the increase of slip, which corresponds to unstable interfacial crack growth on the post-peak behaviour, i.e. the interfacial crack grows even though the pullout load decreases, and full debonding will occur (C). Subsequently, the fiber pullout occurs under frictional slip (CD). In this part of the post-peak branch the load also decreases with the increase of slip, since the available frictional area decreases as well the roughness of the failure surface.

When a straight fiber is submitted to a pullout load, as previously seen, the load transfer at the fiber-matrix interface is effectuated firstly by the adhesion bond stresses and after by
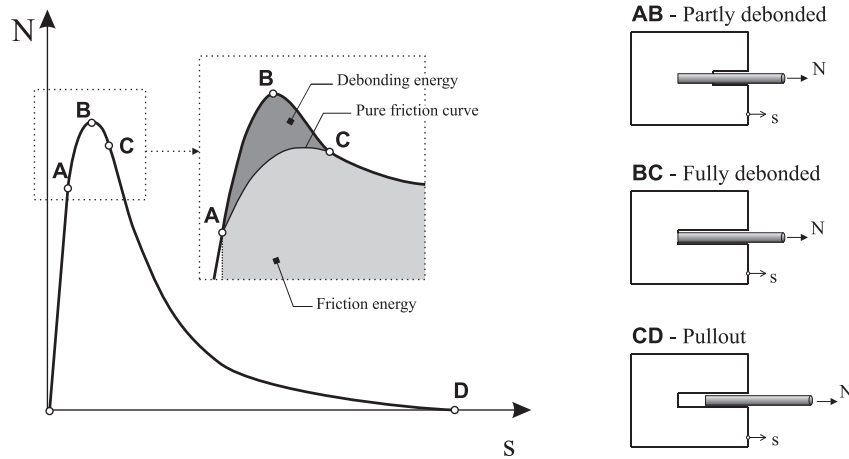
Figure 1.2: Pullout relationship between the load and the end-slip for a smooth straight fibre.

the frictional stresses. However, during the debonding phase, if the pullout load attains the force corresponding to the fiber tension strength without being exceeded the matrix shear strength, it will be observed the fiber rupture. Notice that this case is not very interesting from the reinforcement point of view, since the energy dissipated by this failure mode is limited, and is released abruptly decreasing dramatically the concrete toughness. On the other hand, if the tensile strength of the fiber is not attained, the fiber-matrix interface properties will progressively degrade generating a mechanism with higher dissipated energy.

Hooked-end fibres

The pullout behaviour of hooked-end steel fibres, in similitude to straight fibres, consists also on debonding and frictional pullout. In what concerns to the debonding phase of this type of fibre, the process has generally the same character of the one reported for straight fibres. However, in the frictional pullout, significantly differences can be found between these two types of fibres. In the hooked-end fibres frictional pullout is accompanied by a mechanical bond mechanism correspondent to the mechanical interlock and plastic deformation of the hook.

In Figure 1.3 is depicted the pullout curve for both straight and hooked-end fibres. The pre-peak behaviour of a hooked-end fibre can be described by three branches associated to distinct phenomenon's. The ascending parts OA and AB are associated, respectively, to the adhesive bond and to the debonding process until full debonding occurs at point B. However, in opposite to the straight fibres behaviour, after full debond is attained an additional load increase (BC) is observed due to the mechanical anchorage provided by the fibre hook. At the maximum pullout load (C) both curvatures 1 and 2 are deformed (see Figure 1.3), afterwards the mechanical anchorage starts to become progressively deformed, the pullout load starts to decrease (CD). While the fibre is not fully straightened (DE) another peak load is observed
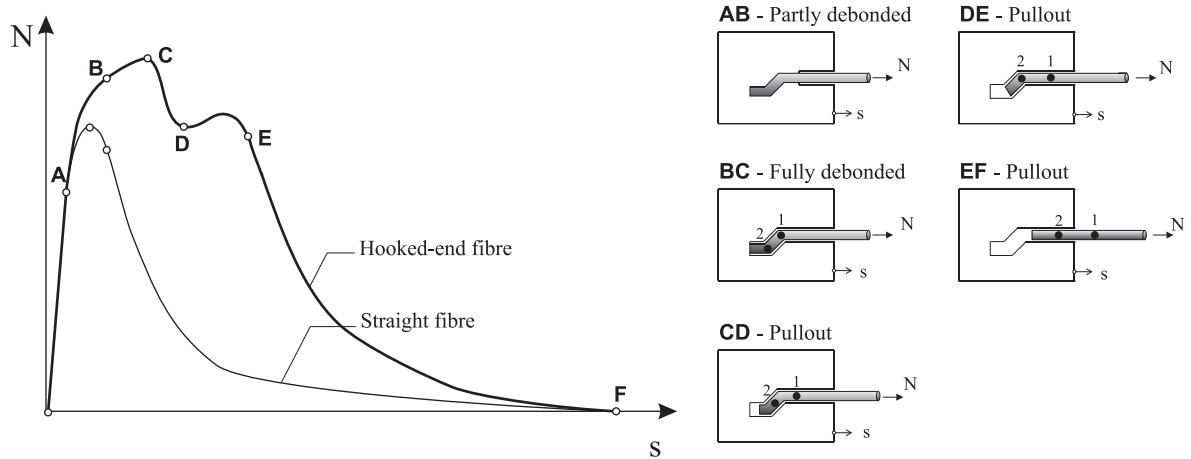
Figure 1.3: Pullout relationship between the load and the end-slip for hooked-end fibre.

which coincide with the fibre (curvature 2) passing the last corner of the fibre imprint made in the matrix. Finally, after the fiber is fully straightened, the pullout process occurs under frictional resistance (EF) as in straight fibres. Remark that in hooked-end fibres, usually the fibre hook is not fully straightened, which will increase the frictional stresses, resulting in a higher residual pullout load at the final stage of the pullout(see Figure 1.3).

1.2.5 Pullout mechanisms of inclined fibres

On the pullout of an inclined fibre with respect to the pullout load, as on the pullout of aligned fibres, debonding of fibre-matrix interface and sliding of the fibre on the debonded interface mechanisms are also observed. However, for inclined fibres other additional mechanisms usually occur: bending of fibres at the matrix crack surface and spalling of the matrix due to the fibre bending.

When a fiber is pulled out from a matrix at an inclined angle, θ, the pullout load, N, can be separated into two components, N_x and N_y (see Figure 1.4). From this two components of the pullout load only the component on the fiber axis, N_x, is dedicated to the debonding/pullout of the inclined fiber generating interfacial stresses along the fibre (S), and is currently termed as the pulley effect (Shah *et al.*, 1995).

The pullout resistance of inclined fibers, for an angle smaller than 45°, usually is higher than the one of aligned fibers (Brandt, 1985). This may be due to several mechanisms associated to the component N_y. As a consequence of the fibre inclination with respect to the pullout load, there are additional concentrated stresses where the fibre is bent. These concentrated stresses may cause local concrete spalling, since the concrete between the fibre and the crack plane is crushed or pushed off. Morton and Groves (1974), and Brandt (1985) proposed that the spalling of the matrix is one of the major mechanisms responsible for the pullout increase. For these

reasons, in the pullout of inclined fibres, the matrix strength is extremely important, whereas a weak matrix is prone to spalling and local damage due to the additional concentrated stresses. However, local stiffness of the matrix can vary significantly, and spalling of the matrix at crack surface fibre exit depends on whether or not there are aggregates or even fibre interlock at this zone (see Figure 1.4). In the case concrete spalling occurs the fibre can easily bend, and the stress carried by the fibre is reduced. The pullout resistance of inclined fibres may also depend on fibre bending (Morton and Groves, 1974) or fibre yielding mechanisms (Brandt, 1985), and on an additional frictional resistance on the fibre matrix interface due to local compression (Li *et al.*, 1990).
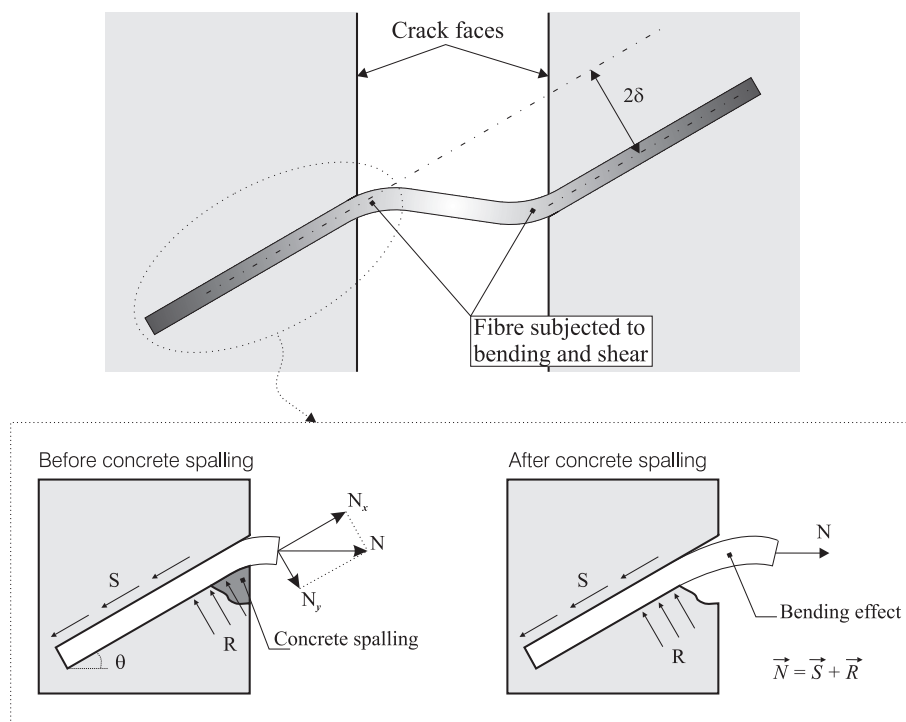
Figure 1.4: Bending and shearing of an inclined fibre across a crack and the components of a crack bridging force (based on Leung and Geng (1998)).

The bending or yielding mechanism is present for small pullout loads, since the fiber will almost immediately be bent when the pullout load starts to apply. On the other hand, frictional stress at the fiber-matrix interface will be generated only when the fiber starts to slip, and for this to occur the interface has firstly to debond. Since the bond slip value prior to peak load is relatively small, the effect of frictional stress on the pullout load of inclined fibers may not be significant before the peak load (Shah *et al.*, 1995). Therefore, both the pulley effect and bending mechanism may be the principle factors to the increase of the peak pullout load for

inclined fibers. Nevertheless, the influence of frictional stress becomes more important after the peak load, since slip is more significant.

1.2.6 Concept of energy dissipated on the fibre pullout

The phase correspondent to the elastic deformation of the fiber is observed for a small slip. Therefore, in the calculus of the energy dissipated on the pullout of the fiber, the component due to the fiber deformation can be neglected, and only the energy dissipated on the frictional phenomena with fiber rigid body displacement is considered. Assuming that the friction behaviour can be simulated by a $\tau_f(s)$ law , the work produced on the fiber pullout is given by:

$$W = \int_0^{l_f} \pi \cdot d \cdot \tau_f(s)(l_f - s) \cdot ds \tag{1.2}$$

where d, l_f and s are the fiber diameter, the fiber embedded length and fiber slip, respectively. Kelly (1970) proposed a constant value for the frictional stress law ($\tau_f(s) = \tau_{fc}$) obtaining the equation (1.3) for the work produced under pullout.

$$W = \pi \cdot d \cdot \tau_{fc} \frac{l_f^2}{2} \tag{1.3}$$

Assuming a polynomial law $h\left(s/l_f\right)$, where (s/l_f) is the normalized slip variable, the equation for determining the work produced is given by:

$$W = \alpha \cdot \pi \cdot d \cdot \tau_{fc} \cdot l_f^2 \tag{1.4}$$

where α is a constant value that depends on the integration of polynomial function $h(s/l_f)$. Equation (1.4) shows that the energy dissipated on the fiber pullout from a matrix varies quadratically with the embedded length of the fiber, for the case of a smooth fiber.

Several authors (Helfet and Harris, 1972; Hing and Groves, 1972; Brandt, 1985) have reported that for inclined fibres an additional amount of work is required to fully pullout a fibre. This additional energy absorption can be assigned to different mechanisms, such as: the plastic deformation under shearing (Helfet and Harris, 1972), or to plastic deformation under bending (Hing and Groves, 1972) both for the fiber. In a simplified way, the plastic deformation energy under shear, W_{shear}, can be considered proportional to the fibre volume deformed, to the ultimate shear resistance of the fiber, τ_{crit}, to the crack opening, w, and to the fibre orientation angle, θ (see Figure 1.4):

$$W_{shear} = \frac{\pi}{4} \cdot d^2 \cdot w \cdot \theta \cdot \tau_{crit} \tag{1.5}$$

However, the previous model presents some limitations. In fact, the deformation under shear can only occur if the matrix surrounding the fibre can support stress increments if submitted to strain increments. As it was previously indicated, local spalling of the matrix can occur, which is followed by bending of the fibre. The energy dissipated calculated by Equation (1.5) can be regarded as the upper limit value of the plastic energy that can be dissipated.

For the case that the dissipated energy is determined assuming a plastic deformation under fiber bending it is necessary to define a criterion for the material behaviour. In case the fibre curvature is sufficiently small, the matrix damage is limited, moreover is realistic to assume the formation of a plastic hinge. Hing and Groves (1972) propose to determine the plastic deformation energy by considering that the fibre is in a first phase bent with an angle θ, and as the fiber deformation process starts this same angle must be updated:

$$W_{bend} = 2 \cdot \frac{\sigma_y \cdot d^3}{6} \cdot \theta \tag{1.6}$$

unfortunately they run up against the problem of the determination of the angle θ and it is then impossible to determine the total dissipated energy.

More recently, assuming the fiber as an elastic material, and considering that the maximum tensile stress in the fiber section reaches the yield stress material under the pullout load, Ouyang *et al.* (1994) presented the following equation, for determining the additional bending energy, which is based on the yield stress of the fiber:

$$W_{bend} = \frac{\sigma_{b,max}^2 \, \pi \, L_b \, r_f^2}{8E_f} \tag{1.7}$$

Where $\sigma_{b,max}$ is the maximum tensile stress due to bending (the stresses resulting from tension are subtracted), L_b is the length of the bent zone of the fibre and is assumed to be proportional to the pullout slip (Stang *et al.*, 1990), and r_f is the fiber radius.

1.3 Experimental research on the pullout behaviour of fibre reinforced composites

The composite behaviour of steel fibre reinforced concrete, SFRC, is governed by the addition of the individual contribution of the single fibre interaction with the matrix. In spite of theoretically being possible to predict the bulk behaviour of SFRC from the single fiber pullout

performance, this task is considerably hard since there are several complex mechanisms involved in the overall composite behaviour. Single pullout tests have been carried out in the past 30 years to optimise the combination of both fibre type and concrete mix, and to understand the mechanisms of fibre reinforcement.

The pullout study of straight fibers has reached its peak during the 80s. Analytical studies were carried out to justify the fiber benefits of fiber addition to cementitious matrices (Bartos, 1981; Brandt, 1985). Over the years, so-called improved shaped fibers have been brought onto the market by different producers with claimed better performances than straight fibers (Naaman and Najm, 1991; Chanvillard, 1993). When the fiber has mechanical anchorages, they can be straightened during its pullout, therefore being necessary to take into account the energy dissipated in the fiber straightening process (Maage, 1977; Chanvillard, 1993). Recently the pullout study of a single fibre is resurging due to the development and increasingly application of new types of concretes, such as: self-compacting fibre reinforced concrete (Groth, 2000) and high performance concretes with hybrid reinforcement (Markovic, 2006). It is well recognised of the importance of fibre-matrix bond in the behaviour of fibre reinforced concrete. Moreover, in these new types of concretes is commonly used the inclusion of fine filler materials which will modify the properties of the interface transition zone, i.e the fibre-matrix bond, therefore its influence on the performance of the composite behaviour should be assessed.

There are several factors which affect the pullout behaviour of steel fibres. Throughout the last 30 years, pullout performance of steel fibers embedded in cementitious matrixes has been assessed as a function of several variables. From these variables can be pointed out: the matrix quality (Wei et al., 1986; Naaman and Najm, 1991; Banthia and Trottier, 1994), fiber inclination (Morton and Groves, 1974; Naaman and Shah, 1976; Ouyang et al., 1994; Banthia and Trottier, 1994), fiber embedment length (Chanvillard, 1993; Li and Stang, 1997; Robins et al., 2002), the rate of loading application (Gokoz and Naaman, 1981; Banthia and Trottier, 1991; Bindiganavile and Banthia, 2001), temperature of the environment (Banthia and Trottier, 1992).

In this section the analysis is restricted to the influence of the fibre type, fibre orientation, matrix quality and fibre embedment length on the pullout response of a single fibre.
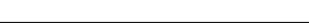
1.3.1   Influence of fibre type

The short fibers used in concrete can be classified in different ways. First, according to the fiber material, which can be natural, both organic and mineral, or man made (e.g. steel, titanium, carbon, glass, etc). Second, according to their physical/chemical properties, such as: density, surface roughness, non-reactivity with cement matrix, fire resistance, etc. Third

according to their mechanical properties such as: tensile strength, elasticity modulus, elongation to failure, surface adhesion properties, etc. Moreover, once a fiber has been selected, an infinite combination of geometric properties related to its cross sectional shape, length, diameter or equivalent diameter, and surface deformation can be selected.

There are several types of steel fibres available, which differ in size, shape and material properties. Due to different materials and manufacturing processes, the mechanical properties such as, tensile strength and grade of mechanical anchorage differ considerably from each fibre. These differences have a significant effect on the fiber pullout behaviour and, consequently, in the overall behaviour of FRC under loading. Some typical profiles of steel fibres commonly used in concrete technology are presented in Table 1.1

Table 1.1: Steel fibers profiles

Longitudinal profile	Cross section
Smooth	Round, flat or any shape
Indented Etched Roughened	
Flat-ended	Round or flat
Buttons-ended	Round
Hooked-ended	
Crimped Corrugated	Round, flat or any shape
Polygonal twisted	Polygonal (triangular or rectangular)

As it was described in a previous section, the behaviour of aligned smooth steel fibres is mainly governed by the adhesion and friction mechanisms, while for non-aligned smooth fibers with the pullout load direction, other mechanisms must be taken into account, such as, the fiber internal work due to its shear and bending deformation. as well as the energy dissipated in the deformation of the matrix surrounding this fiber critical zone. Due to the weak bond between steel-cement matrix, the pullout energy of a straight fibre is small. This problem may be solved by optimising the fibre anchorage properties (Chanvillard, 1993), in order to develop better bond between the fiber and matrix. The fiber can be modified along its length by roughening

or etching its surface, or by inducing other mechanical deformations. Other way of improving the bond is to enhance the chemical and physical bonding of wire surfaces to the cement paste (Hannant, 1987; ACI 544.1R, 1997).

Among various attempts to improve the bond-slip characteristics of steel fibers bonded to cementitious matrices, the most effective is mechanical deforming (Banthia and Trottier, 1994; Li and Stang, 1997). Steel fibers have a significant advantage over other fibers in terms of the facility with which they can be deformed and indented to improve their anchorage to cementitious matrices. Mechanical deformations in the form of hook, cone or crimp placed at the end or along the fiber have proven to be very effective in improving pullout resistance and, consequently, on enhancing several mechanical properties of the composite (Soroushian and Bayasi, 1991; Naaman and Najm, 1991; Banthia and Trottier, 1994; Rossi and Chanvillard, 1996; Groth, 2000).

Recently, Naaman (2003) developed a new kind of steel fiber of optimised geometry to increase the performance of steel fibre reinforced concretes. An originally, triangular or square fibre cross section assumes a polygonal cross section shape after twisting mechanical treatment (see Table 1.1). It is made of high strength steel wire, approximately with a tensile strength of 2000 MPa.

In Figure 1.5 are depicted the typical pullout load – slip responses for some commonly used steel fibres (smooth, hooked-end, crimped, buttons-end) and for the polygonal twisted fiber developed by Naaman (2003). Figure 1.5(a) shows clearly the benefits of the fibers mechanically deformed, when compared with a smooth fibre, on the peak pullout load and pullout energy. In what concerns to the polygonal twisted fibers, the key feature of these fibers is that when pulled-out from a cement matrix, its resistance increases with fiber slip. Increasing the lateral surface area of a fibre, for the same cross section, increases frictional and adhesive bond forces along the fiber that leads to an increase in pullout resistance and thus in fiber efficiency. On the other hand, during the fiber pullout, the fiber additional stiffness provided by the untwisting process will improve the ductility of the pullout load – slip response; since a slip hardening will occur.

In Figure 1.5(b) are compared the pullout responses of deformed fibers. The crimped fiber presents a higher pullout energy, since they have more curved parts than hooked-end fibres, so that more energy is needed to deform them, in comparison with hooked-end fibres (Chanvillard, 1993; Groth, 2000). The button-ended fiber has a higher pullout resistance, in spite of the lower pullout energy due to its rupture at peak pullout force. Remark that the pullout responses of Figures 1.5(a) and 1.5(b) cannot be compared, since the fibre embedment length, L_b, and the matrix compressive strength, f_c, are distinct.

In the case of a deformed fiber, both fiber and matrix are severely stressed during pullout,
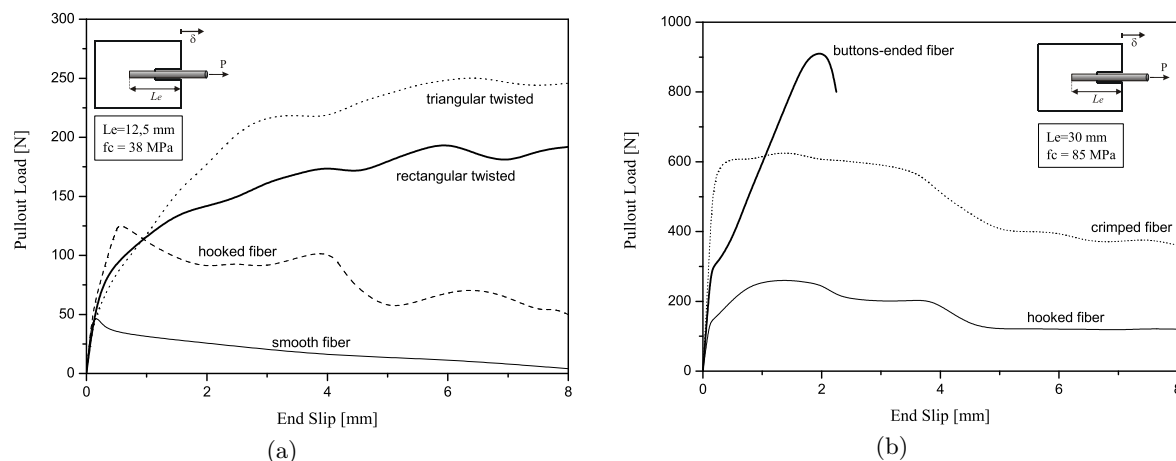
Figure 1.5: Comparison of typical pullout response of different steel fibres: (a) adapted from Naaman (2003), (b) adapted from Banthia and Trottier (1994)

therefore fiber fracture and matrix splitting occur more commonly than in straight fibers. For this reason, material properties like elastic modulus, strength, strain capacity, etc, for both fiber and matrix, are more significant in the case of deformed fibers than for straight fibers (Banthia and Trottier, 1994).

1.3.2   Influence of fibre orientation

In fibre reinforced concrete, the fibres are rarely aligned in the same direction of the pullout load. This is a consequence of the production technology of dispersed reinforcement provided by discontinuous fibres in the bulk material.

In Figure 1.6(a) are depicted different relations between the fibre inclination angle and the normalised values of the maximum inclined pullout force, where $N_{inclined}$ is the pullout force for an angle inclination ranging from 0° and 60°, and $N_{aligned}$ is the pullout force of an aligned fibre with respect to the load. In general, the pullout resistance of inclined fibres is higher than for aligned fibres, even for a significant inclination angle of 60°, the exception are the cases of Bartos and Duris (1994) and Leung and Geng (1998). However, it should be noticed that the values of the fibre slips correspondent to the maximum pullout load of an inclined fibre were much larger than for aligned fibres. Since the fibre slip at maximum pullout load for an inclined fibre can range from 0.5 to 4 mm, the previous remarks do not say much of the fibre performance on a real structural element. Regarding durability, serviceability limit sates or even ultimate load-carrying capacity, an appropriate crack width for a structural element would lay between 0.1 to 1 mm. However, these crack opening values should be taken into account carefully, since distinct allowable crack openings could be established for different fibre reinforced concrete applications, such as: small to moderate crack openings in slab on grade

applications, or large crack openings in tunnel linings and in structures under seismic loading. Taking into account the previous observation, in Figure 1.6(b) are represented the relation between the fibre inclination angle and the pullout load registered at a constant fibre slip of 0.5 mm. For this fiber slip, i.e. crack opening, the pullout forces of inclined fibres are higher than for aligned fibers until an inclination angle of 15°, decreasing significantly for larger values of this angle. The exceptions were the cases of Bartos and Duris (1994) and Leung and Geng (1998), where pullout load of inclined fibers was always lower than of the aligned fibers.

It should be noticed that the scatter of the results found between these authors (Banthia and Trottier, 1994; Bartos and Duris, 1994; Leung and Geng, 1998; Gysel, 1999; Robins *et al.*, 2002) can be assigned to distinct parameters that also influence the pullout response and can not be regarded independently, such as: concrete matrix strength, fiber embedment length and fibre cross section dimensions, fibre strength, dimensions of the fiber mechanical anchorage, fiber surface characteristics, etc. For instance, as fibre inclination angle increases, the pullout response of a hooked-end fibre becomes less influenced by the matrix strength and increasingly more influenced by the mechanical properties provided by the straighten of the fibre with respect with load direction. Another example is whenever the mechanical anchorage of the fibre is not fully mobilised, i.e if the embedment is less than the length of the fiber mechanical anchorage (not larger than 5 mm in the majority of the fibers), the orientation of the fibre has a minor significance on the pullout behaviour (Robins *et al.*, 2002).

(a)   (b)
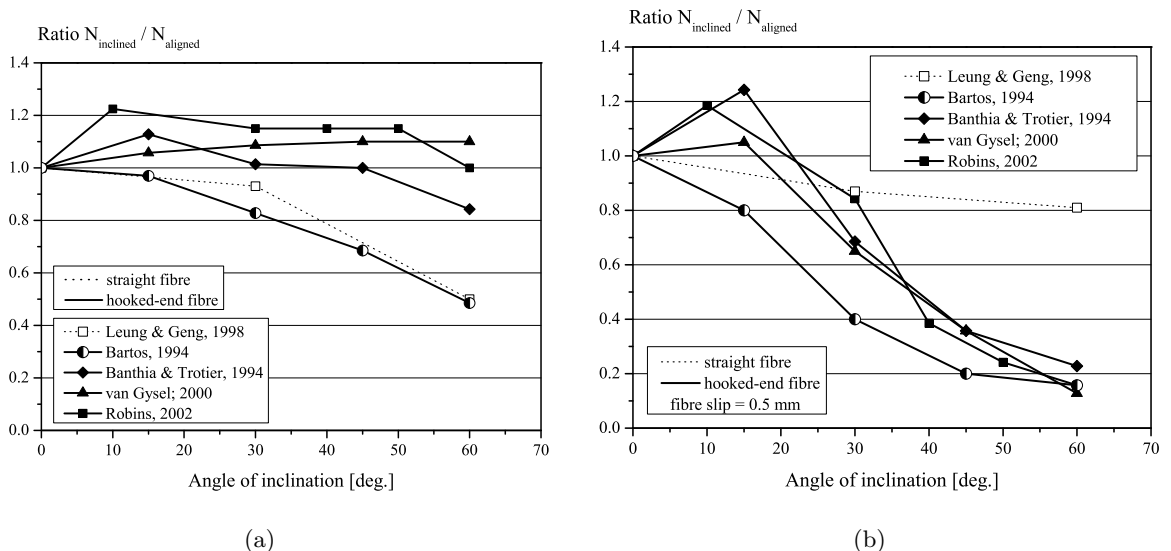
Figure 1.6: Relationship between normalized pullout force of an inclined fibre and the angle of fibre inclination: (a) for fibre slips at which the maximum pullout was achieved, (b) at a constant fibre slip of 0.5 mm.

In Figure 1.7 are depicted the pullout relationships for hooked-end fibres with different inclination angles, the fibre ultimate tensile strength, UTS, is also indicated. The indicated peak loads remained far below the fibre UTS. However, fibres under inclination angles of 45° and 60° fractured below their ultimate tensile strength. This phenomenon was observed by several authors for hooked-end fibres (Banthia and Trottier, 1994; Gysel, 1999; Robins *et al.*, 2002) and corrugated fibres (Banthia and Trottier, 1994; Chanvillard and Aïtcin, 1996) for distinct fibre inclinations, and can be explained by the relatively high stress concentrations at the fibre bending point. According to Banthia and Trottier (1994), the additional shear stresses imposed on inclined fibres, at the point they exit the matrix, will favour the fibre intercrystal slippage within an atomic level point of view, causing a reduction on both the yield and ultimate strength of the material.
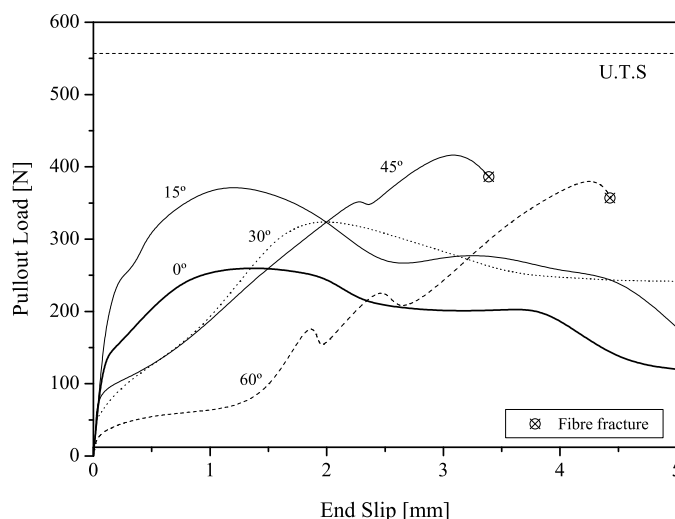
Figure 1.7: Pullout relationships for hooked-end fibre from a high strength matrix (85 MPa) at various inclination angles (Banthia and Trottier, 1994).

In conclusion, the peak load and toughness are, in general, maximized for inclination angles laying between 0° and 20°. Higher angles usually lead to a lower pullout load on the first phase of the pullout behaviour, which should not be neglected, since from the point of view of the fibre performance in the structure, this phase is an important one. However, depending on the fibre type, matrix strength, and other parameters, the maximum pullout load may increase with the fiber inclination up to an angle of about 45° (Naaman and Shah, 1976; Banthia and Trottier, 1994; Robins *et al.*, 2002).

Theoretically, the toughness should increase with the inclination angle, since inclined fibres undergo plastic bending of successive sections of the fibres during pullout. Moreover, as

bigger the inclination angle, as higher is the normal force applied to the fiber at the bend, increasing friction stresses at the debonded interface which contribute also to increase the work requirements to fully pullout a fiber. In spite of that, for deviation angles higher than 20°, the toughness decreases significantly, which may be justified by the fact that for higher inclination angles the fibre generally fractures in an earlier stage.

1.3.3   Influence of embedment length

The pullout response is be expected to improved from the increase of the embedment length, since a larger fibre surface area is in contact with the cement matrix, safeguarding that both the fibre geometry and matrix quality are the same. This holds mainly true for straight fibres (Li and Stang, 1997). However, for some deformed fibres, e.g. hooked-end steel fibres, the maximum pullout load may be higher for a smaller embedment length (Robins *et al.*, 2002; Grünewald, 2004). This may be justified by the fact that in a hooked-end fibre the mechanical component of the bond, corresponding to the plastic deformation of the fibre hook, is more significant than the adhesion component. This was experimentally observed by Naaman and Najm (1991). In addition, Robins *et al.* (2002) observed on the pullout behaviour of hooked-end fibers that a fiber with a embedded length smaller than 5 mm, which is the length of the hook for a 30 and 60 mm fiber length, the mobilisation of the potential fiber pullout strength cannot fully occur. This results on a significantly turn down of both the maximum pullout load and toughness. On the other hand, for fibres with mechanical deformations along the fiber length, the embedded length improves significantly both the maximum pullout load and toughness. This is due to the fact that as higher is the fiber embedded length, more number of mechanical deformations are mobilised. This was observed by Chanvillard (1993) for corrugated fibres and by Groth (2000) for indented straight steel fibre.

1.3.4   Influence of the matrix properties

The mechanical quality of the matrix, which can be evaluated from its compressive strength, depends upon several factors, such as: water/cement ratio or water/binder ratio, presence of fine filler materials, type and quality of the cement, maximum dimension and type of aggregates, etc. Since the fibre-matrix bond is influenced by the properties of interfacial transition zone, the matrix quality plays an important role on the fibre pullout behaviour.

Figure 1.1(b) shows that, the water/binder ratio (w/b) influences the density and micro-hardness of the fiber concrete interfacial transition zone (Wei *et al.*, 1986), therefore influencing the pullout behaviour of fibres. Several authors have reported improvement of the maximum pullout load with the decrease of the w/b ratio for both hooked-end fibres (Banthia and Trot-

tier, 1994; Groth, 2000) and crimped fibres (Banthia and Trottier, 1994; Chanvillard and Aïtcin, 1996). On the other hand, the toughness generally decreases with the decrease of w/b ratio, which can be justified by the brittleness increment of the fiber-matrix interface with the increase of the matrix strength (Banthia and Trottier, 1994). Moreover, within a high strength matrix deformed fibers have higher probability of fracture at an early stage of pullout, and consequently, the fiber pullout toughness decreases significantly.

Several matrix modifications have been examined as a possible way of improving the bond slip of fibers in a cementitious matrix. This include the addition of fine filler materials, e.g. silica fume, fly ash, limestone filler, metakaolin or polymer additions. This additions are often used with several purposes, such as increasing the matrix strength, concrete durability or even its workability. The average grain size of these particles is considerably smaller than the ones of the cement, therefore the empty spaces between the cement particles and the fibre, in the interface zone, can be efficiently filled leading to a higher packing density of the interface. Beyond what has been stated, some additions (e.g. silica fume, fly ash, metakaoline) exhibit a pozzolanic reaction. This reaction improves the strength and quality of the interfacial transition zone, ITZ, since during this reaction the calcium-hydroxide crystals are partly replaced by other stronger crystals (Bentur and Mindess, 1990). The addition of polymers is another technique to dense of the ITZ, i.e. higher packing density. Also, the use of silica fume may also increase the concrete shrinkage 2-3 times when compared to a concrete without it. This will produce a higher clamping pressure on the fibre which could lead to an improvement of the debonding and frictional pullout resistance (Li and Stang, 1997). Robins *et al.* (2002) observed that the addition of silica fume (10 % in vol.) improved both the maximum pullout force and toughness of hooked-end fibres up to approximately 50 %. Guererro and Naaman (2000) also reported an improvement of the maximum pullout force in 50 % with the addition of fly ash (20 % in vol.).

The presence of short fibres, either steel or polypropylene, in the pullout medium can improve the maximum pullout load of hooked-end steel fibres. In the first phase of the pullout, when microcracking starts to develop, short fibres bridge those microcracks mitigating their propagation, which will increase the energy, i.e. pullout force, needed to deform the curvatures of the hook (Markovic, 2006), see Figure 1.2. In Figure 1.8 is depicted the improvement on the pullout behaviour of hooked-end steel fibres on concretes containing short steel fibres. An increase of about 40 % was observed in the maximum pullout load with an addition of 2 vol. % of short steel fibres.
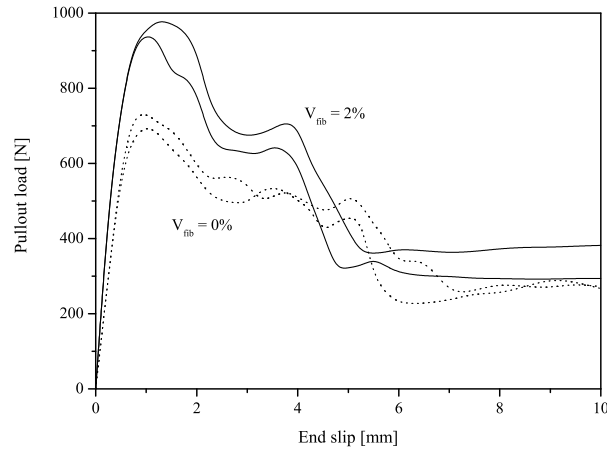
Figure 1.8: Influence of short fibres in the pullout medium on the pullout behaviour of hook ended steel fibres (Markovic, 2006).

1.4   Models for predicting the pullout of fibres

One of the first pullout models was proposed by Lawrence (1972), which relates the shear stress distribution along the fiber to the elastic properties of the matrix and fibre. In addition, the solution was extended for the case of a partially debonded fiber, assuming constant frictional shear stress along the failed interface. Laws *et al.* (1972) applied the analytical model developed by Lawrence (1972) to the study of glass fibre reinforced cement composites failure.

Based on the Lawrence (1972) model, were developed for the fibre pullout problem (Gopalaratnam and Shah (1987), Lim *et al.* (1987), Wang *et al.* (1988), Stang *et al.* (1990), Naaman *et al.* (1991b), Leung and Li (1992)). These models are one-dimensional, with many common features. They include a shear-lag model for the fibre embedded length in full bond conditions, gradual debonding, and frictional sliding for the fibre embedded length where debonding is occurring. In their study, Wang *et al.* (1988) considered only frictional bond. Lim *et al.* (1987) and Naaman *et al.* (1991b) deduced the force distributions in the fibre and matrix. Leung and Li (1992) developed a two-way debonding theory, in which the debonding can progress from both fibre ends. In other models, it is assumed that the interfacial shear bond stresses are elastic to start with, but gradually debonding takes place at the interface and the stress transfer is shifted to a frictional one (Gopalaratnam and Shah, 1987). To describe the debonding criterion, basically two different approaches can be used: a strength-based criterion (or stress-based) and a fracture-based criterion. In the strength based models, it is assumed that debonding initiates when the interfacial shear stress exceeds the shear strength. For the fracture-based models, on the other hand, the debonding zone is treated as an interfacial crack. The conditions for the debonding propagation are considered, in terms of fracture parameters of the interface and an assumption that, to drive the debonded zone forward, adequate energy must be supplied; see

Stang et al. (1990) and Li and Stang (1997).

Nevertheless, the models for straight fibers are of limited use for hooked-end fibers, since the behaviour of hooked-end fibers is dominated by the mechanical anchorage. In hooked-end fibers the bond strength may be meaningless when compared to the parcel provided by the mechanical bond (Naaman and Najm, 1991; Robins *et al.*, 2002).

Alwan *et al.* (1999) developed an analytical model to predict the mechanical contribution of anchorage forces in hooked end steel fibres. This model is based on the concept of frictional pulley along with two plastic hinges. The mechanical bond provided by the hook is considered as a function of the work needed to straighten the fibre during pullout. To predict the full pullout response is needed a two-step process corresponding to the contribution of the two hinges, and then one hinge superposition of the frictional and mechanical components. To overcome this two step process Sujivorakul *et al.* (2000) developed an analytical model where both the frictional bond and mechanical anchorage components are combined in the solution. This model is an extension of the smooth fibre pullout model previously developed by Naaman *et al.* (1991b), where the adoption of a nonlinear spring component in the latter model intends to simulate the mechanical anchorage reinforcement mechanism.

Bentur and Mindess (1990) point out the importance of proper evaluation of the pullout behaviour, which should not be based on the determination of a limited number of numerical parameters (e.g. maximum pull-out load, embedment length and fibre cross-sectional geometry), but rather it should include analysis of the entire curves obtained during such tests. The problems of correctly interpreting fibre pull-out tests can partly explain the huge differences in the quoted values of the interfacial shear bond strength, which in the literature range from 0.5 up to 9 MPa, while the interfacial shear friction ranges from 0.5 to 5 MPa; see Beaumont and Aleska (1978), Bartos (1981), Bentur and Mindess (1990), Gopalaratnam and Shah (1987), Li and Stang (1997), Groth (2000) and Grünewald (2004). In general, the high bond strength values were evaluated from the peak-load values.

1.4.1 Perfectly bonded/debonded smooth fibre model (Stang *et al.*, 1990)

For the current steel fiber dimensions, the pullout problem is mostly governed by frictional pullout, where the fibre slip is of the mm magnitude. On the other hand, the slips that are due to the rupture of the chemical bond can often be neglected, inasmuch as the chemical bond only is mobilised over a very small slip (only a few micrometers). This has lead to the development of perfectly bonded/debonded models.

Amongst these models, the stress-based approach and the fracture mechanics approach are the most referred, therefore they are discussed in the present work. Both approaches have

the aim of checking if the fibre is still perfectly bonded, or has already been debonded. In the stress-based approach the fibre is debonds from the matrix once the shear stress reaches a critical value τ_{crit} in a certain point. On the other hand, in the fracture mechanics approach, an energy criterion for debonding is defined taking into account the chemical bond Γ of the interfacial transition zone, ITZ.
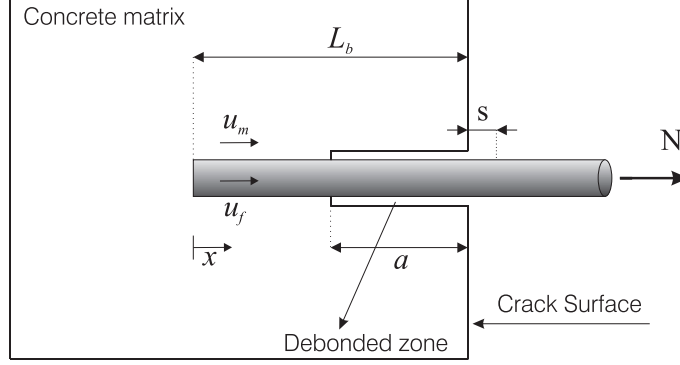
Figure 1.9: Pullout of a single fibre perfectly bonded/debonded.

Stress based approach

Consider the plane model shown in Figure 1.9, where a single fibre is embedded in a matrix with an embedment length L_b. The fiber is assumed to have constant cross sectional area, A_f, and a constant Young's modulus, E_f. The displacement of the fibre in the axial direction, u_f, is assumed to be constant over fibre cross section, and can be calculated when a fibre has a debonded length a, applying equation (1.8). A detailed description of the constitutive relations, as well as the equilibrium equations can be found in Stang *et al.* (1990).

$$u_f(x) = \begin{cases} \dfrac{N - t_f \cdot a}{w \cdot E_f A_f} \cdot \dfrac{\cosh(w \cdot x)}{\sinh[w(L_b - a)]} & 0 \leq x \leq L_b - a \\[2em] \dfrac{N - t_{fr} \cdot a}{w \cdot E_f A_f} \cdot \coth\left[w\left(L_b - a\right)\right] - \dfrac{N - t_f \cdot L_b}{E_f A_f}\left(L_b - a\right) \\[1.5em] \quad - \dfrac{t_f}{2E_f A_f}\left(L_b - a\right)^2 + \dfrac{N - t_f \cdot L_b}{E_f A_f} \cdot x + \dfrac{t_f}{2E_f A_f} \cdot x^2 & L_b - a \leq x \leq L_b \end{cases}$$

$$(1.8)$$

where t_f, d_f and N are, respectively, the frictional shear force per unit length along the debonded interface, the fibre diameter and pullout force that is acting on the fibre; x is the

distance from the embedded fibre end to the point where displacement u_f is considered. In equation 1.8 w and k are defined by:

$$w = \sqrt{\frac{k}{E_f A_f}} \qquad [1/mm] \tag{1.9}$$

and

$$k = \frac{t(x)}{u_m(x)} \qquad [N/mm^2] \tag{1.10}$$

where $t(x)$ and $u_m(x)$ are the shear force per unit length at a distance x from the fibre end, and the displacement of the matrix at a distance x from the fibre end. Remark that, in the aforementioned equations, the length unit is given in [mm], whereas the force unit is in [N].

Equation (1.8) is the general equation of the perfectly bonded - debonded model for obtaining the fibre displacement at any fibre point. However, the total fibre displacement at the crack surface, s, is of special interest (see Figure 1.9). To obtain this displacement, it must be substituted $x = L$ in Equation (1.8). Moreover, to solve this equation, the length of the debonded zone, a, must be defined. For this purpose a stress criterion is defined for debonding, based on the assumption that debonding only occurs when the shear stress at the fibre / matrix interface reaches a critical value. This criterion is expressed in terms of force per length, and assuming that debonding starts once the force per length, t, reaches the critical force per unit length around the fibre, t_{crit}, which is a constant value. It is also assumed that the fictional shear force, t_f, is expressed in terms of t_{crit}. For a certain debonded length a, the shear stress has a maximal value at the place where the debonded zone ends, therefore the condition for debonding can be written as:

$$N = t_f \cdot a + \frac{t_{crit}}{w} \tanh\left[w\left(L_b - a\right)\right] \tag{1.11}$$

This model can simulate the basic pullout behaviour of a aligned straight fibre, since the load - displacement relationship during debonding, $N - s$, can be obtained numerically, by substituting $x = L_b$ in Equation 1.8 and eliminating the length of debonded zone a from Equations (1.8) and (1.11), i.e., $a = 0$.

Fracture mechanics approach

The fracture mechanics is based on an energy approach, which considers that the propagation of the debonding zone requires a certain energy, which is characteristic for the bond between

the fiber and the matrix. In this model (Stang *et al.*, 1990; Li and Stang, 1997), it is assumed that debonding takes place when the energy release rate reaches a critical value, which is related to the fracture work of the interface Γ. Adopting a certain displacement continuity assumption as approximation for the shear lag strain energy, the work done by friction and a constitutive relation for the matrix shear lag, the stress in the fibre can be established in function of the total pullout displacement relative to the crack surface, s, (see Equation 1.12).

$$\sigma_f = \frac{N}{A_f} = 2\sqrt{\left(\frac{t_f}{\pi \cdot d_f}s + \Gamma\right) \cdot \frac{2E_f\left(1+\eta\right)}{d_f}} \tag{1.12}$$

with,

$$\eta = \frac{E_f \cdot V_f}{E_m\left(1 - V_f\right)} \tag{1.13}$$

where σ_f $[N/mm^2]$ and Γ $[N/mm]$ are, respectively, the axial stress in the fibre at the place of the crack surface and the bond energy of the interface transition zone, ITZ, per unit bonded interface area; V_f and E_m $[N/mm^2]$ are the volume fraction of fibres and the Young modulus of the matrix.

Once debonding has just finished, the maximum pullout stress, σ_{max}, is attained. σ_{max} and the corresponding pullout displacement, s_{peak}, when debonding has just completed can be determined by:

$$\sigma_{max} = \frac{t_f \cdot L_b\left(1+\eta\right)}{A_f} + \sqrt{\frac{8\Gamma \cdot E_f\left(1+\eta\right)}{d_f}} \tag{1.14}$$

$$s_{peak} = \frac{t_f \cdot L_b^2\left(1+\eta\right)}{2E_f \cdot A_f} + \frac{L_b}{E_f}\sqrt{\frac{8\Gamma \cdot E_f\left(1+\eta\right)}{d_f}} \tag{1.15}$$

It should be noted that, Equation 1.12 is only valid if the fibre has not yet fully debonded from the matrix. After the fiber has fully debonded, it starts to slip out. Li and Stang (1997) suggest Equation 1.16 for determining the frictional shear stress in the fibre for this stage.

$$\tau = \tau_{crit} + \Delta\tau(s) = \tau_{crit} + a_1 \cdot s + a_2 \cdot s^2 \tag{1.16}$$

where τ_{crit} is the ultimate frictional stress for the interface between concrete and fibre before the

fibre starts to slip. The coefficients a_1 and a_2 are empirical constants to take into account the dependency of frictional shear force per unit length on the pullout length. The latter constants can be obtained from direct pullout tests of single fibres. In Li and Stang (1997) can also be found the values of the parameters of Equation 1.16 for different fibres types and concrete mix compositions.

Moreover, there is evidence that τ_{crit} may be sensitive to lateral pressure, Leung and Geng (1995) found that τ_{crit} obeys a Coulomb type friction law with coefficient of friction μ:

$$\tau_{crit} = \tau'_{crit} + \mu \sigma_n^{shr} + \mu \sigma_n^{ext} \tag{1.17}$$

where τ'_{crit} is the friction of the contact surfaces without any residual normal stress due to shrinkage (σ_n^{shr}) or external normal stress (σ_n^{ext}).

1.4.2   Smooth fibre with an end anchorage model (Sujivorakul *et al.*, 2000)

In Figure 1.10 is schematically represented the pullout model of a smooth fibre with an end anchorage embedded in a matrix. The fibre is decomposed in two parcels, the one corresponding to the smooth part of the fibre and the other corresponding to the anchorage itself. The first one corresponding to the smooth part, is modeled by a fibre that has a cross sectional area A_{f1}, a elastic modulus E_{f1} and is embedded over a length L_b in a matrix with a cross section A_m and elastic modulus E_m. On the other hand, the mechanical anchorage is modeled by a spring which connects the fibre to a similar fictitious fibre along its axis (see Figure 1.10). The fictitious fibre is assumed to have a cross sectional area $A_{f2} = A_{f1}$, a elastic modulus $E_{f2} = E_m$ and length L_{b2}. The fictitious fibre is coupled to the spring to overlap some limitations that would occur if the model had only a nonlinear spring, since the introduction of a fictitious fibre allows to model the movement of the matrix at the embedded end of the fibre, which could not be simulated with the spring exclusively.
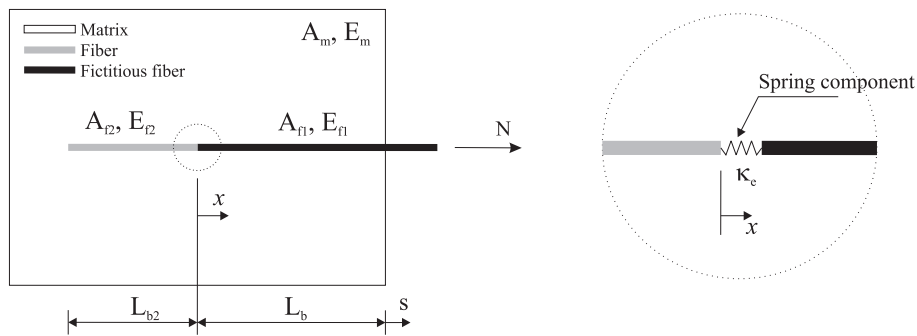
Figure 1.10: Representative pullout model for a smooth fibre with an end anchorage.

To account with the interfacial bond, a bond shear stress versus slip relationship between the fiber and matrix is used. Sujivorakul *et al.* (2000) assumed a linear elastic relation until the bond strength, τ_{crit}, of the interface is attained. Afterwards τ_{crit} is reached at the interface, the shear stress drops to a constant frictional bond, τ_f. On the other hand, the bond shear stress versus slip relation of the fictitious fiber is linear without debonding. In Figure 1.11 are depicted the adopted bond stress versus slip relationships. The influence of the mechanical anchorage is modeled from the stiffness attributed to the spring, κ_e, see Figure 1.10, which expresses the relationship between the force and the displacements at the embedded end of the fiber.
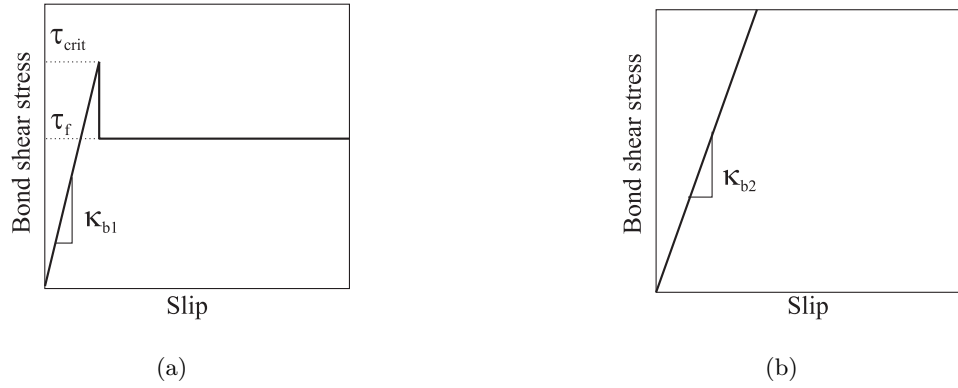
Figure 1.11: Assumed bond shear stress versus slip relationships: (a) Fiber, (b) Fictitious fiber.

The derivation of the mathematical equations of the model are presented elsewhere (Sujivorakul *et al.*, 2000). The complete pullout load versus slip curve is divided the curve in three distinct regions: precritical region, partial debonding region and pullout region. Moreover, for every region an iterative procedure is necessary to obtain the correct value of κ_e that satisfies the boundary conditions.

Precritical region

In this phase, the fiber will not start debonding until the bond shear stress (which is maximum at the crack tip, i.e. $x = L_b$) reaches the shear bond stress τ_{crit}. The critical load, N_{crit}, can be computed when the shear stress is equal to τ_{crit} at $x = L_b$ by:

$$N_{crit} = \frac{\tau_{crit}\psi}{\lambda_1 \left(Ae^{\lambda_1 L_b} - Be^{-\lambda_1 L_b}\right)} \tag{1.18}$$

with,

$$
\left.\begin{array}{l}
\lambda_i = \sqrt{K_i Q_i} \\[2em]
K_i = \dfrac{\psi \kappa_{bi}}{A_m E_m} \\[2em]
Q_i = 1 + \dfrac{A_m E_m}{A_{fi} E_{fi}}
\end{array}\right\} \quad i = 1,2
\tag{1.19}
$$

where ψ, κ_{b1} and κ_{b2} are the fiber perimeter, the bond modulus of the real fiber and fictitious fiber, respectively. The constant κ_{b2} can be assumed from knowing the shear strength of the matrix, whereas κ_{b1} and the other parameters of the bond shear stress relationship can be determined from the inverse problem between the pullout test and the analytical solution on a smooth fiber (Naaman *et al.*, 1991b). The unknown constants A and B are determined from the boundary conditions of the problem.

For a point correspondent to a load $N \leq N_{crit}$, the displacement at the crack tip s can be determined with Equation 1.20. The critical point (N_{crit}, s_{crit}) has to be determined by an iterative procedure, a flowchart for determining this point and others contained in this region is given by Sujivorakul *et al.* (2000).

$$
s = \left(\frac{N}{A_m E_m}\right) \left(\frac{Q_1}{\lambda_1}\right) \left[A \left(e^{\lambda_1 L_b} - 1 \right) + B \left(1 - e^{-\lambda_1 L_b} \right) \right]
\tag{1.20}
$$

Partial debonded region

In this region, afterwards the N_{crit} is reached, the fiber will have two interfacial zones, a bonding zone and debonding zone with a length u. The length of the debonded zone will grow with the displacement at the crack tip s until $u = L_b$. Over the length of the debonded zone the interfacial shear stress is constant and equal to τ_f. The external force N is given by Equation 1.21 and is the sum of the force developed on the bonded zone, N_b, and the force due to frictional resistance on the debonded zone N_d.

$$
N = N_b + N_d = \frac{\tau_{crit}\, \psi}{\lambda_1 \left(A\, e^{\lambda_1 (L_b - u)} - B\, e^{-\lambda_1 (L_b - u)} \right)} + \tau_f\, \psi\, u
\tag{1.21}
$$

In turn, while $u \leq L_b$, the displacement of the fiber at the crack tip δ can be computed by:

$$s = \frac{N\,(Q_1 - 1)\,u}{A_m\,E_m} - \frac{u^2\,\tau_f\,\psi}{2A_m\,E_m}\,(Q_1 - 2) - \frac{u\,L_b\,\tau_f\,\psi}{A_m\,E_m}\left(\frac{n}{A_m\,E_m}\right)\left(\frac{Q_1}{\lambda_1}\right)$$

$$\left[A\left(e^{\lambda_1(L_b - u)} - 1\right) + B\left(1 - e^{-\lambda_1\,(L_b - u)}\right)\right] \tag{1.22}$$

Pullout region

When the debonded zone of the fiber reaches $u = L_b$, a dynamic mechanism of pullout will develop with rigid body displacement of the real fiber, which will be equal to the pullout slip, s. For this region, from the static equilibrium, the pullout load can be determined by:

$$N = \kappa_e s_k + \tau_f\,(s)\,\cdot\psi\,(L_b - s) \tag{1.23}$$

where s_k and $\tau_f(s)$ are the displacement at the embedded end and the frictional stress for the slip s, respectively. Since the fiber undergoes some elongation, the displacement at the embedded end s_k is smaller than the displacement at the fibre tip s. However, for the case of large displacements, the elastic elongation of the fiber is very small compared to the rigid body displacement, so that it can be assumed for large displacements that $s_k = s$. The displacement s_k can be determined by:

$$s_k = \frac{A_{f1}E_{f1}}{(A_{f1}E_{f1} + \kappa_e(L_b - s))}\cdot\left[s - \frac{\tau_f(s)\cdot\psi(L_b - s)^2}{2A_{f1}E_{f1}}\right] \tag{1.24}$$

In turn, the frictional stress for the slip s can be determined with the following equation:

$$\tau_f(s) = \tau_f\cdot\frac{e^{-(s-s_0)^\eta} - \xi e^{-(L_b)^\eta}}{1 - \xi e^{-(L_b - s + s_0)}}\cdot\frac{\left(1 - exp\left(\dfrac{-2\nu_f\cdot\mu(L_b - s + s_0)}{E_f r_f\left(\dfrac{1 + \nu_m}{E_m} + \dfrac{1 - \nu_f}{E_f}\right)}\right)\right)}{\left(1 - exp\left(\dfrac{-2\nu_f\cdot L_b}{E_f r_f\left(\dfrac{1 + \nu_m}{E_m} + \dfrac{1 - \nu_f}{E_f}\right)}\right)\right)} \tag{1.25}$$

that was proposed by Naaman et $al.$ (1991b), since for large slips the assumption of constant friction is not valid due to the deterioration of the τ_f when slip increases. In equation (1.25),

s_0 is the end slip at the full debonding stage, which can be determined by substituting $u = L_b$ in Equation 1.22. The parameter ξ is the damage coefficient related to the rate at which the frictional shear stresses deteriorates, η is a factor that simulates the steepness of the descending branch of the pullout curve, and ν_m and ν_{f1} are the Poisson coefficients for the matrix and the real fiber, respectively.

1.5   Test configuration

The test configuration should simulate the fibre located in the composite under a realistic stress situation, avoiding unrealistic stress concentrations around the fibres. Moreover, a realistic variation of the fibre orientation, embedded length and an accurate measurement of the fibre pullout should be possible. Several tests assemblies have been used for carrying out pullout tests. Nevertheless, up to date a standard method has not yet been acknowledged. It is well described in literature that test set-up and loading conditions can strongly affect the results. The tests results are particulary sensitive to the occurrence of stresses normal to the loading direction. These can be induced by the test set-up configuration, as well as by matrix shrinkage during its curing process. Therefore, the curing conditions and other preparation methods must be maintained constant in order to mitigate the scatter of the results between different tests.

Two major groups of pullout tests configuration arise from experimental research carried out in the past. The pullout tests can be performed on both single-sided specimens (see Figure 1.12(a) to 1.12(c)) and double-sided specimens (see Figure 1.12(d) and 1.12(e)), using both a single fibre or an array of fibres. Single-sided test profiles have been carried out with the configuration as in Figure 1.12(a), by e.g. Grünewald (2004); Markovic (2006). The test set-up as depicted in Figure 1.12(b) has been used by e.g. Naaman and Najm (1991); Groth (2000), whereas the configuration represented in Figure 1.12(c) has been used by e.g. Li and Chan (1994). On the other hand, double-sided test specimens were also used by several authors to access the fibre pullout behaviour (Naaman and Shah, 1976; Chanvillard, 1993; Banthia and Trottier, 1994; Ouyang *et al.*, 1994; Robins *et al.*, 2002).

Both in the case of a single-sided or double-sided specimen configurations some back points can be noticed to each type configuration and several aspects should be paid in attention. For the single-sided specimen, the fibre length that gets out of the matrix block must have the necessary free length to be fixed at the test machine grip, in such a way that the slip between the fibre and the grip can be neglected. Moreover, in case that a steel ring at the upper side of the specimen is used as a support (see Figure 1.12(b)), lateral confinement of the fibre by compressive stresses could exist depending on the sample dimensions. This stress field can unrealistically improve the pullout behaviour of the fibre due to the lateral confinement.
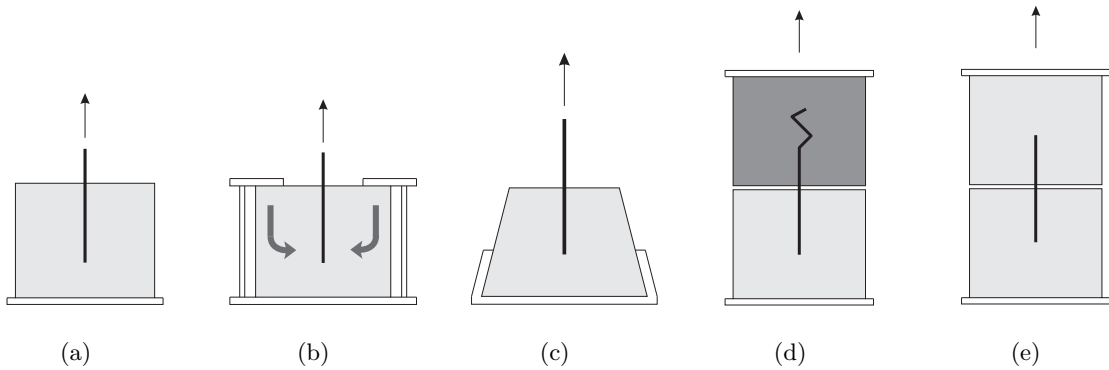
Figure 1.12: Examples of pullout test configurations: (a) to (c) single-sided specimen; (d) and (e) double-sided specimens

In respect to the double-sided specimen, care must be taken to ensure that pullout only occurs at one of the specimen two halves. This can be achieved, by example, applying an additional mechanical anchorage on the fibre end at one of the specimens halves (see Figure 1.12(d)), or with using a matrix strength at one of the halves considerably higher than at the other half, or even taking a higher embedment length on one of the specimens halves (see Figure 1.12(d)). However, in spite of all of these measures, it is highly questioned if the pullout really occurs exclusively on one of the halves. On the other hand, if the fibre is placed perfectly centered in the specimen, the global behaviour would be symmetric, since equal slips would be observed in both specimen halves (Figure 1.12(e)), although this being highly improbable to happen due to lack of sufficient accuracy to exactly place the fibre as well as on assuring symmetry for the material properties. In such case, it is highly probable that the pullout responses would depend on displacements that are mixed from each side during the initial part of the curve, resulting in a more difficult task to interpret the results.

In conclusion, from a conceptual point of view, these assemblies differ in the way of extracting the fibre from the matrix, of maintaining the sample at the time of the test and to position the fibre at the time of manufacture. However, in all the cases the goal of these assemblies is to measure the force necessary to pullout or fracture the fibre.

CHAPTER 2

Experimental results

2.1   Scope of tested parameters

The main scope of this research project is to access the pullout bond-slip mechanisms on a steel fibre reinforced self-compacting concrete medium, SFRSCC. These matrices are rather innovative, since for attaining self-compactibility they have to fulfill high demands with regard to filling and passing ability, as well as segregation resistance. In order to accomplish these requirements, it should be used high percentage of fine materials, low water/binder-ratios, technological advanced admixtures, and considerable high amounts of cement and fine additions. In fiber reinforced cement composite, the interface between fiber and cement paste is the weak link of its micro-structure. Therefore, study of the interfacial behaviour is important for understanding the mechanical behaviour of such composites.

The pullout tests presented here may be divided into two main groups, according to the type of fibres used: hooked and smooth. The benefits of the fibers mechanically deformed (e.g. hook-ended), when compared with a smooth fibre, on the peak pullout load and pullout energy are well documented. In spite of that, in the present work smooth fibres were tested, with the main purpose of isolating the adherence bond from the mechanical bond provided by the hook. This makes it possible the separate assessment of the influence of the various mechanisms of bond. Furthermore it allows to develop rational analytical models to describe bond in fiber reinforced cement-based composites, e.g. SFRSCC. Within these two main groups it was assessed the influence on the pullout response of the fiber embedment length and fiber orientation. In all performed tests only DRAMIX® RC-80/60-BN hook-ended steel fibers were used. The adopted fiber had a length (l_f) of 60 mm, a 0.75 mm diameter (d_f), an aspect ratio (l_f/d_f) of 80 and a yield stress of 1100 MPa (Dramix, 1998). In order to perform the smooth fibre tests, the end hook of the RC-80/60-BN fibre was cut with a pliers.

Code names were given to the tests series, which consist on alphanumeric characters separated by underscore. The first character indicates the fiber type (S - smooth; H - hooked), the second string indicates the embedded length in mm (for instance, lb10 represents a fiber embedded length of 10 mm) and finally the last numeral indicates the fibre inclination angle in degrees with the fiber pullout force orientation. The complete overview of all the fibre pullout tests performed, with reference to their type, aspect ratio, embedded length (l_b) and inclination angle, is given in Table 2.1.

Table 2.1: Overview of the performed pullout tests.

Series	Fibre type	l_b [mm]	Angle [º]	N. Specimens
S_lb10_0			0	3
S_lb10_30		10	30	3
S_lb10_60			60	3
S_lb20_0			0	3
S_lb20_30	Smooth	20	30	3
S_lb20_60			60	3
S_lb30_0			0	3
S_lb30_30		30	30	3
S_lb30_60			60	3
H_lb10_0			0	6
H_lb10_30		10	30	6
H_lb10_60			60	6
H_lb20_0			0	6
H_lb20_30	Hooked	20	30	6
H_lb20_60			60	6
H_lb30_0			0	6
H_lb30_30		30	30	6
H_lb30_60			60	6

2.2 Concrete mixture and test specimens

The materials used in the composition of the steel fiber reinforced self-compacting concrete, SFRSCC, were: cement (C) CEM I 42.5R, limestone filler (LF), superplasticizer (SP) of third generation based on polycarboxilates (Glenium® 77SCC), water (W), three types of aggregates (fine river sand (FS), coarse river sand (CS) and crushed granite 5-12 mm (CA)) and DRAMIX® RC-80/60-BN hook-ended steel fibers.

The method used for defining the composition of the SFRSCC, the mixing procedure and other properties of the SFRSCC in the fresh state can be found elsewhere (Pereira *et al.*, 2004;

Cunha *et al.*, 2006). Table 2.2 includes the composition that has best fitted self-compacting requirements for the adopted fiber content, (Cf). Remark that, in Table 2.2, WS is the water necessary to saturate the aggregates and W/C is the ratio water/cement. The parcel WS was not used to compute the ratio W/C, on the other hand to compute the latter ratio was considered the water parcel from the superplasticizer.

Table 2.2: Final composition for 1 m^3 of SFRSCC.

Cf (kg)	Paste/Total volume (%)	Cement (kg)	LF (kg)	Water (dm^3)	WS (dm^3)	SP (dm^3)	FS (kg)	CS (kg)	CA (kg)	W/C
30	0.34	359.4	312.2	96.9	64.7	6.9	108.2	709.4	665.2	0.29

The pullout tests on single steel fibers were performed using cylindrical concrete specimens. The diameter and height of each specimen was 80 mm. In order to produce the specimens, a special mould was designed, able to accommodate 87 fibers fixed at its bottom (see Figure 2.2). This device was used to cast 87 pullout specimens simultaneously, allowing a correct placement of the fiber and keeping the desired embedded length and inclination angle. After casting, the concrete slab was cured at a temperature of 20ºC and a relative humidity of about 95 %. After 30 days, the concrete was demoulded, and cylindrical specimens containing each one single fiber were drilled out from the slab. The fiber pullout tests were performed at approximately 180 days. The compressive strength of the concrete was assessed by three cubic specimens with an edge length of 150 mm. The average value of the concrete compressive strength, at the testing age, was 83.4 MPa with a coefficient of variation of 0.9 %. Moreover, six single fibers were tested under direct tension in order to assess the fiber tensile strength. The average value of the fiber tensile strength was 1141 MPa with a coefficient of variation of 2.0 %.

2.3 Experimental set-up

The pullout tests were performed on a servo-hydraulic Lloyd LR30K machine with a capacity of 30 kN. The built-in load cell of the test machine, for the expected experimental load values, was not enough accurate. In order to acquire more precise recordings of the loads, a HBM S9 load cell with a capacity of 5 kN and accuracy class 0.05 was attached to the machine test frame.

The single-sided specimen is mounted in a steel frame, see Figure 2.2. This frame incorporates one steel plate attached to testing machine frame and a steel ring coupled to the first by three steel screws. The protruding end of the steel fibre is fastened to a standard "Lloyd" grip which allows a secure hold of the fibre. However due to the small fibre diameter, special
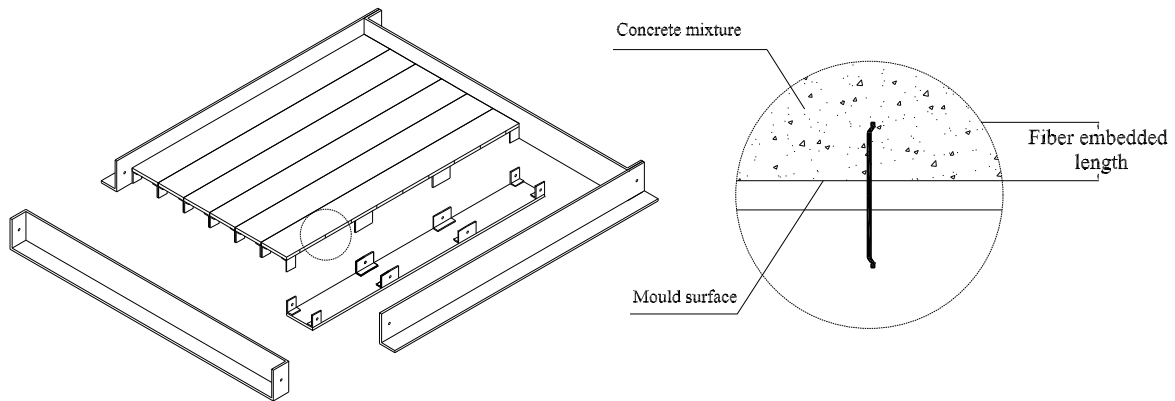
Figure 2.1: Device used to cast the pullout specimens.

attention was given in fastening the fibre, since deforming the fibre end could induce that the
fibre would break at the grip.
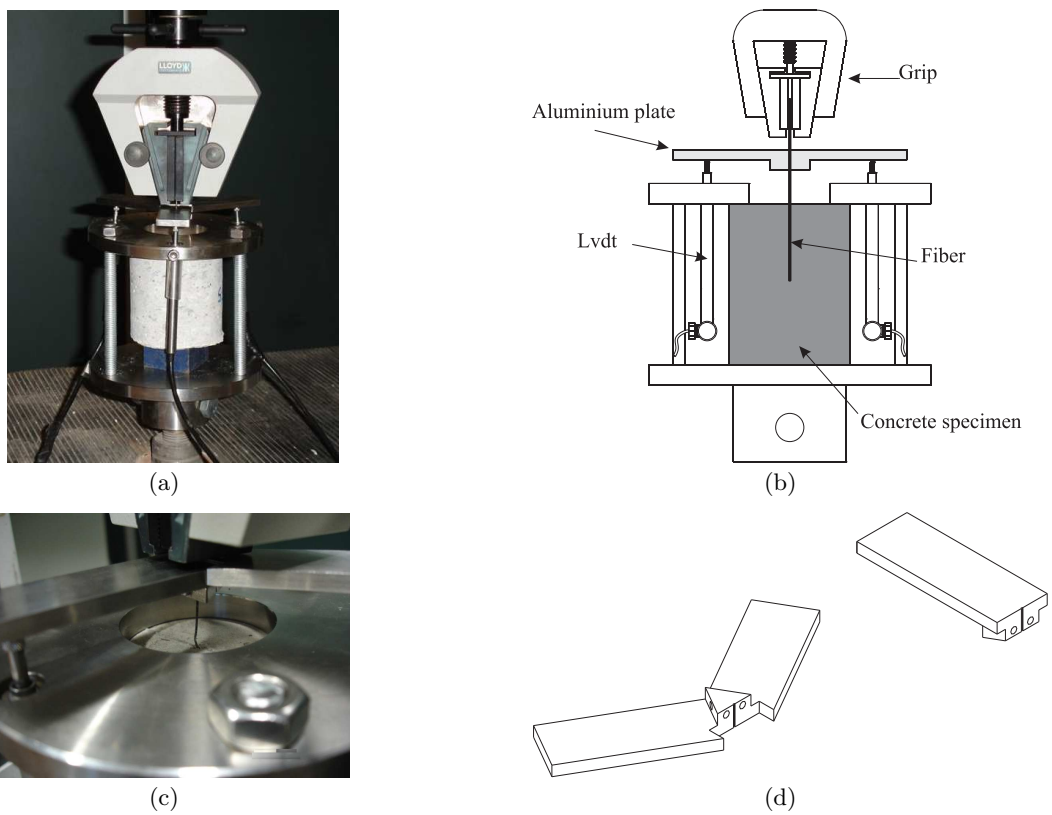
Figure 2.2: Configuration of the single fibre pullout test: (a), (b) general view, and (c), (d) detailed
view of the aluminium plate fixed to the fibre.

For the measurement of the fibre pullout slip, three LVDT's (linear stroke +/- 5mm) were used. In order to exclude measuring deformations of the testing rig and fibre slip at the grip, the LVDT's were fixed at the upper steel ring and touching the bottom surface of an aluminium plate fixed to the fibre. The plate was fixed to the fibre with two fine screws and was used as a support for this LVDT configuration (detail in Figure 2.2(c) and 2.2(d)). Since the three LVDT's were disposed around test specimen forming an angle of 120 degrees between consecutive LVDT's, the actual pullout slip of the fibre is the average of the three LVDT's readouts. The closed-loop displacement control was performed by the testing machine internal displacement transducer. This control procedure guaranties a stable response during the tests and ensures that a constant deformation rate is kept even for e.g. the case of catastrophic debonding during single fibre pullout, i.e it turns possible to obtain the pullout post-peak behaviour. In all pullout tests, it was used the same displacement rate of 10 μm/s.

For the adopted test setup, where a steel ring at the upper side of the specimen is used as a support (see Figure 2.2(b)), lateral confinement of the fibre by compressive stresses could exist depending on the sample dimensions. These stress concentrations can unrealistically improve the pullout behaviour of the fibre due to the lateral confinement. This was observed by Markovic (2006) for a cylindrical specimen with 65 mm diameter and 50 mm height. Taking into account this, a linear-elastic finite element simulation was used to select the steel ring hole and specimen dimensions, in order to avoid the development of arch action by the compressive stresses. With the adopted solution, a cylindrical specimen with 80 mm diameter and height, and a 60 mm diameter ring hole, no compressive stresses nearby the fibre were developed.

2.4 Pullout failure modes

The typical failure modes observed on the pullout tests are schematically represented as the projection on the longitudinal plane of the cylinder from which the fiber was pulled out, and are depicted in Figure 2.3. The totality of both hooked and smooth aligned fibers were completely pulled out (see Figure 2.3(a)). In the case of hooked fibers, after debonding of the fiber-matrix interface, the hooked was fully straightened. This failure is designated as *FM1*. The cross section striction at the end of the hook curvatures produced by the straightening of the hook is depicted in Figure 2.4. A similar failure mode, *FM2*, was observed for some inclined fibers, however in opposite to aligned fibers, spalling of the matrix at the fiber bending point was observed, Figure 2.3(b). Nevertheless, the most common failure mode observed during the pullout tests of inclined hooked fibers was fiber rupture, *FM3* (see Figure 2.3(c)). Another observed failure mode, *FM4* was by matrix spalling, which is depicted in Figure 2.3(d). In this case the fiber is almost fully pulled out of the concrete specimen, however, when the embedded

end of the fiber approaches the exit point of the concrete matrix it detaches a portion of concrete near the fiber bending point. This failure mode was only observed for a few fibers with an inclination angle of 60º and an embedded length of 10 mm. The pullout specimens where the conditions of premature fiber or matrix failure were observed, occurred exclusively for inclined fibers. Moreover, for a 30º inclination angle has occurred predominantly fiber rupture, whereas for an angle of 60º and lower embedded lengths could be found matrix failure. Similar finds were observed for hooked fibers pulled out from a high strength matrix by Banthia and Trottier (1994).
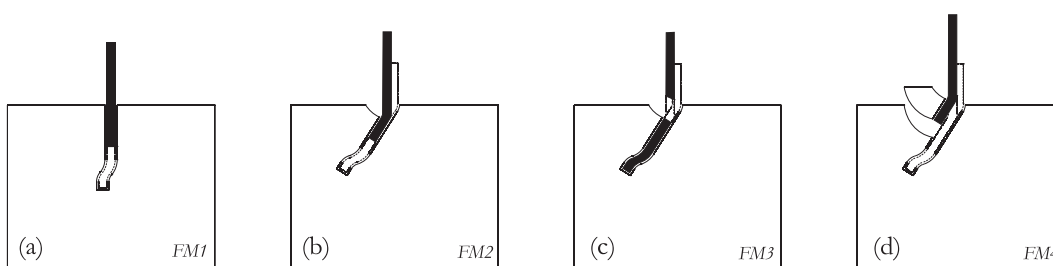
Figure 2.3: Typical failure modes observed during pullout tests.

In Table 2.3 are indicated the correspondent failure modes observed for each series. When more than one failure mode occurred for a specific series, the number of specimens corresponding to each failure type was indicated between round brackets. Due to technical problems, the series S_lb10_0 and S_lb10_30 could not be correctly tested, therefore they are not presented.

Table 2.3: Failure modes observed for eac series.

Smooth series	Failure mode	Hooked series	Failure mode
S_lb10_0	-	H_lb10_0	FM1
S_lb10_30	-	H_lb10_30	FM2(2); FM3(4)
S_lb10_60	FM4	H_lb10_60	FM3(5); FM4(1)
S_lb20_0	FM1	H_lb20_0	FM1
S_lb20_30	FM2	H_lb20_30	FM2(2); FM3(4)
S_lb20_60	FM2	H_lb20_60	FM3
S_lb30_0	FM1	H_lb30_0	FM1
S_lb30_30	FM2	H_lb30_30	FM3
S_lb30_60	FM2	H_lb30_60	FM3

The fibre rupture observed for hooked inclined fibers is a result of both a strong and compact concrete matrix, and a good fibre anchoring in it. Moreover, it was observed that the fiber rupture stresses for inclined fibers were smaller than the fiber tensile strength (1141 MPa).

The average value of the fiber rupture stress for a 30º inclination angle was about 865 MPa, whereas for a 60º angle this value was 736 MPa. This can be explained by the fact that the fiber is submitted to a mixed tensile-bending mode. The fiber rupture for lower stresses than the direct tensile stress is a result of the stress concentrations present in the bent part of the fibre. The strength capacity under composed bending is governed by an interaction diagram between the normal tensile force and the flexure moment. As the bending moment increases, the tensile force corresponding to the ultimate capacity envelope of a section subjected to composed bending must decrease. Moreover, as the inclination angle increases, the bending moment will increase resulting therefore in a decrease of the tensile rupture stress. From an atomic level point of view, the additional shear stresses imposed on the fibers at the matrix exit, favour the intercrystal slippage within the crystal system in steel, hence lowering both the yield and ultimate strength of the material (Banthia and Trottier, 1994).
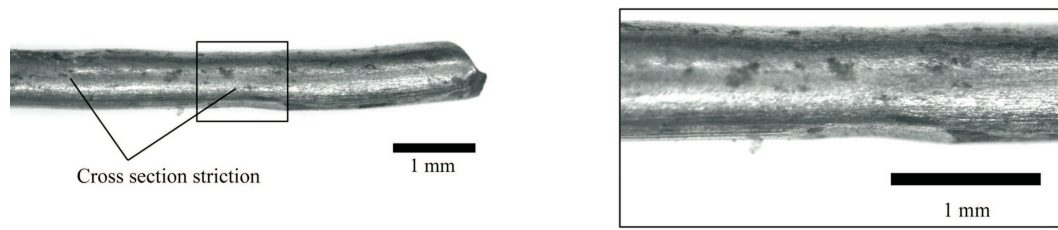
Figure 2.4: Cross section striction at the hooked-end.

2.5 Pullout-slip curves

In Figure 2.5 are depicted the average pullout load-slip curves for the tested series. The pullout curve for each single specimen can be found in Annex I.

In general, for both hooked and smooth aligned fibers analysed, the configuration of the pullout load-slip curve was similar, regardless the fiber embedded length but, as expected, the peak load and the dissipated energy increased with it (see Figures 2.5(a) and 2.5(b)). The vertical offset distance between curves can be regarded as the contribution of the embedded bond increment or decrement between curves. The pre-peak branch of these pullout-slip curves for both hooked and smooth fibers is made up of a linear and non-linear part . The first one is associated with the elastic bonding, whereas the non-linear part starts with the micro-cracking of the interface, corresponding to the debonding process. The non-linear part of the ascending branch is more pronounced in hooked fibers. The lost of stiffness associated to the pre-peak nonlinear branch is justified by the irrecoverable deformation component of the fiber and the

surround paste at the zone of the end hook, when this part of the fiber starts being straightened. On the other hand, for smooth fibers the non-linear part of the ascending branch has a relative small amplitude, since starts very close to the peak load. In smooth fibers, after the peak load is attained a sudden drop is observed, which corresponds to an abrupt increase of damage at the fiber-paste interface (unstable debond). Afterwards, fiber-paste friction is the commanding mechanism of the pullout behaviour. In this part of the post-peak branch, the load decreases with the increase of slip, since the available frictional area decreases, as well as the roughness of the failure surface. On the other hand, the post-peak load decay in hooked fibers was not so abrupt than in smooth fibers, since with the increase of the slip the fiber mechanical anchorage starts to become progressively mobilised. At an approximately 4.5 mm slip (corresponding approximately to the straightened hook length), the pullout process occurs under frictional resistance in similitude to smooth fibers.

In the case of hooked fibers with a 30º inclination angle, as previously seen, occurred two failure modes, which will reflect into two distinct types of pullout-slip curves (see Annex I). In Figure 2.5(c), the average curve is represented up to the slip where the fiber rupture took place, therefore the curve averaging was performed only up to a slip correspondent to the peak load. The pre-peak branch of these curves is similar to the one observed for aligned hooked fibers. However, the non-linear part is more pronounced than for aligned fibers, due to the cracking and spalling of the matrix at the fiber bending point, as a consequence of the additional stress concentration at this zone for inclined fibers. For some specimens, sudden load drops were observed before attaining the peak load (see Annex I), this was a consequence of matrix wedges that have spalled, after each completion of wedge spalling off, a new more stable wedge will be formed, and the remaining fiber segment embedded in the matrix will then be pulled out. Whenever for a 30º inclination angle the hooked fiber did not break, and therefore the fiber was fully pulled out, the post-peak behaviour could be assessed (see Annex I). The post-peak curve of the latter specimens was similar to the observed for aligned series, however, an increment of the residual force was perceived up to a slip of 4 mm. This was more easily noticeable for the hooked fibers with an 20 mm embedded length. Such difference is ascribed to the frictional resistance increase due to the force component perpendicular to the fiber axis. Afterwards at slip of about 4.5 mm (corresponding approximately to the straightened hook length), a significant load decay was observed. For higher slips, only for the fibers with a 20 mm embedded length was seen an increase of the frictional resistance.

On the other hand, smooth fibers with an inclination angle of 30º revealed two distinct pre-peak behaviours. Regarding the series with an embedded length of 20 mm, the pre-peak behaviour was identical to the one observed for the aligned smooth fibers, with the exception that a higher peak load was attained, as a consequence of the bending mechanism associated to
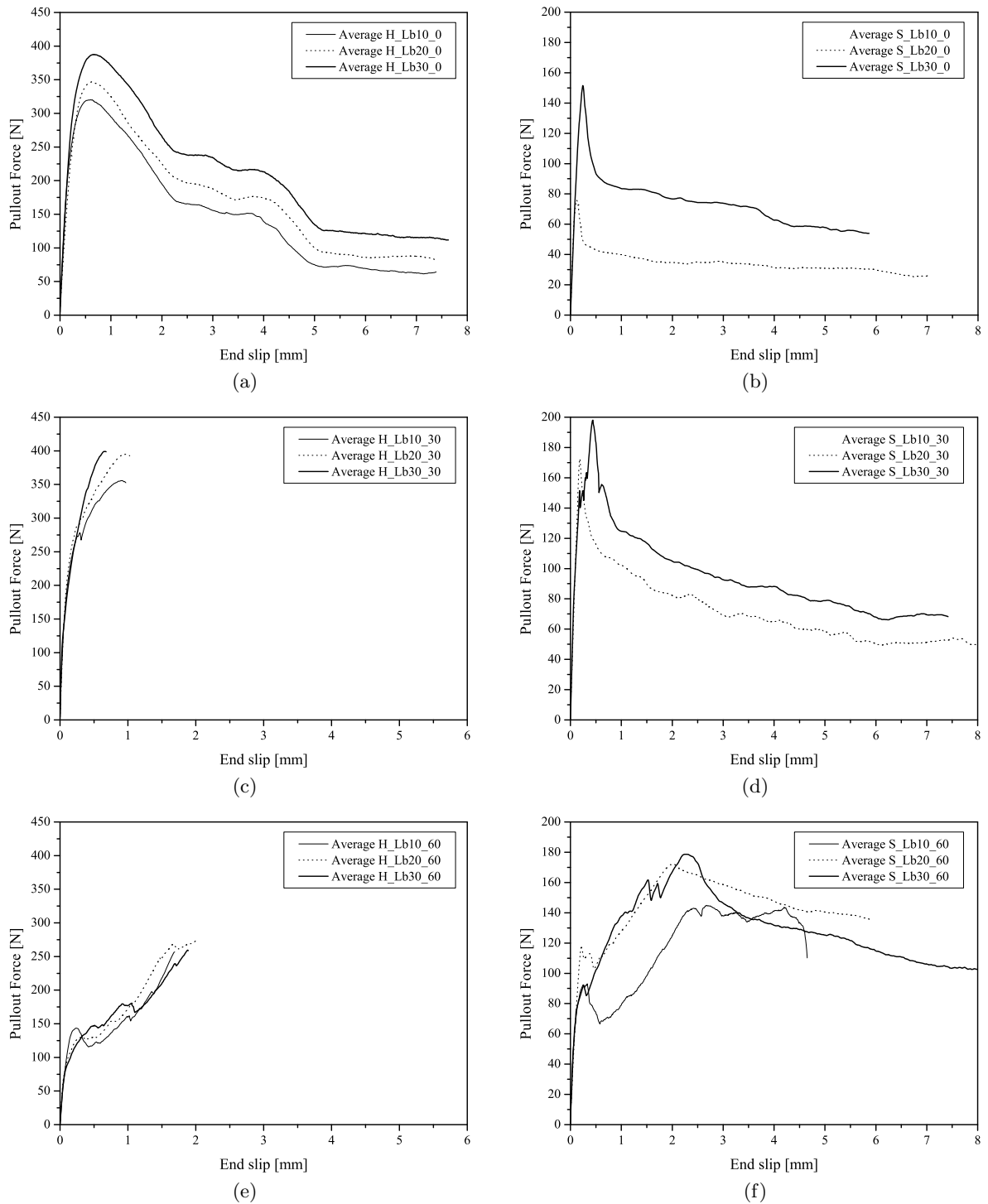
Figure 2.5: Average pullout load-slip curves for a fibre inclination angle: (a), (b) 0 degrees; (c), (d) 30 degrees, and (d),(f) 60 degrees.

fiber inclination angle. For a larger embedded length (30 mm), before reaching the peak load it is observed a decline on the stiffness subordinated to several load decays corresponding to the

cracking or spalling of the concrete matrix (see Figure 2.5(d)). With respect to the post-peak behaviour, the load decreases with the increase of slip. Comparatively to the aligned smooth fibers, the load decay is lesser abrupt, since the influence of the frictional resistance is more significant for inclined fibers.

A completely distinct behaviour was observed for the series with an inclination angle of 60º (Figures 2.5(e) and 2.5(f)). As previously seen, the hooked series with the latter inclination angle failed by fibre rupture, with the exception of one specimen (see Annex I), whereas in the smooth series fibers were fully pulled out. As the inclination angle increases, the stresses concentration at the fiber exit point from the matrix increases, therefore the concrete matrix will be more prone to cracking and spalling. In terms of pre-peak behaviour, this will be decoded in a significant loss of stiffness. Comparing, respectively, Figures 2.5(c), 2.5(d), and Figures 2.5(e), 2.5(f), can be perceived that for the series with an 60º angle, cracking and spalling starts for a lower load level. Moreover, as a larger portion of concrete is pushed or pulled out, a larger fiber length can be more easily bent favouring the stiffness decrease up to the peak load. Regarding the post-peak in smooth fibers a gradual load decay was observed in opposite to smooth fibers aligned and with a 30º angle, since for a 60º inclination angle the frictional resistance due to the force component perpendicular to the fiber axis is much higher. Another interesting point was that the post-peak load decay for a 60º inclination angle was more significant for higher embedded lengths. For the S_lb10_60 series a plateau is observed after the peak load is attained, which abruptly finishes with the matrix spalling, without the fiber being completely pulled out.

2.6 Effect of the embedded length

The influence of the embedded length, L_b, on the maximum pullout load, N_{max}, is represented in Figure 2.6(a). Generally the N_{max} increased linearly with the embedded length for both hooked and smooth fibers. The series H_lb_60º was the only exception, since it was observed a decrease on the N_{max} for a 20 mm embedment length. In the case of aligned fibers the influence of L_b was more significant on the smooth fibers, since an increase of more than 100% on N_{max} occurred, increasing L_b from 20 to 30 mm, while relatively small increments were registered for the hooked end fibers. In fact, for hooked fibers the increment of L_b from 10 to 30 mm provided an increase on the N_{max} of about 20%. These results demonstrate that the pullout response of hooked fibers at given embedment length is predominantly influenced by the mobilisation and straightening of the hook, which is in accordance with published findings (Naaman and Najm (1991) and Robins *et al.* (2002)). For inclined smooth fibers, in resemblance to the aligned hooked fibers, the N_{max} increase with L_b was also relatively small, respectively, 17% and 23% for an inclination angle of 30º and 60º. These results can also point out that, in inclined fibers,

the frictional resistance due to the force component normal to the fiber axis (originated by the inclination angle) plays a more important role on the peak pullout load than the embedded length. This will be even more suggestive on the inclined hooked fibers, since both mechanical deformation of the hook and frictional resistance will actuate together. Therefore, for the latter series, the increase of N_{max} with L_b will be smaller than for smooth fibers. Moreover this increment will decrease with the inclination angle (20%, 15% and 7%, respectively for the hooked series with a 0º, 30º and 60º).
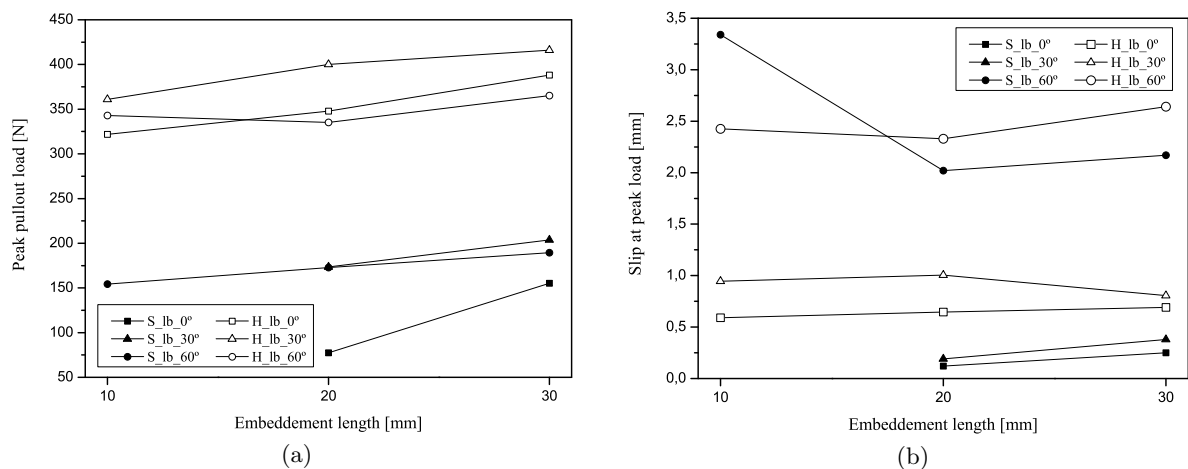
Figure 2.6: Influence of bond length on the (a) peak pullout load and (b) slip at peak load.

Additionally, comparing the curves of the hooked and smooth series in Figure 2.6(a), without regarding to specific details, can be clearly perceived two distinct facts. Firstly, in a general manner the variation of the maximum pullout load with the embedded length can be approximated by a straight line, in which the slope reflects the variation of the pullout load per millimeter. Secondly, a vertical offset between the curves corresponding to the smooth and hooked series can also be identified. This offset distance between those curves represents the contribution of the mechanical anchorage to the N_{max}. Moreover, this contribution was not influenced with the embedment length.

The influence of the embedded length on the slip at the peak load, s_{peak}, is depicted in Figure 2.6(b). For both smooth and hooked aligned fibers a slight increase of s_{peak} with L_b was observed, whereas for inclined fibers was not found any clear relevance of the embedded length influence on the s_{peak}.

The allowable crack opening in fiber reinforced structural elements depend on a specific application. Therefore it is of special interest to assess the mechanical pullout properties, e.g. the maximum pullout load and toughness, for a determined crack opening (i.e. slip). The

pullout toughness was computed by integrating the load-slip curve up to slips of 1 and 3 mm, which were respectively designated by G_{1mm} and G_{3mm}.

In Figures 2.7(a) and 2.7(b) is depicted, respectively, the embedment length influence on G_{1mm} and G_{3mm}. The average values of these parameters, as well as the correspondent variation coefficients are indicated in Annex I. In general, as the the fiber embedded length increases, the toughness to a given slip also increases. However, series H_lb_30º was an exception to the latter assertion, since G_{1mm} and G_{3mm} fall off for an embedded length of 30 mm. The reason of this occurrence was due to distinct types of pullout failure observed for each series (see Table 2.3). For the H_lb30_30º specimens, fiber rupture has always occurred, whereas for the other embedded lengths of the series H_lb_30º there were specimens from which the fiber was completely pulled out. Moreover, the toughness of the latter specimens is considerably larger than the toughness of the ones where fiber rupture occurred (see individual pullout curves in Annex I). As a result, the average toughness value for series H_lb30_30º is smaller than for other embedded lengths with the same inclination angle. Besides, the fact that G_{3mm} of the H_lb30_30º series being smaller than the smooth fiber series with the same inclination angle and embedded length, may also cause bewilderment. Anyhow, once again this was due to the fiber failure modes observed for each series. Since, for the S_lb30_30º all the specimens failed by pullout in opposite to the correspondent hooked series that failed by fiber rupture for an approximate slip of 1 mm. Therefore, the overall toughness is markedly influenced by the type of failure, since fiber fracture will significantly reduce the toughness when comparing to fibers that underwent a complete pullout.

For the aligned series, since always took place the complete fiber pullout, the increase of both G_{1mm} and G_{3mm} with the increase of the embedded length was more significant than for inclined fibers. Regrading the H_lb_0º series, G_{1mm} and G_{3mm} increased with L_b 18 and 28%, respectively. Inasmuch the smooth fibers this increase was even more considerable, since both G_{1mm} and G_{3mm} increased with L_b more than 100%. Once more, previous demonstrates that the pullout response of hooked fibers at given embedment length is predominantly influenced by the mobilisation and straightening of the hook.

2.7 Effect of the fibre orientation angle

In Figure 2.8(a) is depicted the influence of the inclination angle on the maximum pullout load, N_{max}. In general, the N_{max} increases up to a inclination angle of 30º and then decreases for 60º angle. For both hooked and smooth fibers the highest maximum pullout load was observed for an inclination angle of 30º. However, the increase of the maximum pullout load with the inclination angle was more significant on the smooth fibre series. For the latter, the series with
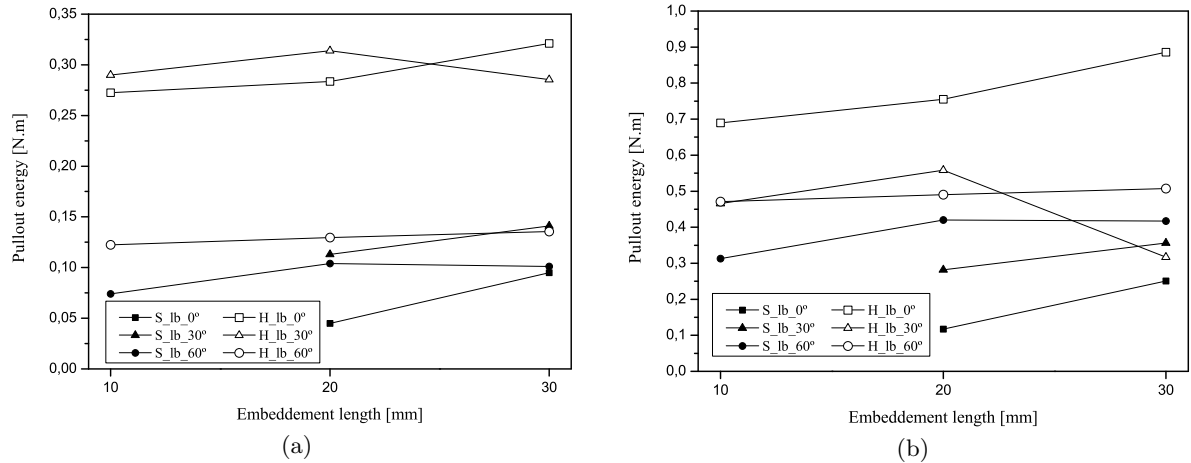
Figure 2.7: Influence of bond length on pullout energy dissipated up to a slip of:(a) 1 mm (b) 3 mm.

a 30° inclination angle have a N_{max} 30-125% higher than the aligned smooth fibre series. On the other hand, for the hooked fibre series with a 30° inclination angle, the N_{max} is just 7 to 15% higher than aligned hooked fiber series. In spite of the increase of the frictional pullout component with the inclination angle, increasing the angle from 30° to 60° will provide a slight decrease on the N_{max}. Remember that for the inclined hooked series the pullout occurred generally by fibre rupture. Moreover, the average fiber rupture load was smaller for the series with a 60° inclination angle than for 30°, as previously explained.

The slip at peak load, s_{peak}, increased with the inclination angle for both hooked and smooth fibers. The trend of the s_{peak} evolution with the inclination angle was very similar for all the series (see Figure 2.8(b)). First a slight increase on the s_{peak} for a 30° angle was observed, afterwards the s_{peak} increased considerably. In fact, for the smooth series with 60° inclination angle, the s_{peak} was approximately 5 to 9 times higher than for a 30° angle, whereas for the hooked series it was 1.3 to 2.3 times higher. The significant higher values of s_{peak} for a 60° angle can be ascribed to other additional mechanisms that usually occur on inclined fibres in opposite to aligned fibres. As the fibre inclination angle increases, the stresses concentrated at the fibre bending point also increase. This will lead to a more significant portion of concrete that is crushed or pushed off at the crack plane. As the volume of concrete that spalls is higher, a bigger fibre length is subjected to bending (see Figure 1.4), which will add to the measured slip a supplementary displacement correspondent to the fibre deformation. So, for large inclination angles, such as 60°, the slip includes a significant parcel which is due to fibre deformation.

The capacity level of a fibre can be given as the ratio of the maximum tensile stress observed in the fibre during pullout (σ_{max}) and the tensile strength of the fibre steel (σ_y). The analysis of this ratio allows to assess the optimisation level of the fibre utilised in conception of the present self-compacting concrete, i.e if the fibre type and aspect ratio are adequate to the matrix
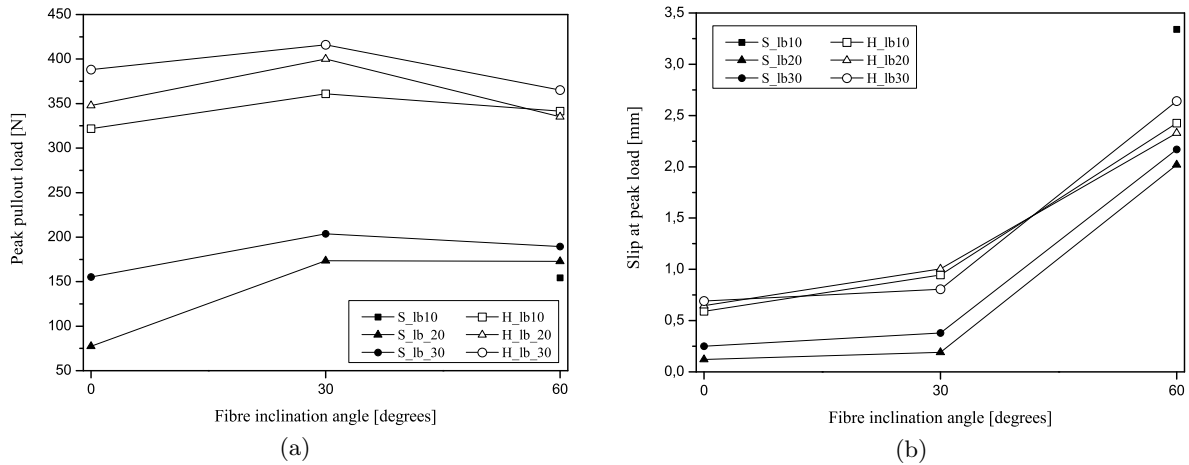
Figure 2.8: Influence of inclination angle on the: (a) peak pullout load and (b) slip at peak load.

strength. As perceived in a previous section, the rupture stress for inclined fibres was smaller than the one obtained experimentally in the direct tension tests, since composed bending will arise for inclined fibres (see Figure 2.9). As the inclination angle increases, the bending moment will increase and the axial force must decrease in order to attend the ultimate capacity diagram of the cross section under composed bending. Therefore, for the computation of the latter ratio for the inclined series, the tensile strength obtained in direct tension tests was not used. In order to accomplish a better interpretation of the results, for the inclined series, the tensile strength was computed as the ratio between the average rupture load observed in the pullout tests and the fibre cross section area (N_{max}/A_f). The influence of the inclination angle on the ratio σ_{max}/σ_y is depicted in Figure 2.10.
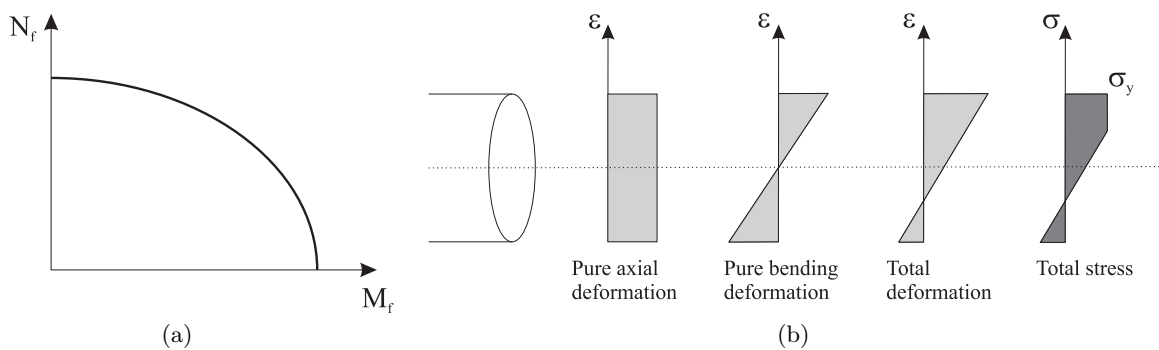
Figure 2.9: Composed bending: (a) interaction diagram between bending moment and axial force (b) Strain and stress distribution on the fibre cross section.

The peak pullout force of a fibre, or its corresponding tensile stress, should not be determined exclusively at the maximum stage, i.e at the correspondent slip at peak load, since this

will not say much about the performance of fibres in real structures. In fact they should be
determined at normative values of the fibre slip, i.e. of the crack width. As it was previously
seen, the maximum pullout load can be observed for distinct slips (see Figure 2.8(b)), ranging
0.2 to 3.3 mm depending on the type of fibre, embedment length or inclination angle. The
allowable crack openings (fibre slip) in real structural elements depend either on the durability
or the ultimate load-bearing capacity. These values can lay out between 0.1-0.3 mm regarding
durability, or 1-3 mm concerning the ultimate load-bearing capacity depending of type appli-
cation. In Figure 2.11 is depicted the ratio between the tensile stresses of aligned and inclined
fibres, at fibres slips (which is related to crack widths) of 0.1, 0.25, 0.5 and 1 mm, for both
hooked and smooth fibres.
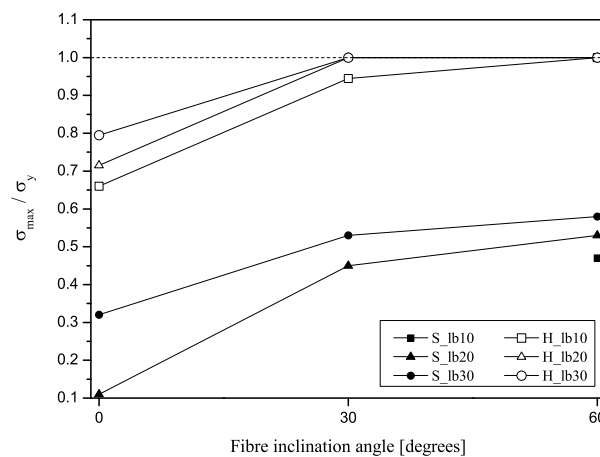
Figure 2.10: Ratio between the maximum achieved tensile stress (σ_{max}) and the fibre strength (σ_y).

Figure 2.11(a) shows, that hooked fibres inclined at 60º possess the lowest efficiency for
all fibre slips (i.e. at all crack widths). Fibres inclined at 60° are 1.5 to 2.6 times lesser
effective when compared to fibres aligned with the tensile load. Regarding the fibres with a 30º
inclination, a positive effect is mainly observed at very small fibre slips (0.1 mm). For the latter
inclination, no significant differences were observed for larger slips, when compared to aligned
fibres. In opposite to this observation, results of several researchers, shows that for a 30º angle
the efficiency of hooked fibres is significantly smaller than for align fibres. The tensile stress in
a 30º inclined fibre can be up to 2.5 times smaller than for aligned fibres (see Figure 1.6). The
discrepancy between the obtained results and those depicted in Figure 1.6 can be due to the
differences between the self-compacting and conventional concrete matrices. The high strength
matrix of the self-compacting concrete used is in general considerably more compact, i.e has
fewer voids, than a conventional matrix. Remark that as consequence of the fibre inclination,

there are additional concentrated stresses nearby the concrete surface fibre exit. Therefore, a weaker matrix or less compact (e.g. conventional concrete) is more prone to spalling and local damage. As concrete spalling occurs the fibre can easily bend, and the stress carried by the fibre is reduced. On the other hand, on fibres with a 30° inclination angle pulled-out from high performance reinforced concrete (with smaller fibres to increase the splitting tensile strength of the matrix) was also observed a positive effect (Markovic, 2006). Consequently, in opposite to conventional matrices, high compacity matrices (e.g. self-compacting concrete or high performance cement composites) can improve the effectiveness of inclined fibres for 30° angles.
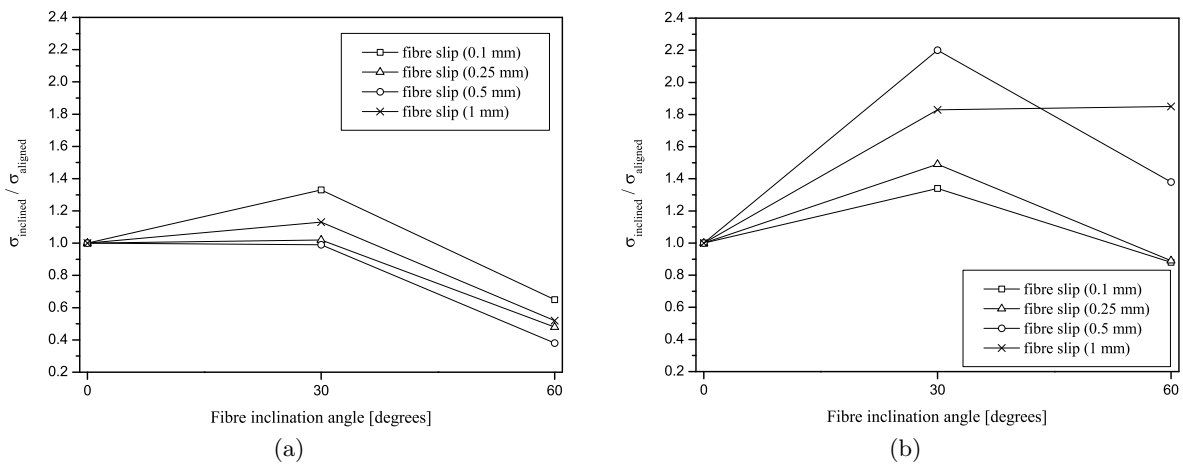
Figure 2.11: Ratio between the tensile stresses in aligned and inclined fibres (0°, 30° and 60°), at different fibre slips for: (a) hooked and (b) smooth fibres.

Inasmuch as for smooth fibres, the efficiency for both inclinations studied was higher, comparatively to hooked fibres (see Figure 2.11(b)). For a 30° inclination angle depending on the fibre slip the efficiency of the inclined fibre can reach up to 2.2 times of an aligned smooth fibre. This increase is more significant in smooth fibres, since this kind of fibres did not failed by fibre rupture, in opposite to the hooked fibres. On the other hand, for fibres with a 60° inclination angle the efficiency increased only for higher slips, i.e. 0.5 and 1 mm, whereas for the other fibres slips the fibre efficiency was almost the same as for aligned fibres. The absence of a mechanical anchorage in the smooth fibres will lead to smaller pullout forces, consequently, the concentrated stresses nearby the concrete surface fibre exit due to fibre angle will be smaller. Considering the abovementioned, when pulling out smooth fibres, the fraction of concrete matrix damaged will be smaller. Therefore, the efficiency of a smooth fibre at an inclination angle of 60° is not so compromised as for the hooked fibres.

In Figures 2.12(a) and 2.12(b) is depicted, respectively, the influence of the inclination angle on the toughness up to a slip of 1 mm, G_{1mm}, and 3 mm, G_{3mm}. In general, an increase of G_{1mm} was observed up to an inclination angle of 30º followed by a decrease for a 60º angle. With regard to the hooked series a significant reduction (118 - 155%) of G_{1mm} for a 60º inclination angle was observed. As the inclination angle increases, the frictional resistance also increases supplying an additional parcel to the overall energy necessary to pullout the fibre. In spite of that, when pulling out at an angle, the fibre will appoint the matrix nearby the fibre bending point under additional stress. As the angle increases more, splitting of the matrix becomes more considerable and arises for lower load levels. Additionally, for the last mentioned series, as the matrix becomes more spalled for smaller slips, the loss of stiffness due to the fibre bending starts also for a lower load level, repercussing on a lower toughness (see Figure 2.5). On the other hand for the smooth series with a 60º inclination angle, though the decreasing of toughness, a significantly smaller decrease was observed than the one for the latter hooked series.
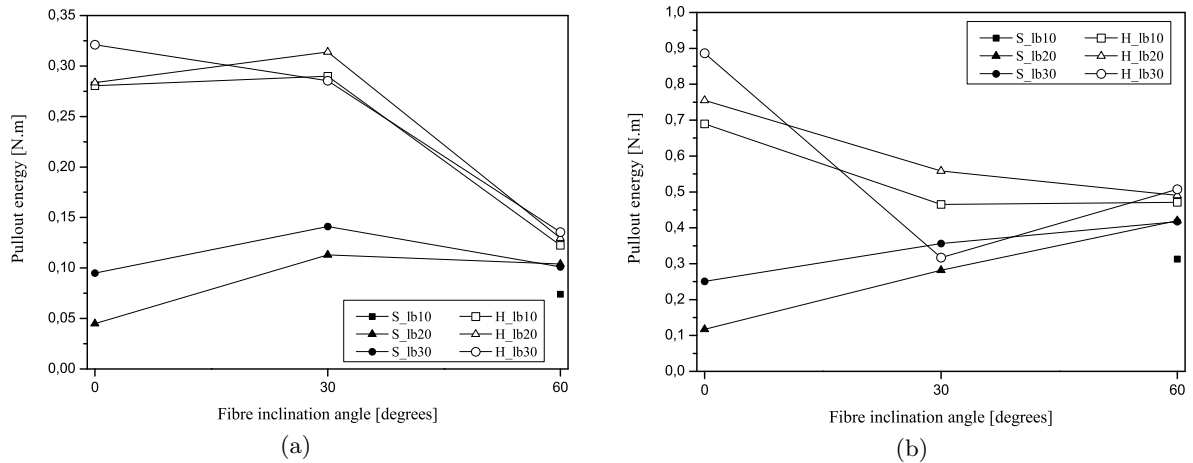
Figure 2.12: Influence of the inclination angle on pullout energy dissipated up to a slip of:(a) 1 mm (b) 3 mm.

Looking upon the influence of the inclination angle on the G_{3mm}, two distinct trends could be perceived for each the smooth and hooked fibres. Concerning the smooth series an increase of G_{3mm} was observed with the increase of the inclination angle, while for the hooked series it was observed the opposite. The prior finding as a feasible explanation. In the case of inclined smooth fibres, as previously said, the principal mechanism that contributes to the toughness increase is the additional frictional resistance provided by the inclination angle. This was only reflected for G_{3mm}, and not for G_{1mm}, since the frictional resistance will become more important for higher slips, which is in accordance with other authors findings (Shah *et al.*,

1995). In opposite, regarding the inclined hooked series, as also previously said, the influence on the pullout mechanisms of the additional frictional resistance is less significant than the mobilisation of the hook. This fact, associated to the fibre rupture observed in these series at a slip smaller than 3 mm, contributed to the decrease of toughness. The toughness of the series H_lb30_30º was smaller than expected, in comparison to the other series with a 30º angle, since fibre rupture occurred for the totality of the series specimens.

2.8   Effect of the hooked end

In Figure 2.13(a) is depicted the contribution of the end hook mechanism on the overall pullout behaviour of aligned fibres. The mechanical component of bond (curve 3 in Figure 2.13(a)) was obtained by subtracting the average curve of the hooked series (curve 1 in Figure 2.13(b)) to the correspondent average curve of the smooth series (curve 2 in Figure 2.13(a)). Comparing curves 3 obtained for both the 20 mm and 30 mm embedment lengths, respectively Figures 2.13(a) and 2.13(b), it can be observed that the curves are extremely similar. This also reveals that if the full mobilisation of the hook is attained, the mechanical component of the hook is not influenced by the embedment length. This will not be true if the embedment length is smaller than the length of the hooked end (Robins *et al.*, 2002), which is not the case of the present work.

In order to assess in a quantitative way the contribution of the hook straightening and deformation on the overall pullout behaviour of aligned hooked fibres, it was used the curve 3 depicted in Figure 2.13 to compute the maximum pullout load and toughness ratios between the later curve and the correspondent average curve of the hooked series (curve 1). For the maximum pullout load, the contribution of the hook mechanism was of 88% and 77%, respectively for a 20 and 30 mm embedded length. Regarding both G_{1mm} and G_{3mm} the endowment of the hook was about 84% and 71% for an embedded length of 20 and 30 mm, respectively. Obviously, in the case of aligned hooked fibres the influence of the hook on the pullout behaviour decreases with the embedded length increase, since the debonding process proceeds throughout a larger distance on the case of the series with 30 mm, and, additionally, the mechanical component was not influenced by the embedded length.

On the other hand, for inclined fibres, the assessment of the contribution of the hook is not so easy, since for inclined hooked fibres several other mechanisms arise in comparison with aligned fibres. Those mechanisms are respectively: the additional frictional resistance due to the force component normal to the fibre axis, the deformation, bending and plastification on the bending point of the fibre, and finally, spalling of the concrete matrix nearby the fibre exit point of the concrete. Moreover, these mechanisms during the pullout process will interact
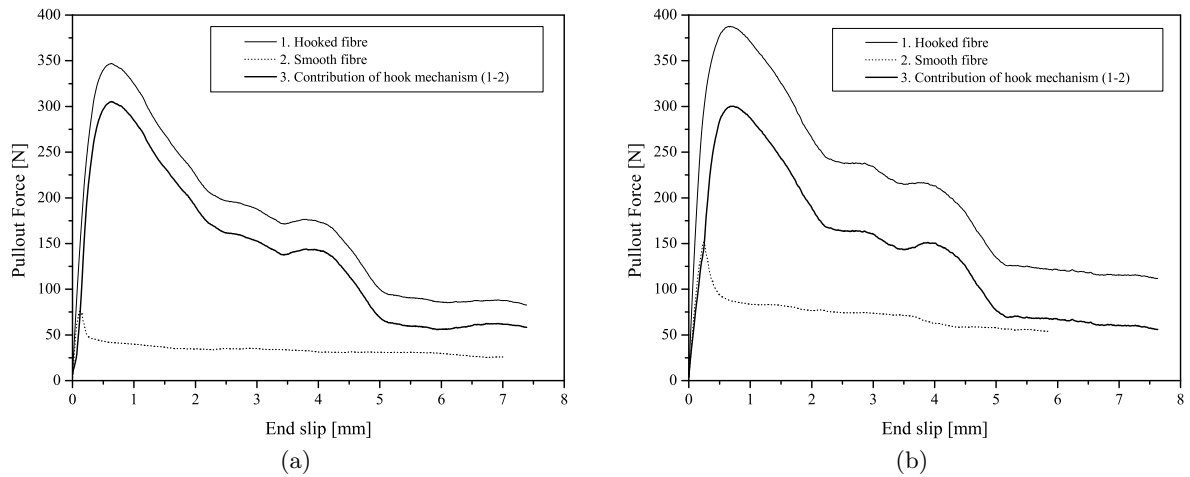
Figure 2.13: Contribution of the end hook to the overall pullout behaviour in aligned hooked-end fibres with an embedded length of: (a) 20 mm and (b) 30 mm.

with each others. In Figures 2.14 and 2.15 is depicted, respectively, the contribution of the end hook mechanism on the overall pullout behaviour of fibres with a 30º and 60º inclination angle. The contribution of the hook mechanism for inclined fibres was assessed in a similar way to the aligned fibres. Comparing this contribution for aligned and inclined fibre (see Figures 2.13, 2.14 and 2.15), can clearly be observed that as the inclination angle increases, the contribution of the hook mechanism decreases. In fact, for inclined fibres with a 30º angle, the hook influence on the maximum pullout behaviour was about 54%, whereas for a 60º inclination angle was of 48%. Regarding the G_{1mm}, the hook contribution was about 58% for a 30º angle and 20% for the 60º angle.
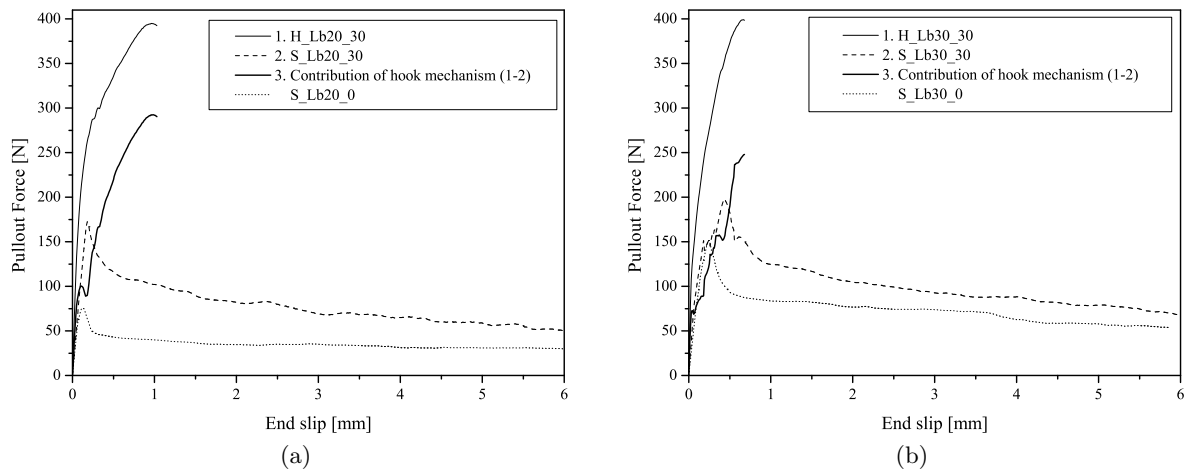
Figure 2.14: Contribution of the end hook to the overall pullout behaviour in hooked-end fibres with a 30º inclination angle: (a) 20 mm and (b) 30 mm.

The previous assertions for the inclined series (30° and 60°) must be regarded with care, since in the present work fibre rupture occurred. Therefore, these assumptions can only be applied to the pre-peak behaviour. Moreover, for fibres with a considerable inclination angle, such as 60°, there is significant parcel of the slip that is due to the bending deformation of the fibre. From analysing Figures 2.14(b) and 2.15(b), it points out that the end hook only starts to be mobilized for large slips (over 1 mm).
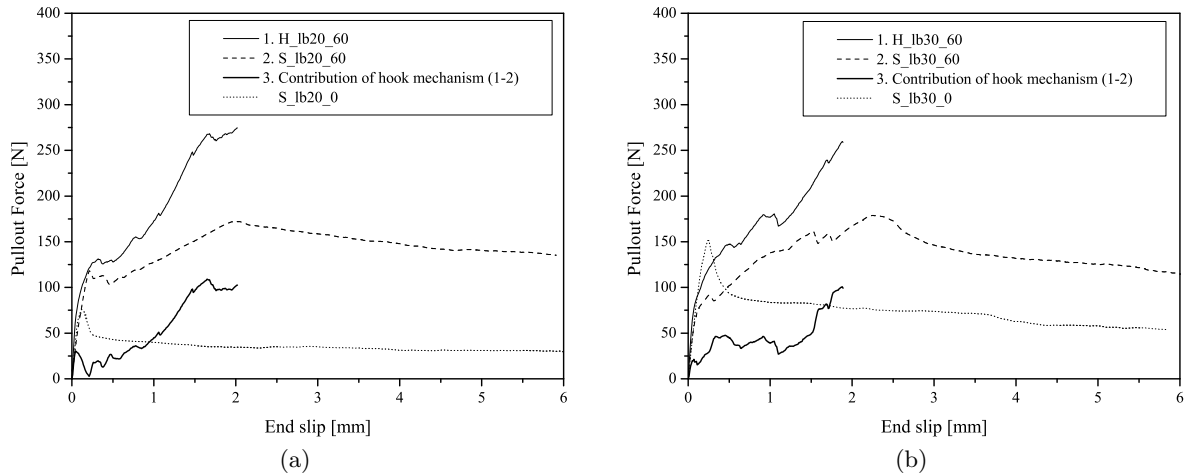
Figure 2.15: Contribution of the end hook to the overall pullout behaviour in hooked-end fibres with a 60° inclination angle: (a) 20 mm and (b) 30 mm.

In order to enlighten the validity of these arguments, the mechanical contribution of the end hook was acquired for a single specimen from the series with an inclination angle of 30° and 60° which has been fully pulled out (see Figure 2.16). The mechanical contribution curve withdrawn from the H_lb20_30 specimen is very similar to the one obtained for the aligned series (see Figure 2.13). Regarding the curve of the mechanical contribution related to the H_lb10_60 specimen, can be withdrawn that the contribution of the hook to the maximum pullout load was of 60%, whereas the input to G_{3mm} was 45%. This also points out that even in the case that fibre rupture does not occurs, for a high inclination angle (60°), the contribution of the end hook to the overall pullout behaviour is not so significant as in aligned fibres.
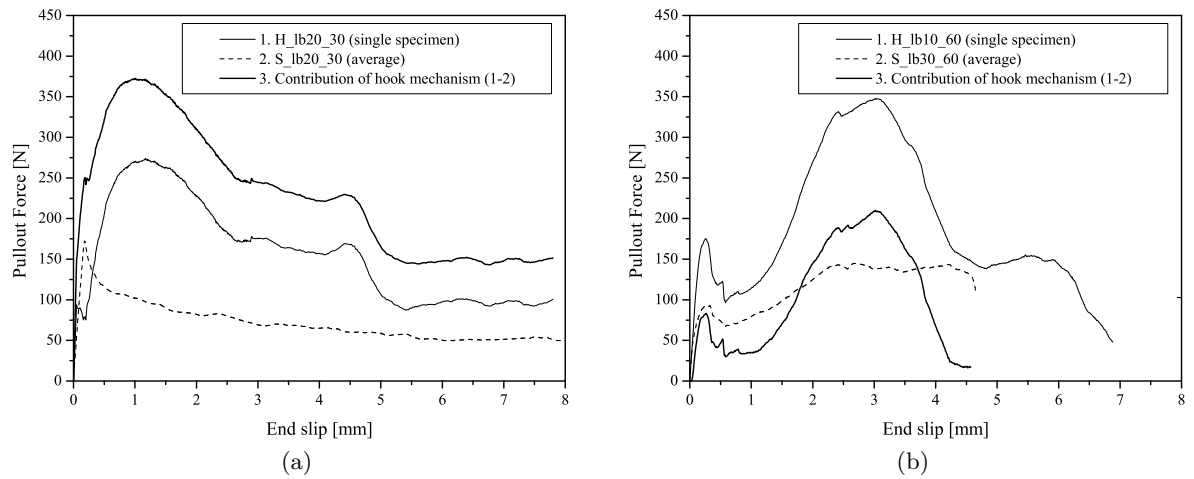
Figure 2.16: Contribution of the end hook to the overall pullout behaviour for the single specimen from series: (a) H_lb20_30 and (b) H_lb10_60.

Analytical modeling of the bond-slip relationship

Analytical models for pullout problems are only capable to determine a load-slip relationship $N(s)$ of a pullout test on basis of a given bond law, $\tau(s)$, i.e. the direct problem, where with $\tau(s)$ is obtained $N(s)$. The straightforward analytical determination of the bond stress versus slip relationship for a given pullout curve, i.e. the inverse problem where with $N(s)$ is obtained $\tau(s)$, is extremely difficult due to considerable complexities from mathematical point-of-view (Banholzer *et al.*, 2005). Actually, to overcome this concern, the inverse problem must be approached as a direct problem complemented with a numerical fitting tool.

In the present section, the developed numerical method for obtaining an analytical bond stress-slip relationship will be described. The mathematical representation of the pullout problem is often expressed by a second order differential equation expressed in terms of forces (Naaman *et al.*, 1991b; Sujivorakul *et al.*, 2000; Banholzer *et al.*, 2005). However since in the present model the displacements of the concrete points at the interface between concrete and fiber were neglected, the differential equation was derived in terms of slip, after Russo *et al.* (1990), Focacci *et al.* (2000) and Sena-Cruz (2005). This model was used for both smooth and hooked fibers. However, for hooked fibers, in order to account for the mechanical anchorage resistance at the embedded end, an additional spring component at the embedded end of the fiber was included, Figure 3.1. The pullout problem of hooked fibers is markedly a three dimensional problem. Nevertheless it was approached as two dimensional problem, since otherwise it would be extremely difficult to plant an analytical model. Moreover, it seemed feasible to model the interfacial bond of the hooked fiber as a two dimensional axisymmetric problem, since the hook length is relatively smaller than the fiber length, and then introduce the anchorage component by a spring.

3.1   Theoretical relationships

3.1.1   Local bond-slip

The equilibrium of the free body of an infinitesimal length dx of a fibre bonded to a concrete matrix can be given by (see Figure 3.1(c)):

$$\sigma_f \cdot A_f + \tau \cdot P_f \cdot dx = (\sigma_f + d\sigma_f) \cdot A_f \tag{3.1}$$

where $\tau = \tau\left(s\left(x\right)\right)$ is the local bond shear stress acting on the contact surface between fibre and concrete, and s is the slip, i.e. the relative displacement between the fibre and the concrete. σ_f, A_f and P_f are the normal stress, cross section area and perimeter of the fiber, respectively.
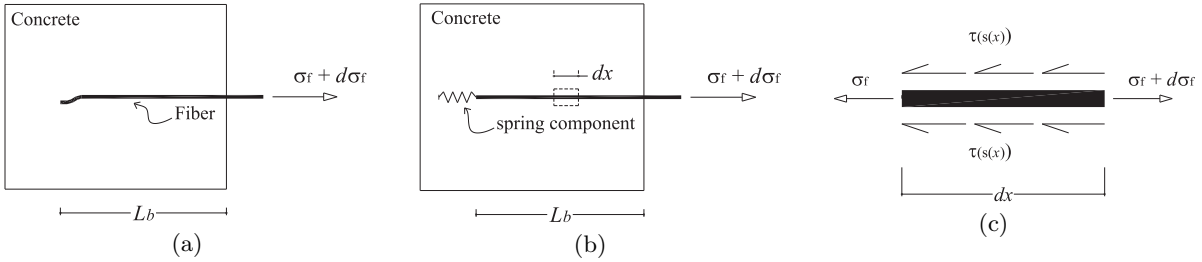
Figure 3.1: Axisymetric pullout model: (a) general problem, (b) simplified model (c) equilibrium of an infinitesimal fiber free-body.

Assuming that the fiber has a linear elastic constitutive law in the longitudinal direction ($d\sigma_f = E_f\ d\varepsilon_f$), equation 3.1 can be rewritten into:

$$\tau = \frac{E_f A_f}{P_f} \cdot \frac{d\varepsilon_f}{dx} \tag{3.2}$$

where E_f and ε_f are, respectively, the Young modulus and the strain of the fibre.

The strain components in a representative bulk of the fibre - concrete interface are indicated in Figure 3.2. The slip variation over an infinitesimal length, ds/dx is given by:

$$\frac{ds}{dx} = \varepsilon_f - \varepsilon_c \tag{3.3}$$

where ε_c is the concrete strain. However, the contribution of the concrete deformability in the slip assessment may be neglected, since the fibre is subjected to large inelastic deformations. Several authors have neglected this component, on the evaluation of the bond-slip relationship

of reinforcing bars (Russo *et al.*, 1990) or of FRP reinforcement (Focacci *et al.* (2000), Sena-Cruz (2005)). In spite of this belief, in order to validate this assumption for small fibres, it was used an analytical model which took into account the deformation of the matrix surrounding the fibre (Sujivorakul *et al.*, 2000) in the assessment of the pullout load - slip relationship. A sensitivity analysis was carried out using the latter model to evaluate the influence of the matrix deformation on the pullout response. For the current fibers lengths and matrix stiffness, the ε_c did not influence the slip value determination, since $\varepsilon_c << \varepsilon_f$.
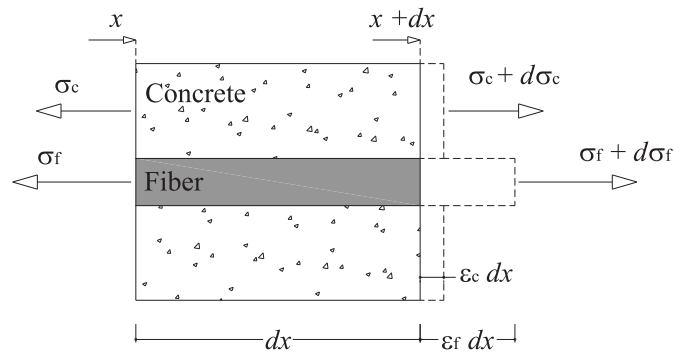
Figure 3.2: Stresses and strains on the fiber bond region.

Considering the abovementioned, neglecting the concrete deformability in the slip determination ($\varepsilon_c = 0$), incorporating the equation 3.3 into 3.2, the second order differential equation that governs the local bond phenomena of the fiber - matrix interface is given by:

$$\frac{d^2s}{dx^2} = \frac{P_f}{E_f \, A_f} \cdot \tau \tag{3.4}$$

3.1.2 Pullout load-slip relationship

The pullout load and slip relationship can be determined using either an energy approach (Focacci *et al.*, 2000) or an equilibrium approach (Russo *et al.*, 1990; Naaman *et al.*, 1991b). In the present work will be adopted the energy approach.

Consider a steel fiber embedded on a concrete matrix over a bond length $\tilde{L}_b = L_b$, where N is the generic applied pullout force, and s_f and s_l are, respectively, the free and loaded end slips, with respect to the longitudinal axis of the fiber, x, starting at the free end (see Figure 3.3). When the fiber is slipping due to an applied pullout load, $\overline{N}$, the following functions can be

evaluated along the fiber bond length: slip along the fiber, $s(x)$; bond shear stress along the embedded length, $\tau(x)$; fiber strain, ε_f; and the axial force, $N(x)$.
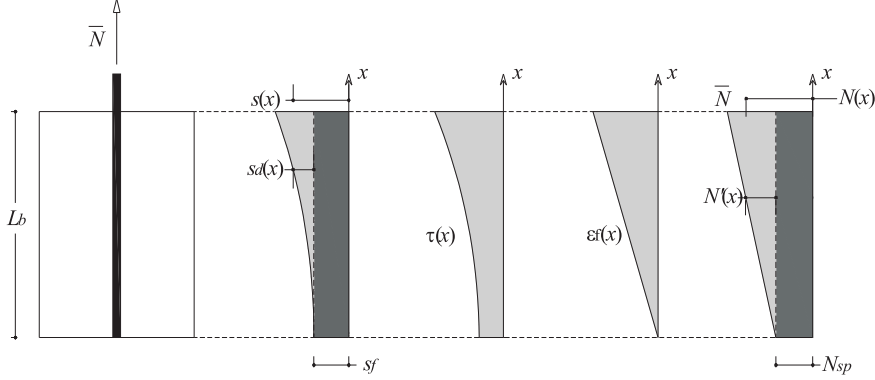
Figure 3.3: Entities evolved in the developed method.

In Figure 3.3 the slip diagram along the fiber, $s(x)$, can be regarded as the sum of two components. A constant component s_f which produces a rigid body displacement of the fiber, whereas the $s_d(x)$ component results from the deformation of the fiber. Moreover, for any point x of the fiber embedded length, just the $s_d(x)$ component will result in a fiber length change, and, therefore, contributing to the fiber deformation energy. Likewise, the axial force along the fiber $N(x)$ can be decomposed into two components. A constant component N_{sp} due to the spring load (only in the case of hooked fibers) and the $N'(x)$ component. Only the latter will contribute to the fiber deformation energy, since in the adopted model it was assumed that N_{sp} will not produce a fiber length change. Therefore, the fiber deformation at a point x would be $\varepsilon_f(x) = N'(x)/(E_f A_f)$. Considering a generic fiber cross section, constrained by $0 \leq \overline{x} \leq \tilde{L}_b$, and that the fiber lateral surface over embedded length is $\Omega = P_f \cdot \overline{x}$, the work performed by external forces acting on the range $0 \leq \overline{x} \leq \tilde{L}_b$ is :

$$W_{ext} = \int_{\Omega} \left(\int_{s_f}^{s(x)} \tau\left(s\right) ds \right) d\Omega = P_f \int_{0}^{\overline{x}} \left(\int_{s_f}^{s(x)} \tau\left(s\right) ds \right) dx \qquad (3.5)$$

On the other hand, remarking $V_f = A_f \cdot \overline{x}$ as the fiber volume over the embedded length, the elastic energy of the fiber is:

$$W_{int} = \int_{V_f} \left(\int_0^{\mathcal{E}(x)} \sigma_f\left(\varepsilon_f\right) d\varepsilon \right) dV_f = A_f \int_0^{\overline{x}} \left(\int_0^{\mathcal{E}(x)} E_f \varepsilon_f d\varepsilon \right) dx \tag{3.6}$$

$$= \frac{A_f}{2E_f} \int_0^{\overline{x}} \sigma_f^2\left(x\right) dx$$

From Equations 3.5 and 3.6 is obtained:

$$\int_0^{\overline{x}} \left(P_f \int_{s_f}^{s(x)} \tau\left(s\right) ds - \frac{A_f}{2E_f} \sigma_f^2\left(x\right) \right) dx = 0 \tag{3.7}$$

Since Equation 3.7 must be satisfied for each value of $0 \leq \overline{x} \leq L_b$, this equation may be rewritten as:

$$P_f \int_{s_f}^{s(x)} \tau\left(s\right) ds - \frac{A_f}{2E_f} \sigma_f^2\left(x\right) = 0 \tag{3.8}$$

At $x = L_b$ equation 3.8 becomes:

$$P_f \int_{s_f}^{s\left(x=\tilde{L}_b\right)} \tau\left(s\right) ds - \frac{N'^2}{2E_f A_f} = 0 \tag{3.9}$$

$$N' = \sqrt{2E_f \cdot A_f \cdot P_f \int_{s_f}^{s\left(x=\tilde{L}_b\right)} \tau\left(s\right) ds} \tag{3.10}$$

Equation 3.10 allows to determine the generic applied pullout force for a smooth fiber, or in the case of a hooked fiber, the pullout load component at the fiber free end due to the interfacial bond of the fiber. Remarking that in the case of hooked fibers, the generic applied load is $\overline{N} = N' + N_{sp}$ (see Figure 3.3), for the latter fibers the generic applied load is given by:

$$\overline{N} = \sqrt{2E_f \cdot A_f \cdot P_f \int_{s_f}^{s\left(x=\tilde{L}_b\right)} \tau\left(s\right) ds} + N_{sp} \tag{3.11}$$

3.2   Determination of the local bond stress-slip relationship

The local bond stress-slip relationship, $\tau - s$, was determined throughout the previous described theoretical relationships. The adopted method is supported on the work developed by Focacci *et al.* (2000) and Sena-Cruz (2005). In order to improve the performance of the method and to adapt it to the specificities of the present study, some modifications were performed. In this section, it is described in detail the implemented algorithm.

3.2.1   Analytical bond stress-slip relationship

The obtained experimental pullout load-slip curves (see Figure 2.5) revealed a distinct pullout behaviour for the different fiber inclination angles studied, as previously described in Chapter 2. Therefore, in the present work, three distinct local bond were defined stress-slip relationships for each inclination angle.

For the series with an inclination angle of 0$^\text{o}$ and 30$^\text{o}$ were used, respectively, equations 3.12 and 3.13.

$$\tau(s) = \begin{cases} \tau_m \left(\dfrac{s}{s_m}\right)^{\alpha} & \text{IF } s \leq s_m \\[2em] \tau_m \dfrac{1}{1 + \left(\dfrac{s - s_m}{s_1}\right)^{\alpha''}} & \text{IF } s > s_m \end{cases} \tag{3.12}$$

$$\tau(s) = \begin{cases} \tau_m \left(\dfrac{s}{s_m}\right)^{\alpha} & \text{IF } s \leq s_m \\[2em] \tau_m \left(\dfrac{s}{s_m}\right)^{-\alpha'} & \text{IF } s > s_m \end{cases} \tag{3.13}$$

Where τ_m and s_m are, respectively, the bond strength and its corresponding slip. Parameter α defines the shape of the pre-peak branch, whereas α', α'' and s_1 describe the configuration of the post-peak branch of the curve. These relationships were selected due to its easiness and aptitude to accurately model the local bond stress-slip behaviour, as previously ascertained by several researchers (Eligehausen *et al.* (1983), Stang and Aarre (1992), Lorenzis *et al.* (2002), Sena-Cruz (2005)).

On the other hand, for the series with a 60$^\text{o}$ inclination angle, the pullout load-slip curve could not be correctly simulated with the abovementioned laws. Consequently, for this inclination was adopted the quadrilinear law with the following generic form:

$$\tau(s) = \frac{\tau_i - \tau_{i-1}}{s_i - s_{i-1}} \cdot s + \tau_{i-1}, \quad s_{i-1} < s \le s_i \tag{3.14}$$

where $i = 1, ..., 4$; τ_i and s_i are, respectively, the bond stress and its correspondent slip at point i, and τ_0 and s_0 are both zero and define the origin point of the bond stress-slip relationship.

3.2.2   Analytical relationship for the mechanical anchorage

The contribution of the end hook mechanism on the overall pullout behaviour was obtained separately for the series with a 0º, 30º and 60º inclination angle. The adopted procedure was described in section 2.8. In Figure 3.4 is depicted the analytical simulation of the hook mechanical contribution for the distinct inclination angles studied.
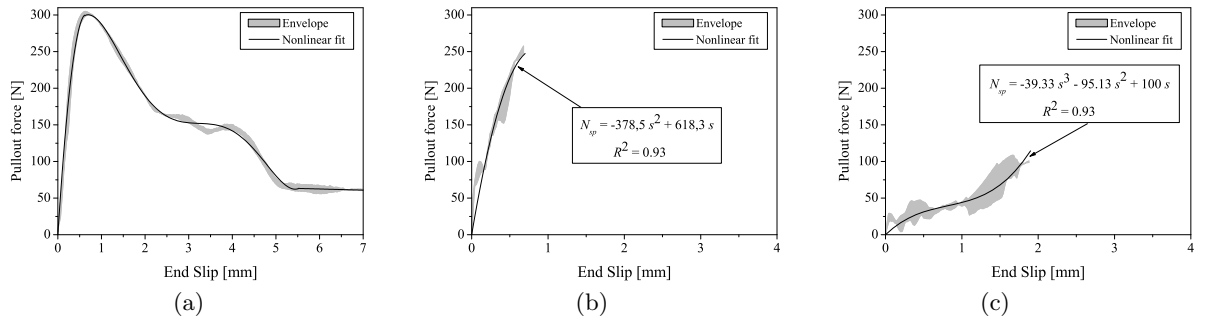
Figure 3.4: Analytical simulation of the hook mechanical contribution for the series with an inclination angle of: (a) 0º, (b) 30º and (c) 60º

The analytical expressions for the series with a 30º and 60º inclination angle are given in Figure 3.4, whereas for the aligned series the analytical expression is given by Equation 3.15. Remark that for the inclined series the contribution of the hook was only assessed for an initial stage, since, in general, fibre rupture occurred during the fibre pullout on these series.

$$N_{sp} = \begin{cases} 918.98 \cdot s - 717.1 \cdot s^2 & \text{IF} \quad s \le 0.6 \\[2em] 2.2423 \cdot s^5 - 35.326 \cdot s^4 + 201.61 \cdot s^3 \\ \quad -497.84 \cdot s^2 + 444.79 \cdot s + 171.96 & \text{IF} \quad 0.6 < s \le 5.5 \\[2em] -1.57 \cdot s + 70.0 & \text{IF} \quad s > 5.5 \end{cases} \tag{3.15}$$

3.2.3   Description of the method

Regarding the entities described in Figure 3.3, can be stated the following boundary conditions at the free and loaded ends, Equation 3.16 for smooth fibers, whereas Equation 3.17 for hooked fibers. In the present method, both numerical and experimental entities are simultaneously used, hence the experimental one was distinguished by an overline, i.e $\overline{N}^i$ stands for the pullout force experimentally measured in the i-th scan read-out. Additionally, remark that for a smooth fibre $N'(\tilde{L}_b) = \overline{N}$. On the other hand, for a hooked fibre, $\overline{N} = N'(\tilde{L}_b) + N_{sp}$.

$$x = 0 \rightarrow \begin{cases} s(0) = s_f \\ N(0) = 0 \\ \varepsilon_f(0) = 0 \end{cases} \qquad x = \tilde{L}_b \rightarrow \begin{cases} s(\tilde{L}_b) = s_l \\ N(\tilde{L}_b) = \overline{N} \\ \varepsilon_f(\tilde{L}_b) = N'(\tilde{L}_b)/(E_f A_f) \end{cases} \qquad (3.16)$$

$$x = 0 \rightarrow \begin{cases} s(0) = s_f \\ N(0) = N_{sp} \\ \varepsilon_f(0) = 0 \end{cases} \qquad x = \tilde{L}_b \rightarrow \begin{cases} s(\tilde{L}_b) = s_l \\ N(\tilde{L}_b) = \overline{N} \\ \varepsilon_f(\tilde{L}_b) = N'(\tilde{L}_b)/(E_f A_f) \end{cases} \qquad (3.17)$$

Where s_f and s_l are, respectively, the slips at the free and loaded ends, and A_f and E_f are the cross section area and elasticity modulus of the fibre.

   The fibre pullout tests provide in terms of pullout load, $\overline{N}$, and loaded end slip, $\overline{s}_l$ several scan read-outs, being $\overline{s}_l^i$ and $\overline{N}^i$ the values of the i-th scan read-out. Regarding these experimental results, the set of unknown parameters of a given local bond relationship (equations 3.12, 3.13 and 3.14) are desired to be found in order to fit the differential equation 3.4 as accurately as possible. A computational code was developed and implemented, supported on the algorithm described in Figure 3.5. The second order differential equation 3.4 included in the algorithm is solved by the Runge-Kutta-Nyström (RKN) method (Kreyszig, 1993), which is detailed in Annex II. The algorithm is build up from the following main steps :

1. the $\tau - s$ relationship is defined attributing values to the unknown parameters. The error, e, defined as the area between the experimental and analytical curves, is initialized;

2. the loaded end slip is calculated at the onset of the free end slip, $\tilde{s}_l$, (see Module A in Figure 3.6);

3. for the experimental i-th scan reading, the loaded end slip, $\overline{s}_l^i$, and the pullout force, $\overline{N}$ are read;

4. taking the loaded end slip, $\overline{s}_l^i$, and using 3.4, the pullout force at the loaded end, $N^i(s_l^i)$, is evaluated. In this case the following two loaded end slip conditions must be considered:

i) if $\overline{s}_l^i < \tilde{s}_l$, the determination of $N^i(s_l^i)$ must take into account that the effective bond length is smaller than the fibre embedded length (see Module B on Figure 3.6). For the case of hooked fibers, the mechanical anchorage contribution is not considered, since the fibre is not yet fully debonded;

ii) if $\overline{s}_l^i \geq \tilde{s}_l$, the evaluation of $N^i(s_l^i)$ is based on Module C (see Figure 3.6). In the latter module, the contribution of the hook end, $N_{sp}(s_l^i(L_b))$, is assessed by the equations presented in section 3.2.2;

5. the error associated with $N^i(s_l^i)$ is calculated. This error is the area between the experimental ($A_{exp,f}^i$) and numerical ($A_{num,f}^i$) curves. The points $(\overline{s}_l^{i-1}, N^{i-1}(s_l^{i-1}))$ and $(\overline{s}_l^i, N^i(s_l^i))$ are used to define the numerical curve, whereas the experimental curve is represented by the points $(\overline{s}_l^{i-1}, \overline{N}^{i-1})$ and $(\overline{s}_l^i, \overline{N}^i)$;

6. the error is updated.

In Modules B and C the Newton Raphson method is used. Whenever the Newton Raphson method fails, the bisection method is used as an alternative.

The algorithm previously detailed was used for both aligned and inclined fibers. In order to use it for inclined fibers must be clarified several issues. As previously said, the pullout behaviour of inclined fibers is a very complex problem, since several mechanisms will interact with each others during pullout. The establishment of an analytical model which took in consideration those mechanisms would be more difficult. Therefore, for simulating inclined fibers, the following aspects were neglected: bending and plastification of the fibre, spalling of the concrete matrix at the fibre exit point, and finally, the change on the embedded length due to matrix spalling. Moreover, for ascertaining the local bond stress-slip law of inclined fibers was only used the pullout load component on the fibre axis, since is the only component dedicated to generate interfacial stresses along the fibre. In practical terms, the pullout load component on the fibre axis is $\overline{N}^i / \cos \alpha$

The determination of the unknown parameters defining the bond stress-relationship, $\tau - s$, was performed by a back-analysis, i.e. determining the $\tau - s$ relationship in such a way that the difference between the numerical and experimental load-slip curves with a minimum error, e. Additionally two restriction conditions were added in order to assure similar values between the numerical and experimental peak pullout load and its corresponding slip (with a tolerance smaller than 2%). The back-analysis was performed by the exhaustive search method (brute force method), based on several parameters sets ascertained by a predefined range and step for each parameter of the corresponding set.

3.3   Parameters for the local bond stress-slip relationship

The values of the parameters of the defined local bond stress-slip relationships (see equations 3.12, 3.13 and 3.14) were determined using the numerical strategy described in section 3.2.3. The local bond stress-slip relationship for each series was calibrated from the average experimental pullout load-slip curve. In the model was adopted a Young modulus, E_f, of 200 GPa, a cross sectional area, A_f, of 0.562 mm^2 and a cross section perimeter, P_f, of 2.356 mm.

In Figures 3.7, 3.8 and 3.9 are depicted both the numerical pullout load-slip relationship and the experimental envelope for each tested series. On the other hand, the values of the parameters defining the local bond relationships obtained by back analysis are included in Table 3.1 (0º series), Table 3.2 (30º series) and Table 3.3 (60º series). Moreover, in the abovementioned tables is also included the corresponding normalised error, $\overline{e}$, which was defined as the ratio between e and the area under the experimental curve.

The numerical curves fitted the experimental data extremely accurate even for high slips, as the normalised error in each series is quite low. In Tables 3.1, 3.2 and Table 3.3 are also indicated the average values and corresponding coefficients of variation of the local bond law parameters. In spite of the accurateness of the numerical simulation, the coefficients of variation of the bond law parameters were extremely high. This fact can be related to the method used in back-analysis (exhaustive search), since the parameters search is based on a previously defined range and step, i.e the parameter variables are discrete. Moreover it was used only one objective function, i.e. difference between the area under the experimental and numerical curves, to determine the best fit for each series. A possible way to solve this problem could be the utilisation of a multi-objective function.

Regarding the abovementioned, the interpretation of the obtained results can not be conclusive. However, in spite of the high coefficients of variation, some trends can be observed. For the series with a 30º and 60º inclination angle, the bond strength, τ_m (30º) and τ_1 (60º), decreased with the bond length increment. Moreover, the bond strength average value increased for the series with a 30º angle, and afterwards decreased abruptly. The smaller bond strength value for the series with a 60º inclination angle was expected, since for this series cracking of the matrix, and consequently degradation of the local bond strength, started for a lower load level. The higher value of the bond strength for the series with a 30º angle can be explained by the fact that, the frictional resistance increases with the inclination angle, additionally remark that the post-peak branch of the local bond law is defined by the bond strength (see equation 3.13). On the other hand, the increase of the frictional resistance was even more pronounced for the 60º series, however, with a lower bond strength. For these reasons the bond laws used for the

series 0º and 30º are not suitable for the series 60º. Additionally, the multi-linear bond law used to model the series 60º allowed that the post-peak branch of this law could be defined independently from the bond strength parameter. Therefore, parameter τ_3 of the multi-linear bond stress-slip law can not be regarded as the bond strength, although being considerable higher than τ_1 (see Table 3.3).

Table 3.1: Parameters for the local bond stress-slip relationship obtained by back analysis for the aligned series.

Series	s_m [mm]	τ_m [MPa]	α	α''	s_1 [mm]	$\bar{e}$ [%]
S_lb20_0	0.14	1.77	0.60	0.22	0.44	3.2
S_lb30_0	0.24	2.27	0.69	0.42	1.30	5.0
H_lb10_0	0.25	1.61	0.22	0.88	0.53	4.3
H_lb20_0	0.23	1.80	0.84	0.45	1.10	2.2
H_lb30_0	0.14	2.10	0.89	0.42	2.21	1.9
Average	0.20	1.91	0.65	0.48	1.11	-
	(24%)	(11%)	(37%)	(45%)	(57%)	

Values in round brackets are the coefficients of variation of the corresponding series.

Table 3.2: Parameters for the local bond stress-slip relationship obtained by back analysis for the series with an inclination angle of 30º.

Series	s_m [mm]	τ_m [MPa]	α	α'	$\bar{e}$ [%]
S_lb20_30	0.16	3.12	0.90	0.30	4.1
S_lb30_30	0.40	2.34	0.42	0.36	3.4
H_lb10_30	0.28	4.31	0.13	0.34	2.2
H_lb20_30	0.11	3.29	0.70	0.25	1.4
H_lb30_30	0.40	1.99	0.21	0.16	1.3
Average	0.27	3.01	0.47	0.28	-
	(50%)	(30%)	(69%)	(28%)	

Values in round brackets are the coefficients of variation of the corresponding series.

Table 3.3: Parameters for the local bond stress-slip relationship obtained by back analysis for the series with an inclination angle of 60°.

Series	s_1 [mm]	τ_1 [MPa]	s_2 [mm]	τ_2 [MPa]	s_3 [mm]	τ_3 [MPa]	s_4 [mm]	τ_4 [MPa]	$\bar{e}$ [%]
S_lb10_60	0.15	1.92	0.58	1.40	2.40	3.07	4.58	5.80	3.1
S_lb20_60	0.18	1.27	0.44	1.08	1.94	3.63	20	0	1.6
S_lb30_60	0.12	0.91	2.17	1.95	3.19	1.82	30	0	3.8
H_lb10_60	0.12	2.62	0.54	1.90	1.72	1.39	10	0	3.2
H_lb20_60	0.05	0.88	0.41	0.95	1.55	3.33	20	0	4.1
H_lb30_60	0.06	0.58	0.62	0.84	2.22	1.85	30	0	2.8
Average	0.11 (44%)	1.36 (56%)	0.79 (85%)	1.35 (36%)	2.17 (27%)	2.51 (37%)	19.1 (54%)	0.98 (245%)	-

Values in round brackets are the coefficients of variation of the corresponding series.
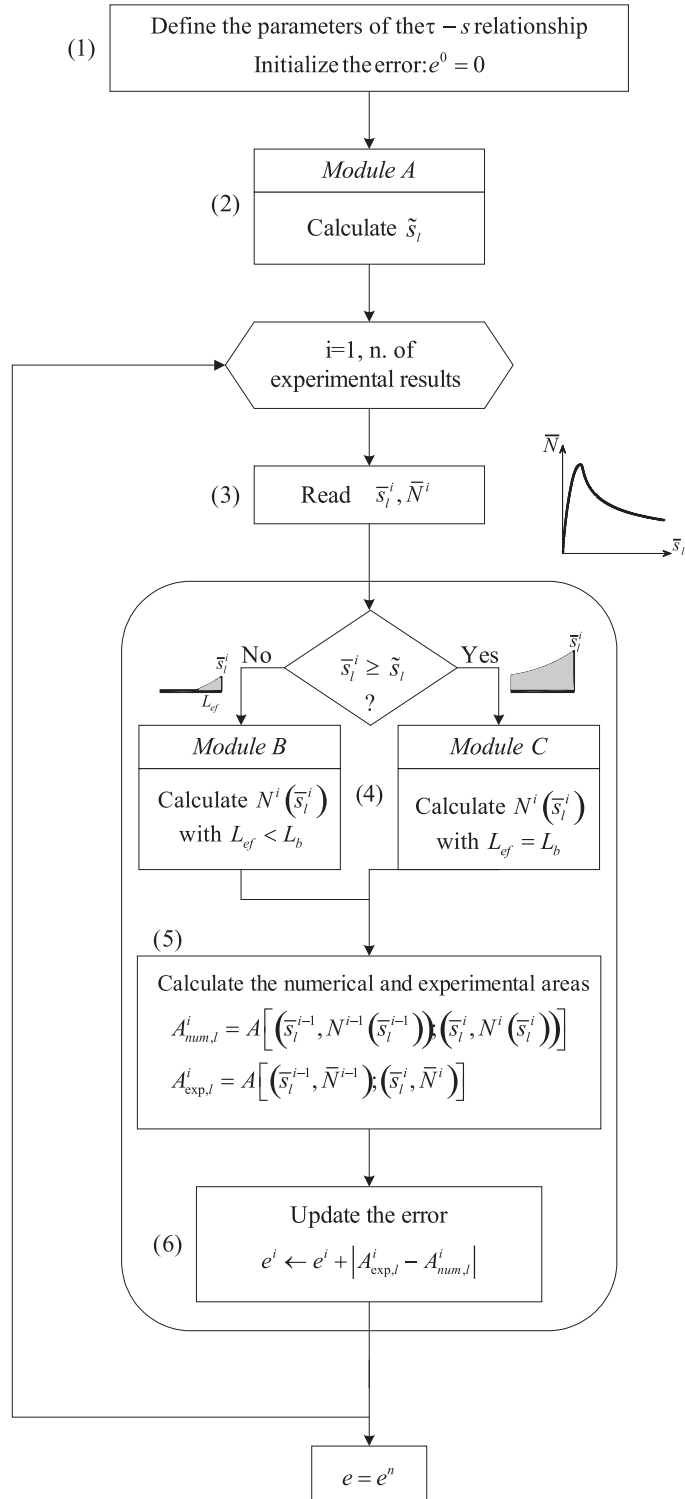
Figure 3.5: Algorithm implemented to obtain the local bond-stress slip relationship.
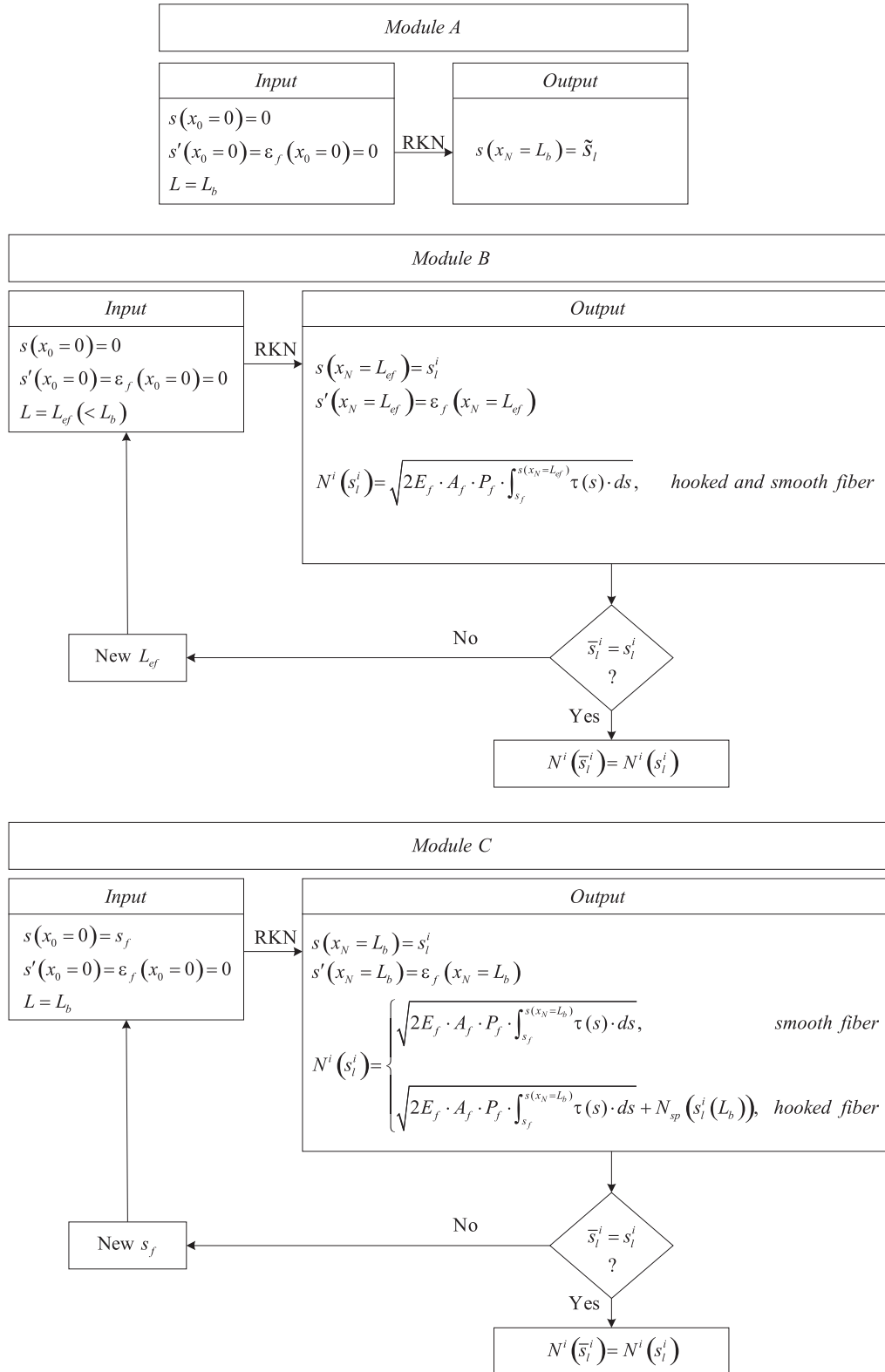
Figure 3.6: Modules A, B and C of the algorithm shown in Figure 3.5.
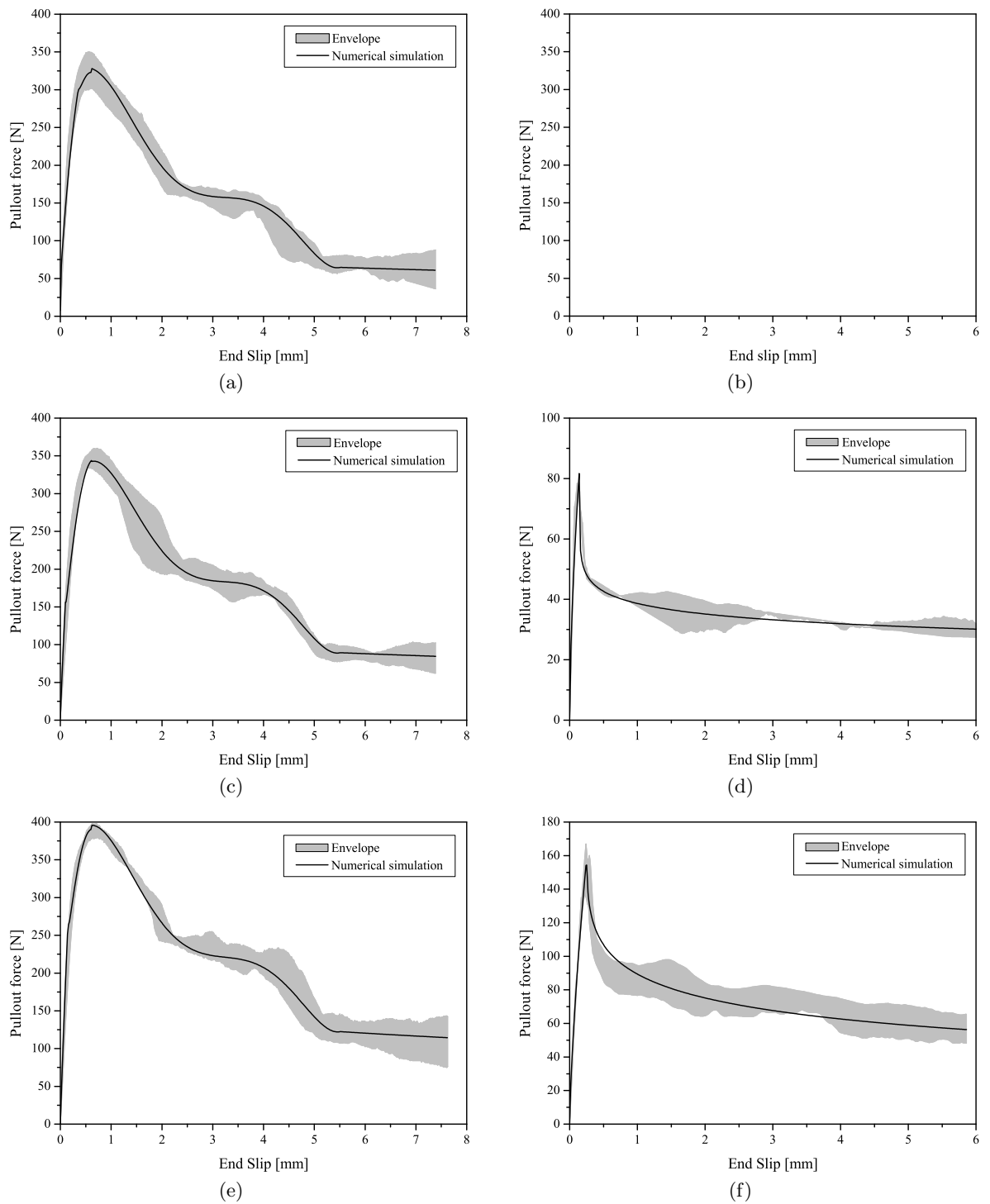
Figure 3.7: Pullout load-slip numerical simulation for a 0° fibre inclination angle: (a), (c) and (e) hook-ended fibres with an embedded length of 10, 20 and 30 mm, respectively. (b), (d) and (f) smooth fibres with an embedded length of 10, 20 and 30 mm, respectively.
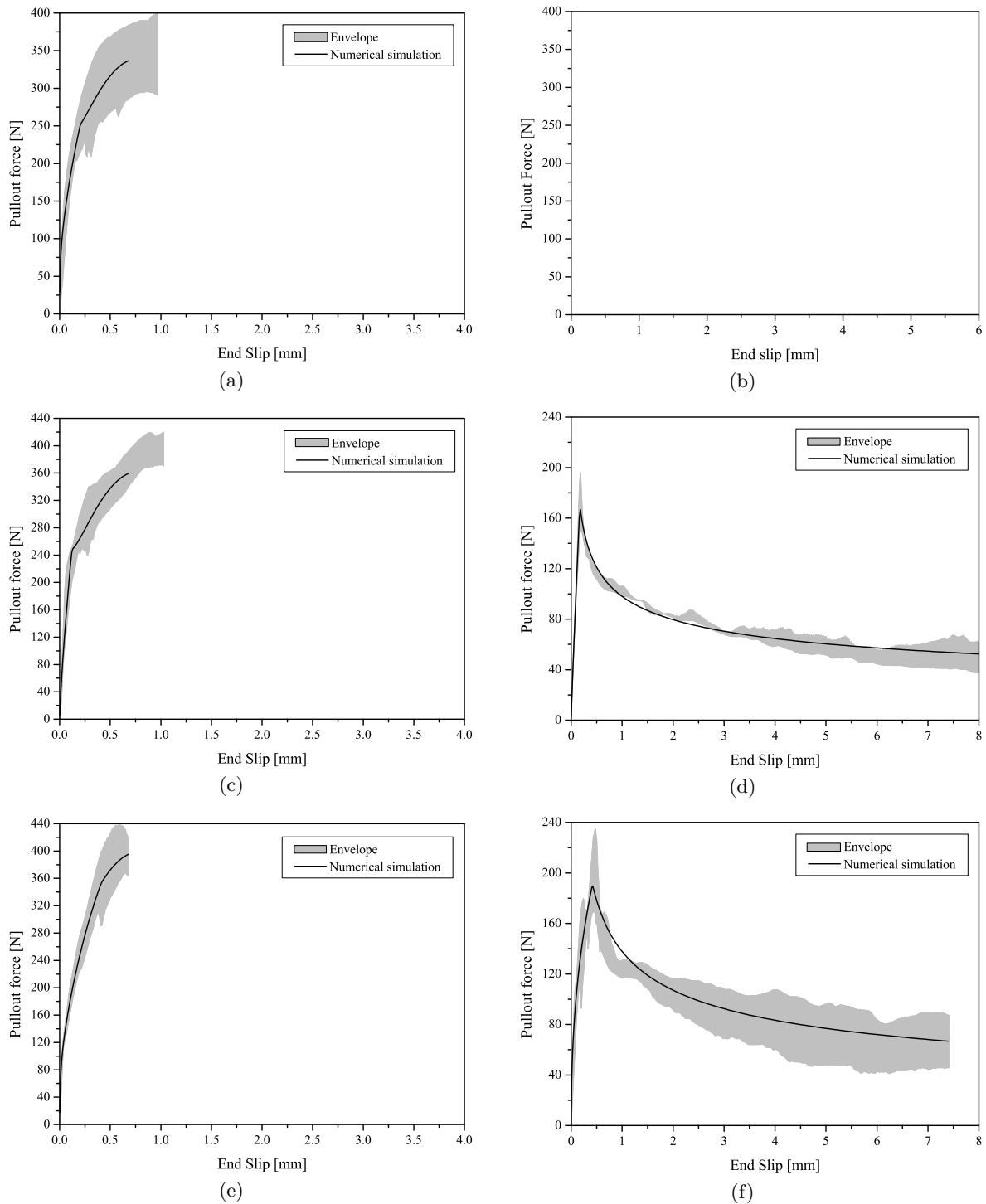
Figure 3.8: Pullout load-slip numerical simulation for a 30° fibre inclination angle: (a), (c) and (e) hook-ended fibres with an embedded length of 10, 20 and 30 mm, respectively. (b), (d) and (f) smooth fibres with an embedded length of 10, 20 and 30 mm, respectively.
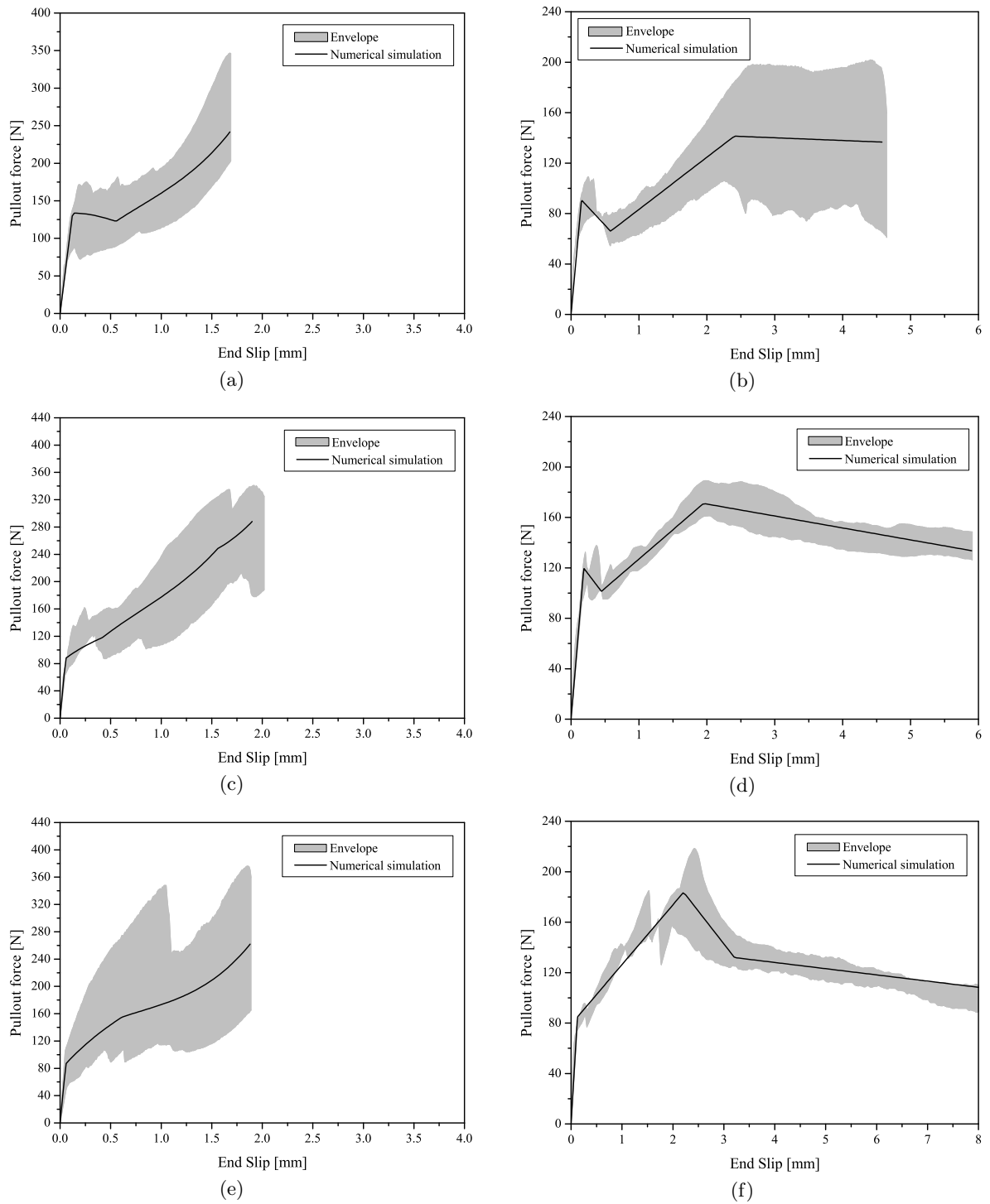
Figure 3.9: Pullout load-slip numerical simulation for a 60° fibre inclination angle: (a), (c) and (e) hook-ended fibres with an embedded length of 10, 20 and 30 mm, respectively. (b), (d) and (f) smooth fibres with an embedded length of 10, 20 and 30 mm, respectively.

CHAPTER 4

Conclusions

The experimental results of hooked-end steel fibres pullout tests on a SFRSCC medium were presented and discussed in this work. Emphasis was given to the accurate acquirement of the pullout load versus end-slip relationship. The influence of the fibre orientation, as well as, the fibre embedment length on the fibre pullout behaviour was studied. Additionally, the role of the end hook, on the overall pullout behaviour, is attained by isolating the contribution of the frictional bond component. Finally, the experimental pullout load-slip were modeled by an analytical model. For this purpose a computational code was implemented with the developed analytical model. The local bond stress-slip law parameters were obtained by a back-analysis performed by the exhaustive search method. In the following section the main conclusions withdrawn in the present study will be presented.

4.1 Experimental results

In general, two main pullout failures modes were observed during the pullout tests. The complete fiber pullout was observed for aligned hooked fibers, aligned smooth fibers and inclined smooth fibers, whereas for inclined hooked fibers the principal failure mode observed was fiber rupture. The latter failure mode observed for hooked inclined fibers was a result of both a strong and compact concrete matrix.

Generally, the maximum pullout load increased linearly with the embedded length for both hooked and smooth fibers. However, this increase was more significant on the smooth fibers, since the pullout response of hooked fibers at a given embedment length is predominantly influenced by the mobilisation and straightening of the hook. Regarding the effect of the orientation angle, the maximum pullout load increased up to a inclination angle of 30° and then decreased for a 60° inclination angle. For both hooked and smooth fibers the highest maximum pullout load was observed for an inclination angle of 30°. However, the increase of

the maximum pullout load with the inclination angle was more significant on the smooth fiber series.

For both smooth and hooked aligned fibers a slight increase of the slip at peak load with the embedded length was observed, whereas for inclined fibers was not found any clear relevance of the embedded length influence on the slip at peak load. On the other hand, regarding the influence of the orientation angle, a slight increase on the slip at peak load was observed for a 30º angle, whereas for a 60º angle, the slip at peak stress increased considerably. The significant increase of the slip at peak load for a 60º angle can be ascribed to other additional mechanisms that usually occur on the pullout of inclined fibers in opposite to aligned fibers, those phenomenons will add to the measured slip a supplementary displacement correspondent to the fiber deformation.

The pullout toughness was computed by integrating the load-slip curve up to slips of 1 and 3 mm, respectively G_{1mm} and G_{3mm}. In general, as the fiber embedded length increased, the toughness to a given slip also increased. Moreover, for the aligned fibers, since always took place the complete fiber pullout (in opposite to inclined fibers in which, frequently, occurred fiber rupture), the G_{1mm} and G_{3mm} increase with the embedded length was more significant than for inclined fibers. Looking upon the influence of the inclination angle on the toughness, in general, an increase of G_{1mm} was observed up to an inclination angle of 30º followed by a decrease for a 60º angle. On the other hand for the G_{3mm}, two distinct trends were perceived for each the smooth and hooked series. Concerning the smooth series, an increase of G_{3mm} was observed with the orientation angle, while for the hooked series the opposite was observed. The overall toughness was markedly influenced by the type of failure, since fiber fracture significantly reduced the toughness when comparing to fibers that underwent a complete pullout.

4.2   Numerical analysis

The analytical model presented was able to simulate with extreme accuracy the experimental pullout load-slip curves, even for high slips for both hooked and smooth fibers (aligned or inclined). In the simulation of inclined fibers, the present model neglected the following aspects: bending and plastification of the fiber, spalling of the concrete matrix at the fiber exit point and, finally, the change on the embedded length due to matrix spalling. In spite of the accurateness of the numerical simulation, the coefficients of variation of the bond law parameters were extremely high. This fact can be related to the method used in back-analysis (exhaustive search), since the parameters search is based on a previously defined range and step, i.e the parameter variables are discrete. Moreover, it was used only one objective function, i.e. difference between the area under the experimental and numerical curves, to determine the best fit for each series. A

possible way to solve this problem could be the utilisation of a multi-objective function, hence additional study should be performed in order to ascertain the local bond law parameters with a lower coefficient of variation.

In spite of the high coefficients of variation for the local bond law parameters, some trends could be observed. For the inclined series, the bond strength decreased with the bond length increment. Regarding the influence of the inclination angle, the bond strength average value increased for the of fibres at 30°, and afterwards decreased abruptly. The smaller bond strength value for the series with a 60° inclination angle was expected, since for this series cracking of the matrix and, consequently, degradation of the local bond strength started for a lower load level. A higher value of the bond strength parameter was obtained for the series with a 30° angle due to two main reasons. The higher frictional resistance observed for the inclined series, and to the fact that the post-peak branch of the local bond law used, for the series with a 30° inclination angle, was defined in function of the bond strength. The increase of the frictional resistance was even more pronounced for the 60° series, however, with a lower bond strength, since the bond law used for the 60° series allowed that the post-peak branch of this law could be defined independently from the bond strength parameter.

References

ACI 544.1R. "State-of-the-art report on fiber reinforced concrete." Technical report, American Concrete Institute (1997).

Alwan, J. M., Naaman, A. E. and Guerrero, P. "Effect of mechanical clamping on the pull-out response of hooked steel fibers embedded in cementicious matrices." *Concrete Science and Engineering RILEM*, 1(1): 15–25 (1999).

Banholzer, B., Brameshuber, W. and Jung, W. "Analytical simulation of pull-out tests - the direct problem." *Cement & Concrete Composites*, 27: 93–101 (2005).

Banthia, N. and Trottier, J. "Deformed steel fiber cementicious matrix bond under impact." *Cement and concrete research*, 21(1): 158–168 (1991).

Banthia, N. and Trottier, J. "Micromechanics of steel pull-out, rate sensitivity al very low temperatures." *Cement and concrete composites*, 14: 119–130 (1992).

Banthia, N. and Trottier, J. "Concrete reinforced with deformed steel fibers, Part I: Bond – slip mechanisms." *ACI Materials Journal*, 91(5): 435–446 (1994).

Bartos, P. J. M. "Bond in fibre reinforced cement and concretes." *The International Journal of Cement Composites*, 3(3): 159–177 (1981).

Bartos, P. J. M. and Duris, M. "Inclined tensile strength of steel fibres in a cement-based composite." *Composites*, 25(10): 945–952 (1994).

Beaumont, P. W. R. and Aleska, J. C. "Cracking and toughning of concrete and polymer concrete dispersed with short steel wires." *Journal of Materials Science*, 13(8): 1749–1760 (1978).

Bentur, A. and Mindess, S. *Fibre reinforced cementitious composites.* Elsevier Applied Science, London (1990).

Bindiganavile, V. and Banthia, N. "Polymer and steel fiber-reinforced cementicious composites under impact loading - Part 1: Bond slip response." *ACI Materials Journal*, 98(1): 10–16 (2001).

Brandt, A. M. "On the optimal direction of short metal fibres in britle matrix composites." *Journal of Materials Science*, 20: 3835–3841 (1985).

Chandra, S. *Properties of concrete with mineral and chemical admixtures.* Spon Press, London (2002).

Chanvillard, G. *Analyse expérimentale et modelisation micromécanique du comportament des fibres d'acier tréfilées, ancrées dans une matrice cimentaire.* Ph.D. thesis, Laboratoire Central de Ponts et Chaussées (1993).

Chanvillard, G. and Aïtcin, P.-C. "Pull-out behavior of corrugated steel fibers (qualitative and statical analysis)." *Advanced Cement Based Materials*, 4: 28–41 (1996).

Cunha, V., Barros, J. and Sena-Cruz, J. "Compressive behaviour of steel fibre reinforced self-compacting concrete at early ages." Technical report, 06-DEC/E-04, University of Minho, Portugal (2006).

Dramix. "Product data sheet – RC-80/60-BN." Technical report, N.V. Bekaert S.A., Zwevegem, Belgium (1998).

Eligehausen, R., Popov, E. P. and Bertero, V. "Local bond stress-slip relationships of deformed bars under generalized excitations." Technical report, Report No. UCB/EERC-83/23, Earthquake Engineering Research Center, College of Engineering, University of California, Berkeley, California, US, 162 pp (1983).

Focacci, F., Nanni, A. and Bakis, C. "Local bond-slip relationship for FRP reinforcement in concrete." *Journal of Composites for Construction ASCE*, 4(1): 24–31 (2000).

Gokoz, U. N. and Naaman, A. E. "Effect of strain rate on the pullout behaviour of fibres in mortar." *International Journal of Cement Composites and Lighweight Concrete*, 3(3): 187–202 (1981).

Gopalaratnam, V. and Shah, S. P. "Failure mechanisms and fracture of fiber reinforced concret." In A. SP-105 (editor), "Fiber Reinforced Concrete Properties and Applications," 1–25. Oslo, Norway (1987).

Gray, R. J. "Analysis of the embedded fibre length on fibre debonding and pull-out from an elastic matrix - Part 1: Review theories." *Journal of Materials Science*, 10(3): 861–870 (1984).

Grünewald, S. *Performance-based design of self-compacting fibre reinforced concrete.* Ph.D. thesis, Delft University, Netherlands (2004).

Grünewald, S. and Walraven, J. C. "Self-compacting fibre reinforced concrete - orientation effect of steel fibres in large beams." In "Workshop - Design rules for steel fibre reinforced concrete structures," 107–113. Oslo, Norway (2003).

Groth, P. *Fibre reinforced concrete - Fracture mechanics methods applied on self-compacting concrete and energetically modified binders.* Ph.D. thesis, Department of Civil and Mining Engineering, Lulea University of Technology, Sweden (2000).

Guererro, P. and Naaman, A. E. "Effect of mortar fineness and adhesive agents on pullout response of steel fibres." *ACI Materials Journal*, 97(1): 12–20 (2000).

Gysel, A. V. "A pullout model for hooked end steel fibres." In RILEM (editor), "HPFRCC3 - High performance fiber reinforced cement composites," 351–359. Mainz, Germany (1999).

Hannant, D. J. *Fibre cements and fibre concretes.* John Wiley & Sons, Chischester (1987).

Helfet, J. and Harris, B. "Fracture toughness of composites reinforced with discontinous fibres." *Journal of Materials Science*, 7(5): 494–498 (1972).

Hing, P. and Groves, G. "The strength and fracture toughness of polycristalline magnesium oxide containing metallic particles and fibers." *Journal of Materials Science*, 7(4): 427–434 (1972).

Homrich, J. and Naaman, A. "Stress-strain properties of sifcon in compression." In u. SP 105 (editor), "Fiber Reinforced Concrete Properties and Applications," 283–304. Oslo, Norway (1987).

Hughes, B. P. and Fattuhi, N. I. "Fiber bond strengths in cement and concrete." *Magazine of Concrete Research*, 27(92): 161–166 (1975).

Kelly, A. and Sweben, C. "Poison effects in aligned fibre composites showing pull-out." *Journal of Materials Science Letter*, 11(3): 583–586 (1976).

Kreyszig, E. *Advanced Engineering mathematics.* John Wiley & Sons, Inc (1993).

Lawrence, P. "Some theoretical considerations of fibre pull-out from an elastic matrix." *Journal of Materials Science*, 7(1): 1–7 (1972).

Laws, V., Lawrence, P. and Nurse, R. "Reinforcement of britle matrices by glass fibers." *Journal of Physics: D Applied Physics*, 6: 523–537 (1972).

Leung, C. K. Y. and Geng, Y. "Effect of lateral stresses on fiber debonding pull-out." *J. Compos. Eng.*, 5(10-11): 1331–1348 (1995).

Leung, C. K. Y. and Geng, Y. P. "Micromechanical modeling of softening behaviour in steel fibre reinforced cementicious composites." *Int. Journal Solids Strucutres*, 35(32): 4205–4222 (1998).

Leung, C. K. Y. and Li, V. "Effect of fiber inclination on crack bridging stress in brittle fiber reinforced brittle matrix composites." *Journal of Mechanics and Physics of Solids*, 40(6): 1333–1362 (1992).

Li, V. C. "Postcrack scaling relations for fiber reinforced cementicious composites." *ASCE Journal of Materials in Civil Engineering*, 4(1): 41–57 (1992).

Li, V. C. and Chan, Y.-W. "Determination of interfacial debond mode for fiber-reinforced cementitious composites." *ASCE Journal of Engineering Mechanics*, 120(4): 707–719 (1994).

Li, V. C. and Stang, H. "Interface pproperty characterisation and strengthening mechanisms in fibre reinforced cement based composites." *Advanced Cement Based Composites*, 6: 1–20 (1997).

Li, V. C., Wang, Y. and Backer, S. "Effect of inclining angle, bundling, and surface treatment on surface treatment on synthetic fiber pull-out from a cement matrix." *Composites*, 21(2): 132–140 (1990).

Li, V. C., Wang, Y. and Baker, S. "A micromechanical model of tension softening and bridging toughning of short random fiber reinforced britle matrix composites." *J. Mech. Phys. Solids*, 39(5): 607–625 (1991).

Lim, T., Paramasivam, P. and Lee, S. "Analytical model for tensile behavior of steel-fibre concrete." *ACI Materials Journal*, 84(4): 286–298 (1987).

Lorenzis, L. D., Rizzo, A. and Tegola, A. L. "A modified pull-out test for bond of near-surface mounted frp rods in concrete." *Journal of Composites Part B: Engineering*, 33(8): 589–603 (2002).

Maage, M. "Interaction between steel fibres and cement-based matrices." *Materials and Structures, Research and Testing* (RILEM), 10(59): 297–301 (1977).

Maalej, M., Li, V. C. and Hashida, T. "Effect of fiber rupture on tensile properties of short fiber composites." *ASCE Journal of Engineering Mechanics*, 121(8): 903–913 (1995).

Markovic, I. *High-Performance Hybrid-Fibre Concrete - Development and utilization.* Ph.D. thesis, Delft University, Netherlands (2006).

Morton, J. and Groves, G. W. "The cracking of composites consisting of discontinous ductile fibres in a britle matrix - effect of fibre orientation." *Journal of Materials Science*, 9: 1439–1445 (1974).

Naaman, A. "Engineered steel fibers with optimal properties for reinforcement of cement composites." *Journal of Advanced Concrete Technology*, 1(3): 241–252 (2003).

Naaman, A. and Shah, S. "Pullout mechanism in steel fibre reinforced concrete." *ASCE Journal Struct. Div.*, 102: 1537–1548 (1976).

Naaman, A. E. and Najm, H. "Bond-slip mechanisms of steel fibers in concrete." *ACI Materials Journal*, 88(2): 135–145 (1991).

Naaman, A. E., Namur, G. G., Alwan, J. M. and Najm, H. S. "Fiber pullout and bond slip I: Analytical study." *Journal of Structural Engineering ASCE*, 117(9): 2769–2790 (1991b).

Ouyang, C., Palacios, A. and Shah, S. P. "Pullout of inclined fibers from cementicious matrix." *ASCE Journal of Engineering Mechanics*, 120(12): 2641–2659 (1994).

Pereira, E. B., Barros, J. A. O., Ribeiro, A., Cunha, V. M. C. F. and Antunes, J. A. B. "Self compacting steel fibre reinforced concrete for precasted sandwich panels - experimental and numerical research." In "Proocedings BeFib," Ancona, Italy (2004).

Robins, P., Austin, S. and Jones, P. "Pull-out behaviour of hooked steel fibres." *RILEM Journal of Engineering Mechanics*, 35(251): 434–442 (2002).

Rossi, P. and Chanvillard, G. "New geometry of steel fibre for fibre reinforced concrete." In H. W. Reinhardt and A. E. Naaman (editors), "High Performance Fiber Reinforced Cement Composites," 129–139. E. & F. N. Spon, London (1996).

Russo, G., Zingone, G. and Romano, F. "Analytical solution for bond-slip of reinforcing bars in R.C. joints." *Journal of Structural Engineering ASCE*, 116(2): 336–355 (1990).

Sena-Cruz, J. M. *Strenghning of concrete structures with near surface mounted CFRP laminate strips.* Ph.D. thesis, Dep. Civil Engineering, Universidade do Minho, Portugal (2005).

Shah, S. P., Swartz, S. E. and Ouyang, C. *Fracture machanics of concrete (application of fracture mechanics to concete, rock and other quasi-britle materials).* John Wiley & Sons, Inc. (1995).

Soroushian, P. and Bayasi, Z. "Fiber-type effects on the performance of steel fiber reinforced concrete." *ACI Materials Journal*, 88(2): 129–134 (1991).

Stang, H. and Aarre, T. "Evaluation of crack width in FRC with conventional reinforcement." *Cement & Concrete Composites*, 14(1): 143–154 (1992).

Stang, H., Li, Z. and Shah, S. P. "Pullout problem: Stress versus fracture mechanical approach." *Journal of Engineering Mechanics*, 116(10): 2136–2150 (1990).

Stroeven, P. "Stereology of concrete reinforced with short steel fibres." *Fract. Mech. Struct. Aspects Concr.*, 31: 15–28 (1986).

Sujivorakul, C., Waas, A. M. and Naaman, A. "Pullout response of a smooth fiber with an end anchorage." *Journal of Engineering Mechanics*, 126(9): 986–993 (2000).

RILEM TC 162-TDF. "Test and design methods for steel fibre reinforced concrete - design of steel fibre reinforced concrete using the σ-w method: principles and application." *Journal Materials and Structures*, 35(249): 262–276 (2002).

Visalvanich, K. and Naaman, A. E. "Fracture model for fiber reinforced concrete." *ACI Journal*, 80(2): 128–138 (1983).

Wang, Y., Li, V. and Backer, S. "Modelling fiber pullout from a cement matrix." *International Journal of Cement Composites and Lightweight Concrete*, 10(3): 143–149 (1988).

Wei, S., Mandel, J. and Said, S. "Study of the interface strength of steel fibre reinforced cement based composites." *ACI Journal*, 83: 597–605 (1986).

Experimental pullout results

In Tables I.1, I.2 are indicated, respectively the average maximum pullout load and the average slip at peak load.

Table I.1: Average values of the maximum pullout load, N_{max}.

	L_b [mm]	FIBRE ORIENTATION ANGLE					
		0º		*30º*		*60º*	
		N_{max} [N]	CoV [%]	N_{max} [N]	CoV [%]	N_{max} [N]	CoV [%]
Smooth	*10*	-	-	-	-	154.2	43.8
	20	77.4	2.0	173.5	18.2	172.8	8.7
	30	155.2	9.7	203.7	13.8	189.4	15.0
Hooked	*10*	321.8	5.6	360.9	13.9	342.0	2.3
	20	347.8	2.8	400.1	4.9	335.2	3.0
	30	388.2	1.6	416.0	3.4	365.1	2.5

Table I.2: Average values of the slip at maximum pullout load, s_{peak}.

	L_b [mm]	FIBRE ORIENTATION ANGLE					
		0º		*30º*		*60º*	
		s_{peak} [mm]	CoV [%]	s_{peak} [mm]	CoV [%]	s_{peak} [mm]	CoV [%]
Smooth	*10*	-	-	-	-	3.34	45.6
	20	0.12	11.8	0.19	7.4	2.02	2.0
	30	0.25	14.4	0.38	32.3	2.17	11.8
Hooked	*10*	0.59	8.7	0.94	11.4	2.40	20.81
	20	0.65	9.4	1.00	9.7	2.33	15.1
	30	0.69	11.0	0.80	19.3	2.64	23.2

Tables I.3 and I.4 contain respectively the average values of the energy dissipated up to a 1 mm and 3 mm slip.

Table I.3: Average values of the energy dissipated up to a 1 mm slip, G_{1mm}.

	L_b [mm]	FIBRE ORIENTATION ANGLE					
		0°		30°		60°	
		G_{1mm} [mm]	CoV [%]	G_{1mm} [mm]	CoV [%]	G_{1mm} [mm]	CoV [%]
Smooth	10	-	-	-	-	0.074	19.1
	20	0.046	3.1	0.114	6.9	0.105	2.0
	30	0.095	5.9	0.141	7.4	0.100	4.4
Hooked	10	0.273	5.6	0.290	11.7	0.125	19.4
	20	0.283	3.6	0.314	5.6	0.129	15.4
	30	0.322	2.5	0.286	11.8	0.126	37.8

Table I.4: Average values of the energy dissipated up to a 3 mm slip, G_{3mm}.

	L_b [mm]	FIBRE ORIENTATION ANGLE					
		0°		30°		60°	
		G_{3mm} [mm]	CoV [%]	G_{3mm} [mm]	CoV [%]	G_{3mm} [mm]	CoV [%]
Smooth	10	-	-	-	-	0.263	13.4
	20	0.117	8.5	0.282	4.0	0.420	6.4
	30	0.251	9.3	0.356	9.7	0.418	5.8
Hooked	10	0.689	5.1	0.465	41.9	0.482	21.3
	20	0.756	5.5	0.558	53.6	0.490	15.3
	30	0.886	1.3	0.317	23.7	0.523	15.2

In Figures I.1, I.2 and I.3 are depicted, respectively, for a fibre inclination angle of 0°, 30° and 60°, the pullout load-slip curves for each specimen tested.

Figure I.1: Pullout load-slip curves for a 0° fibre inclination angle: (a), (c) and (e) hook-ended fibres with an embedded length of 10, 20 and 30 mm, respectively. (b), (d) and (f) smooth fibres with an embedded length of 10, 20 and 30 mm, respectively.

Figure I.2: Pullout load-slip curves for a 30° fibre inclination angle: (a), (c) and (e) hook-ended fibres with an embedded length of 10, 20 and 30 mm, respectively. (b), (d) and (f) smooth fibres with an embedded length of 10, 20 and 30 mm, respectively.
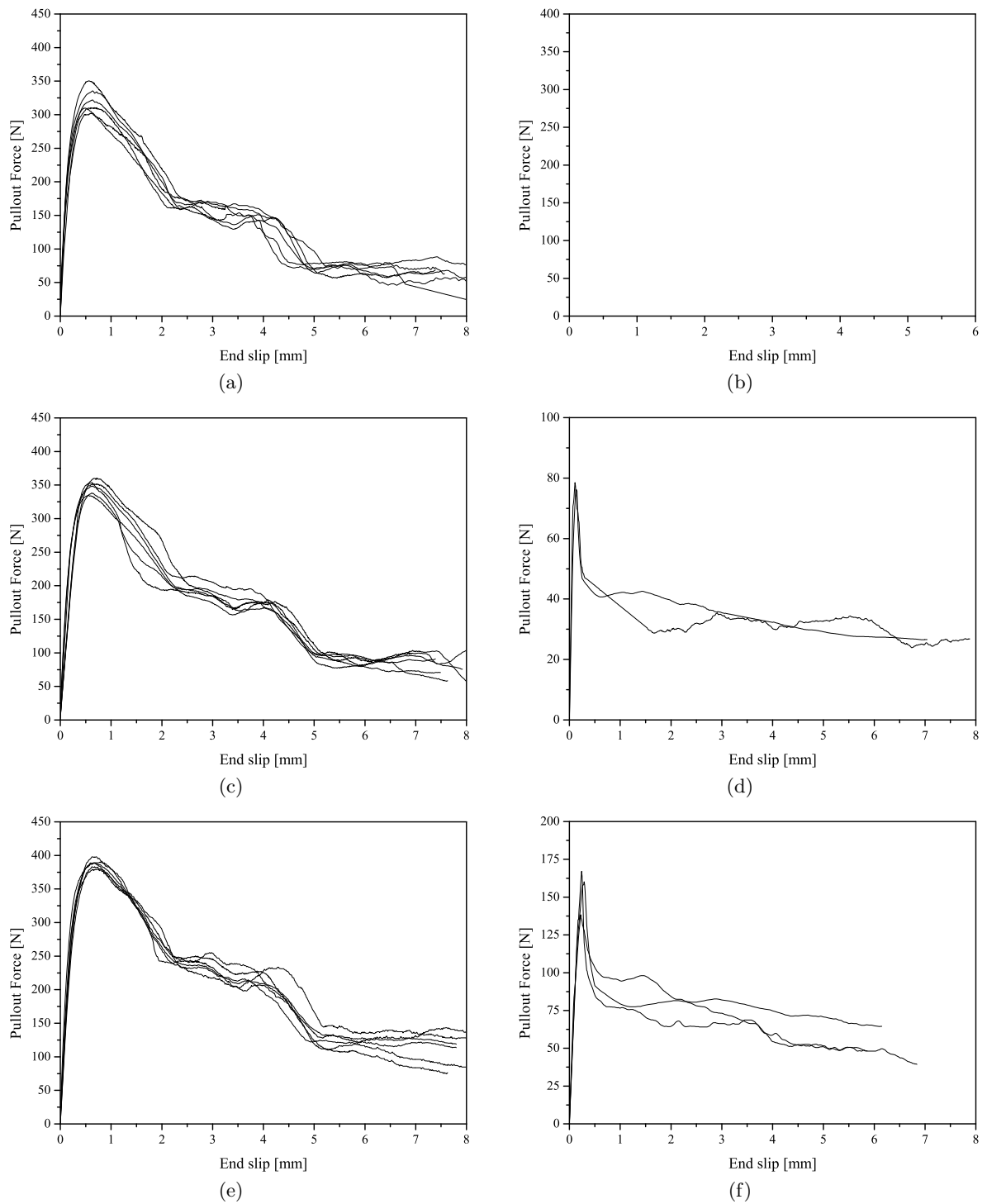
Figure I.3: Pullout load-slip curves for a 60° fibre inclination angle: (a), (c) and (e) hook-ended fibres with an embedded length of 10, 20 and 30 mm, respectively. (b), (d) and (f) smooth fibres with an embedded length of 10, 20 and 30 mm, respectively.
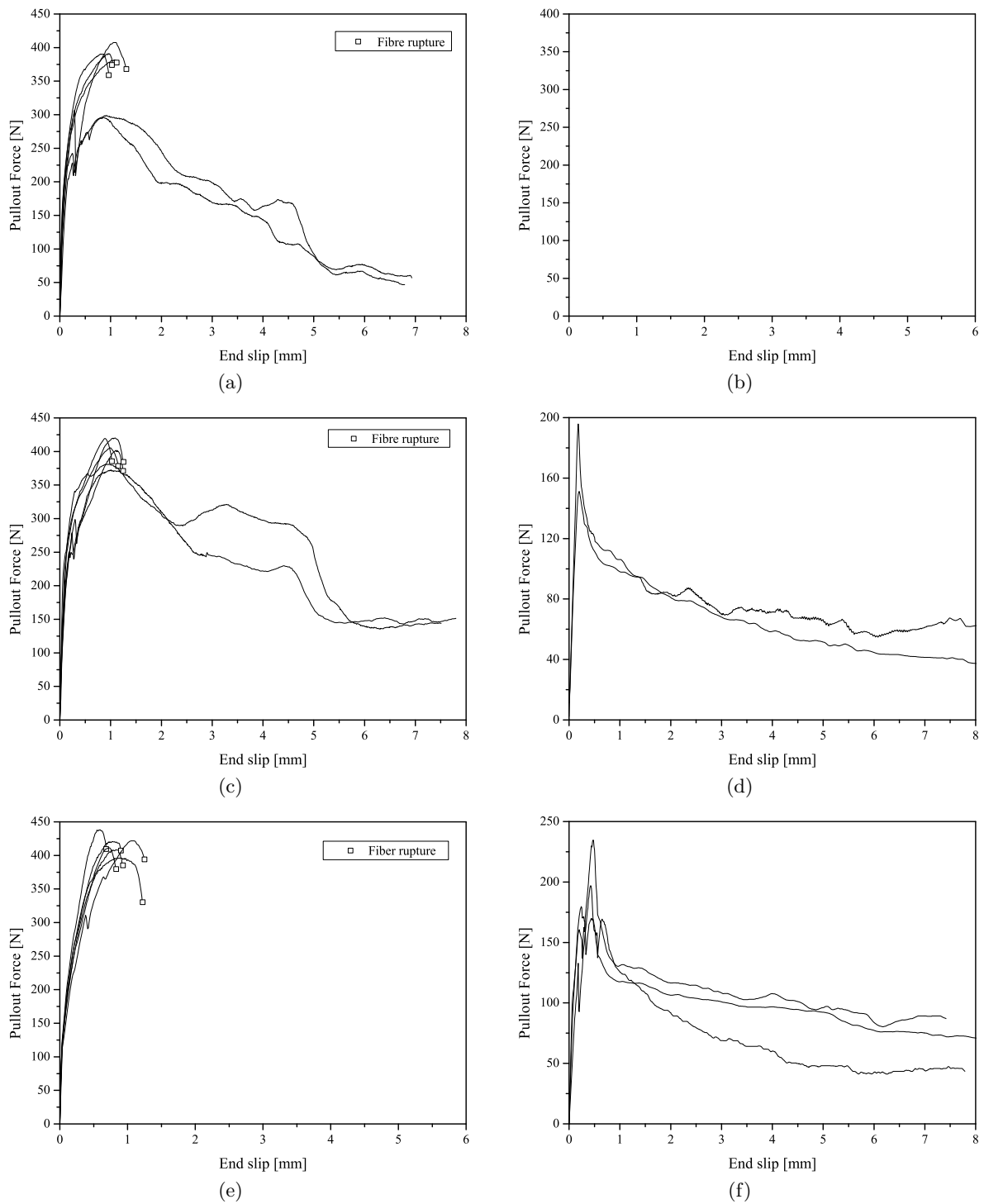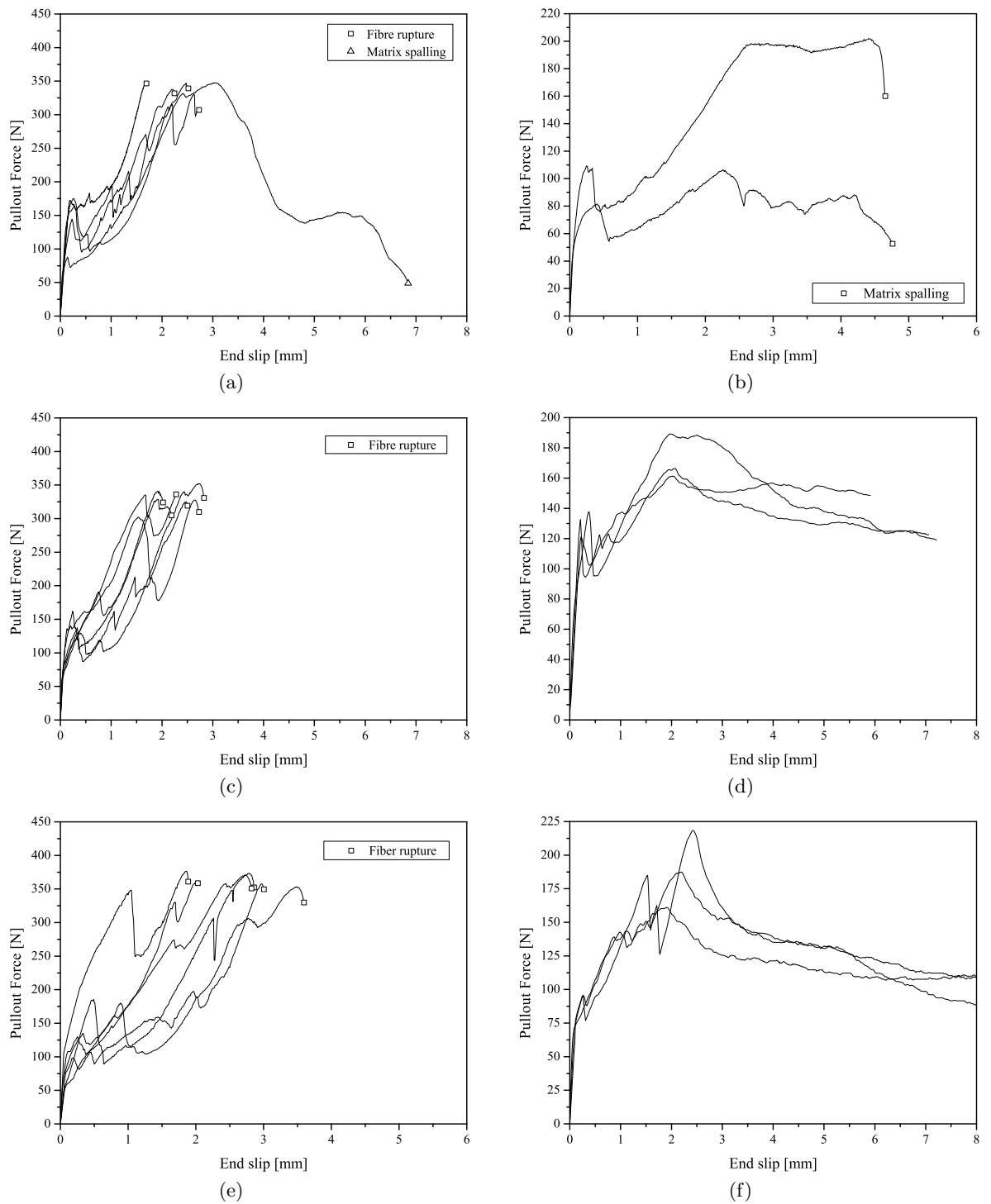
Annex II

Runge-Kutta-Nyström Methods

The Runge-Kutta-Nyström (RKN) method (Kreyszig, 1993) computes the solution of $y'' = f(x, y, y')$ using the initial values $y(x_0) = y_0$, $y'(x_0) = y'_0$ at equidistant points $x_1 = x_0 + h$, $x_2 = x_0 + 2h$, ..., $x_N = x_0 + Nh$, h the step length and N the number of steps. Figure II.1 shows the corresponding algorithm.

The following functions are used in the present study:

$$y'' = \frac{d^2 s}{dx^2}$$

$$f(x, y, y') = \frac{P_f}{(E_f A_f)} \cdot \tau(s)$$

(2.1)

The first point of the effective bond length, L_{ef}, is $x_0 = 0$ and the last one is $x_N = L_{ef}$. The effective bond length was divided in 100 segments of equal width ($N = 100$).

The initial values are the free end slip, $y(x_0) = s_f$, and the fiber strain at the free end, $y'(x_0) = (ds/dx)_0 = \varepsilon(x = 0) = 0$. According to the algorithm represented in Figure II.1, the loaded end slip, $y(x_N) = s_l$, and the laminate strain at the loaded end, $y'(x_N) = \varepsilon(x_N)$, are calculated.
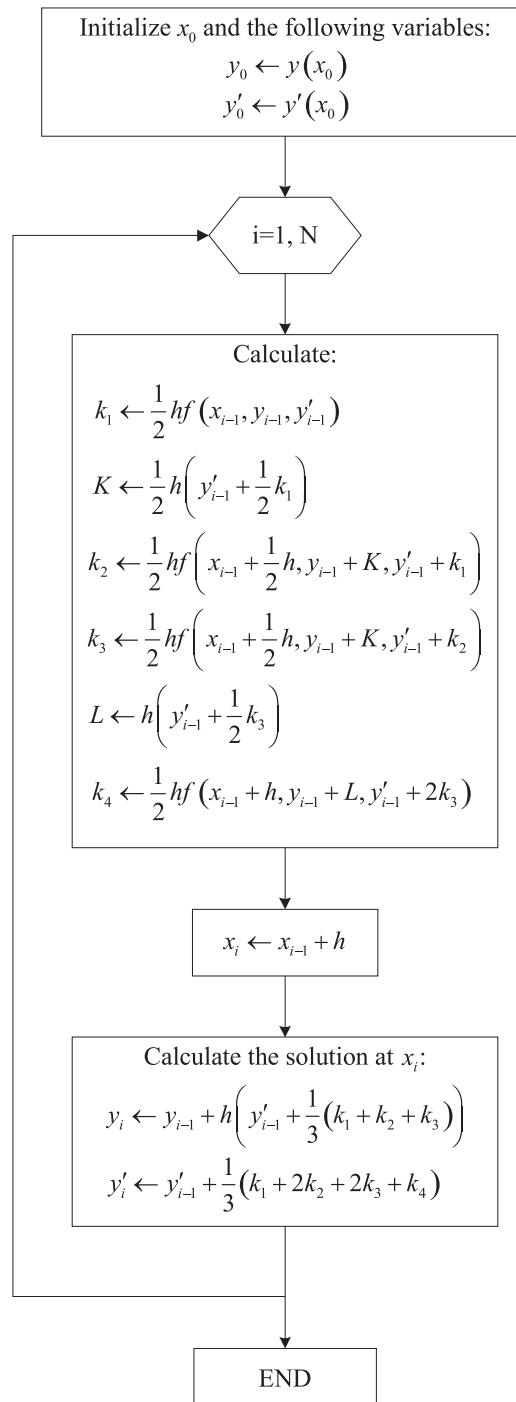
$$\boxed{\begin{array}{c}\text{Initialize } x_0 \text{ and the following variables:}\\ y_0 \leftarrow y(x_0)\\ y'_0 \leftarrow y'(x_0)\end{array}}$$

$$\langle\,i=1,\ N\,\rangle$$

Calculate:

$$k_1 \leftarrow \frac{1}{2}hf\left(x_{i-1}, y_{i-1}, y'_{i-1}\right)$$

$$K \leftarrow \frac{1}{2}h\left(y'_{i-1} + \frac{1}{2}k_1\right)$$

$$k_2 \leftarrow \frac{1}{2}hf\left(x_{i-1} + \frac{1}{2}h, y_{i-1} + K, y'_{i-1} + k_1\right)$$

$$k_3 \leftarrow \frac{1}{2}hf\left(x_{i-1} + \frac{1}{2}h, y_{i-1} + K, y'_{i-1} + k_2\right)$$

$$L \leftarrow h\left(y'_{i-1} + \frac{1}{2}k_3\right)$$

$$k_4 \leftarrow \frac{1}{2}hf\left(x_{i-1} + h, y_{i-1} + L, y'_{i-1} + 2k_3\right)$$

$$x_i \leftarrow x_{i-1} + h$$

Calculate the solution at x_i:

$$y_i \leftarrow y_{i-1} + h\left(y'_{i-1} + \frac{1}{3}\left(k_1 + k_2 + k_3\right)\right)$$

$$y'_i \leftarrow y'_{i-1} + \frac{1}{3}\left(k_1 + 2k_2 + 2k_3 + k_4\right)$$

END

Figure II.1: Runge-Kutta-Nyström algorithm.